Understanding the optical and electronic properties of organic semiconductors using high pressure

Malte Schmidt

Directores:

Dr. Mariano Campoy Quiles

Prof. Alejandro R. Goñi

Dra. Mª Isabel Alonso Carmona

Tutor:
Prof. Javier Rodríguez Viejo

Tesis doctoral

Departamento de Física
Universidad Autónoma de Barcelona
Instituto de Ciencia de Materiales de Barcelona (ICMAB-CSIC)
2013

Abstract

This thesis deals with the optical properties of organic semiconductors which are used for organic light emitting diodes (OLEDs) and organic solar cells (OSCs). This comprises also the charge transfer (CT) state in donor/acceptor blends, an intermediate state on the way to charge collection in OSCs. The aim of this work is to understand how different mechanisms influence the energy levels of organic semiconductors (conjugated polymers and small molecules) and the properties of the CT state.

The most important part in this study involved the application of high hydrostatic pressure, which allows for the observation of the effects of smaller intermolecular distances on the energy levels in organic semiconductors and the properties of the CT state. We explain the observed pressure-induced red-shifts in the absorption and photoluminescence (PL) spectra by the effect of four parameters - bond length, planarity, intermolecular interaction and the dielectric environment - and estimate their contribution to these shifts.

Thick spin-coated films of poly(9,9-dioctylfluorene) (PFO) were investigated under hydrostatic pressure. The comparison between a completely amorphous film and a film with an additional very planar conformation (β-phase) allowed us to clearly estimate the effect of planarisation. Additionally, the absolute value of the refractive index of a conjugated polymer film (PFO) under high hydrostatic pressure was determined for the first time, for which we used an interferometric method.

Two different types of poly(3-hexyl thiophene) (P3HT) were studied in dilute solutions and in thin films both under ambient conditions and under hydrostatic pressure. Especially, the effect of interchain interaction on the optical properties of the thin films was discussed. Raman measurements were used to address the issue of planarisation of the P3HT chains in thin films under hydrostatic pressure.

Studies on spin-coated thin films of blends of P3HT and fullerene derivatives yielded information about the clustering and crystallisation of the fullerenes in an amorphous polymer matrix and its effect on the properties of the CT state. Changes of the CT state energy and emission intensity with fullerene concentration and with hydrostatic pressure were investigated. The observations were used to draw conclusions on the reason for the observed red-shifts and the efficiency of the dissociation of the CT state.

Contents

1 Motivation **7**

2 Introduction and background **13**

2.1 Semiconducting polymers and small molecules 13

2.2 Introduction to organic solar cell 16

2.3 Organic solar cells: from absorption to charge extraction . . . 19

2.3.1 Absorption and photoluminescence 19

2.3.2 Charge transfer state and charge separation 23

2.4 Energy levels and decay mechanisms in organic semiconductors 26

2.4.1 Energy level changes 26

2.4.2 Photoluminescence quenching 30

2.5 Organic materials 31

2.5.1 Phenyl-C61-butyric acid methyl ester (PCBM) 31

2.5.2 Poly(3-hexyl thiophene) (P3HT) 32

2.5.3 Poly(9,9-dioctylfluorene) (PFO) 33

2.5.4 Poly(3,4-ethylenedioxythiophene) poly(styrenesulfonic acid) (PEDOT:PSS) 35

3 Experimental Details **37**

3.1 Preparation of samples by spin coating 37

3.2 The diamond anvil cell 38

3.2.1 Preparation of a sample for the pressure cell 41

3.3 Raman scattering 43

3.4 Photoluminescence and absorption 45

3.5 Ellipsometry 46

4 Planarity and dielectric constant: PFO **49**
4.1 At ambient pressure 51
4.2 PL and absorption under pressure 56
4.3 Refractive index and interchain interaction under pressure . . 60
4.4 Dependence on interchain distance 72
4.5 Chapter conclusions 74

5 Intermolecular interaction: P3HT and PCBM **75**
5.1 From solution to solid film (ambient pressure) 77
5.2 Low temperatures 83
5.3 PL and absorption under pressure 85
5.4 Raman studies under pressure 98
5.5 Chapter conclusions 104

6 Effects of mixing on structure and energy levels **107**
6.1 Clustering of PCBM 108
6.2 Influence of PCBM concentration on P3HT and on the charge transfer state 113
6.3 Influence of temperature 129
6.4 Blends under high hydrostatic pressure 130
6.5 Chapter conclusions 138

7 Conclusions and Outlook **141**

- You have a power she lacks.
- Only because I have a bow.
- She has never seen a bow. Doesn't exist in her world. To you it's a simple tool, to her... it's magic.

Star Trek - The Next Generation: Who Watches The Watchers

1 Motivation

Imagine you are going on a long awaited camping trip. You discover a small secluded place with picturesque scenery. It is the perfect spot; the sun shining down on you, the fragrance of the eucalyptus trees floating on the air. Exhilarated, you assemble your new tent and then sit down to enjoy a nice hot cup of tea. To harvest the abundance of sunlight, the roof of your tent contains organic solar cells. These will be suitable for all your energy needs while camping. With your hands trembling with anticipation, you plug in your electric kettle and open the new pack of Earl Grey tea. By the time the sun begins to disappear behind the trees, the batteries are fully charged. Even though now the sun withholds its energy, you can watch a nice relaxing film, using your organic light-emitting diode screen with bright colours and low energy consumption. To finish this wonderful day you fancy reading a nice old-style book. It lies in the interior of your tent. The whole ceiling of your tent is covered with organic light-emitting diodes to serve you as a solid state light source. They illuminate the interior of your tent so homogeneously and efficiently that you find your book in a trice. As you snuggle down in your bed you thank organic materials for revolutionising your camping trip. At your return, your friends are fascinated to hear about your tales and are even more astonished to hear how cheap and light-weight the tent is.

This possible future camping trip describes, how the way we think about

energy production and usage might change if the research in organic electronics manages to improve the efficiency and applicability of the optoelectronic devices like organic solar cells (OSCs) and organic light-emitting diodes (OLEDs). The photoactive part of these thin film devices could be made out of polymers, which are known to be flexible, light-weight and relatively cheap in production.

For these devices no ordinary polymers are used, which are additionally known to be transparent and quite good insulators, but conjugated polymers. They have (in their undoped state) often semiconducting properties, i.e. they conduct electrical charges and absorb light in the visible part of the spectrum. This opens up the opportunity to build devices which until recently were the preserve of inorganic materials like silicon. The huge opportunity for the application of these conjugated polymers to combine typical optical and electrical properties of inorganic semiconductors with typical mechanical properties of polymers in one and the same material - maybe some researchers with daydreams like the camping trip - lead to the development of a wide variety of semiconducting polymers for the different organic optoelectronic devices.

Organic optoelectronic devices are very thin and can be shaped into any form and thus could be used on a great scale on the many usually unused spaces of structures or vehicles at very low cost [1, 2]. They could even be introduced between glass panes of insulated windows [3] or on flexible surfaces [2] like textiles [4] (as a tent for a camping trip).

OLEDs have established themselves already on the market for displays for small portable devices, and recently (January 2013) SONY presented even the first large scale television prototype [5]. Apart from displays, OLEDs can also be used as high intensity solid state light emitter [6]. For large area devices, solution based processing, using polymers instead of small molecules, are desirable because of the cheaper processing (by ink-jet printing and/or roll-to-roll processing) [7].

OSCs are up to date still not widely commercially available. Because of their good mechanical properties and their cheap fabrication, they might be used for places where silicon solar cells would be too expensive, too heavy,

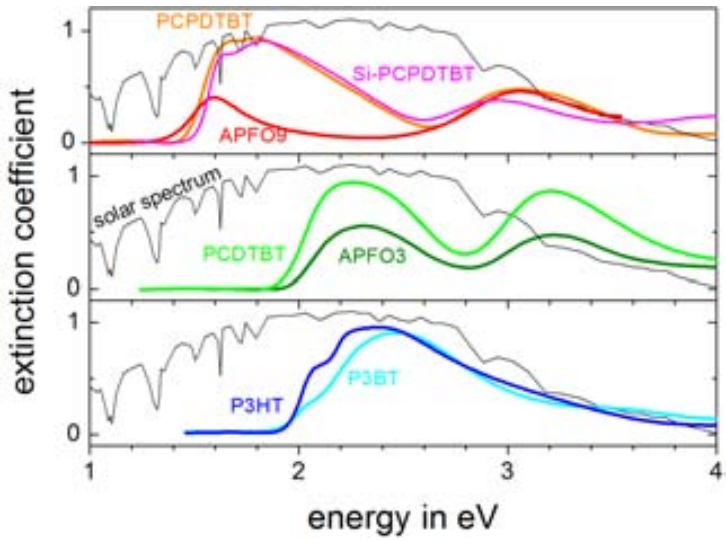

Figure 1.1: Extinction coefficients of various polymer thin films. Most conjugated polymers absorb just in the high energy region of the solar spectrum. (with permission of Dr. Mariano Campoy-Quiles)

too bulky, too fragile or simply not conducive to the beauty of the place. As they will probably not compete with inorganic solar cells in terms of power conversion efficiency or lifetime [8], they are believed to be complementary to inorganic solar cells rather than substitutes [9]. Much progress has been already achieved until now for OSCs [1, 10–18] with the best reported power conversion efficiency of 12 % (March 2013) [19]. But the efficiency of the devices still have to be improved and also the costs have to be lowered in order to make solar cells attractive to the market [8].

For both kind of devices it is very important to control the energy (wavelength/colour) at which the active layer absorbs or emits, which is influenced by their band gap. For OLEDs the application might demand a certain colour; for OSCs, the emission spectrum of our sun demands an efficient low-energy absorption in order to enhance the absorption of sunlight. For OSCs, this is a major reason for low efficiencies at the moment, since the best compromise for a band gap for OSCs is assumed to be between 1.1 eV and 1.5 eV [20], which is much lower than the band gap of most polymers used in OSCs (above 1.9 eV [21], see figure 1.1). For this reason low-bandgap copolymers are being developed, but they usually show low charge carrier

transport leading to low power conversion efficiencies despite the better absorption properties compared to high-bandgap polymers like poly (3-hexyl thiophene) (P3HT)[22]. Thus, it seems very important for improvements of OSCs to be able to find alternative ways to reach desired low absorption of the active film. This is closely related to the question: **How can a polymer in the active film be influenced in order to adjust the band gap for the specific need?**

This is one major question which shall be discussed in the course of this thesis. The other question deals with the so called charge transfer state, an intermediate state on the way to charge collection in OSCs. Its energy is closely related to the the output voltage in OSCs [3]. The reasons for the dissociation of the charge transfer state, which is important to allow for the collection of the charges and their energy, are still not well understood [23, 24]. At the moment, the formation and dissociation of the charge transfer state involves also major losses which manifests itself in a low power conversion efficiency. Thus, the desired increase in the charge transfer energy while maintaining a high dissociation efficiency raises the question: **On what does the charge transfer energy depend and how can its dissociation be stimulated?**

This thesis is contributing to the endeavour to improve optoelectronic devices and answering the proposed questions in a very fundamental way. The main objective of the thesis was to understand how optical properties of semiconducting polymers can be influenced without chemically modifying the molecules. This is important because a deeper understanding allows us to get insight into which properties a molecules should have or which morphology the polymer film should have to get the desired optical properties.

The disadvantage of a chemical modification is that it is difficult to assign the observed optical changes to certain parameters, since intermolecular distance, band gap and the film morphology can all change at the same time and many different molecules would have to be systematically investigated to disentangle the different influences on the absorption and emission of materials and blend systems. For this reason, we used a diamond anvil cell to induce changes by high hydrostatic pressure, which allowed us to gradually

change the parameters as the intermolecular distance and thus modify the optical properties in a very controlled and "clean" way.

Spin-coated films of poly(9,9-dioctylfluorene) (PFO) and P3HT were investigated this way. The former is a polymer with possible applications in OLEDs, the latter is one of the most important high-bandgap polymers for OSCs. Furthermore, blends of P3HT with phenyl-C61-butyric acid methyl ester (PCBM), a very important model system for OSCs, were studied [25]. Mostly optical measurements like absorption, photoluminescence and Raman measurements were performed. With these various aspects of the molecules like their energy levels, conformations and morphology in thin films are discussed in pure polymer films of poly(9,9-dioctylfluorene) (PFO) and P3HT.

Structure of the thesis

The thesis is structured as follows:

The second chapter gives a deeper introduction into the field and provides the necessary theoretical basis of organic semiconducting materials (such as P3HT, PCBM and PFO). A review of the pertinent literature is given in order to facilitate the later discussion of the experiments. The third chapter describes the preparation of the samples and the measurements.

The results will be presented and discussed in the subsequent chapters. Chapter 4 deals mostly with the planarisation of the polymer chain and the change in the refractive index under pressure by the example of PFO. In chapter 5 the different behaviour of the semicrystalline and the amorphous versions of P3HT and of PCBM under pressure is presented with a focus on planarisation and intermolecular interaction. In chapter 6, the effect of mixing P3HT and PCBM - as in the active layer of a real working OSC - is presented focusing on clustering of PCBM and the effect of PCBM concentration and hydrostatic pressure on the charge transfer state and the efficiency of the charge transfer state dissociation. Finally, in the seventh chapter, the conclusions will be given and the results and their importance for the design of new molecules and solar cells will be discussed in a broader context.

Y nosotros leemos, y, a partir de esa lectura, creemos, votamos, discutimos, perdemos la memoria, nos olvidamos generosa, cretinamente, de que hoy dicen lo contrario de ayer.

Mario Benedetti, **La tregua**

2

Introduction and background

The experiments performed for the thesis are mostly fundamental and of a rather general character interesting for any device with organic semiconductors. However, the greatest part was performed in order to understand the processes happening in organic solar cells. This includes the properties of the pure conjugated polymers but also the so called charge transfer state, an intermediate state on the way towards charge collection at the electrodes. Furthermore, the influence of pressure on the optical properties of organic semiconductors is a central point in the thesis. To give sufficient background for the discussion of the performed experiments we will introduce conjugated polymers, then give a broad outline of the most important processes happening in organic solar cells and explain in detail the literature available about the optical properties of conjugated polymers and small molecules under pressure.

2.1 Semiconducting polymers and small molecules

Polymers consist of carbon based repeat units (monomers) connected by covalent bonds to usually long chains, which can be linear or branched. The properties of polymers are virtually independent from their number of repeat

units. For shorter chains this is not true and to distinguish these molecules from polymers they are called oligomers (from the greek $o\lambda\iota\gamma o\sigma$ meaning "a few"). There is no exact number which determines when oligomers become polymers, and it depends also on whether one refers to the optical, electrical or thermodynamical properties. Common polymers out of everyday life have very similar mechanical properties to the ones which are discussed in this thesis but completely different optical and electrical properties. Both types have a low density, are ductile and strong; hence they are resistant to many mechanical influences. But while polymers are known to be mostly transparent and good electrical insulators, some conjugated polymers can exhibit a certain degree of conductivity, thus opening up the way for organic electronics.

The difference of these two types of polymers can be found in the bonds they form. The C-atoms of *common* polymers have predominantly sp^3 hybridised orbitals, which form σ-bonds. The energy gap, formed by the occupied bonding σ-state and the empty anti-bonding σ^*-state, is in these case very high[1] giving the polymers their transparent and insulating property. C-atoms in semiconducting molecules, in contrast, have typically sp^2 hybridised orbitals, forming σ-bonds, and one p_z-orbital, forming π-bonds. The π-bonds are weaker (they have a higher energy) and a smaller energy splitting between the bonding and anti-bonding state, which form the band gap of the semiconducting molecules. The transition from the π- to the π^*-orbital is in the range of a few electronvolts and as a result conjugated molecules have semiconducting properties. This transition does not lead to free charges, however, but to a strongly bound Frenkel[2]-exciton[3] because of

[1] high compared to energy of photons of visible light and of typical voltages applied at electronic devices
Alessandro Giuseppe Antonio Anastasio Volta (1745, Como - 1827, Como)

[2] Yakov Il'ich Frenkel (1894, Rostov-on-Don, Russia - 1952, Leningrad)

[3] Strictly speaking one has to take into account that in polymers a strong interaction between vibrational and electronic states exists. The excitation is always accompanied by the distortion of the molecule in its vicinity, which influences the excitation's properties. The electron or hole with the distortion together is called a polaron. However, as the difference is most of the times of minor importance for the understanding of the processes, in this thesis the concepts more familiar to physicists of free electrons/holes and excitons will be mostly used.

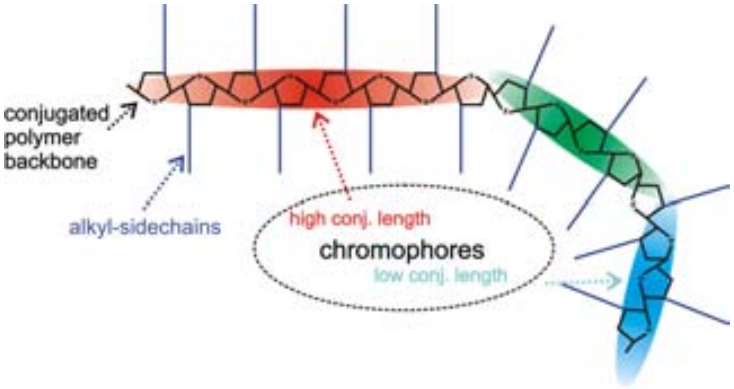

Figure 2.1: Sketch showing P3HT with chromophores of different conjugation lengths. In reality, the borders are not as clearly defined and many reasons exist to impede the movement of the exciton.

the high exciton binding energy between 0.1 eV and 0.5 eV [23, 26–30]. That the exciton binding energy is so much higher than in inorganic materials, e.g. silicon, can be explained by two main differences: a) The strong localisation of the wave functions to a one dimensional system over a few monomers [30] compared to a three dimensional extension of the wave function in inorganics; b) the much lower dielectric constant in polymers (approx. 3-4 compared to about 11 for silicon and gallium arsenide) resulting in less screening of the charges.

The (de)localisation of the exciton along the polymer backbone is one of the most important characteristics and is described by the (effective) conjugation length. The conjugation length states over how many monomers the exciton is delocalised. For poly(3 hexyl thiophene) (P3HT) a typical number reported is 7-10 monomers [31]. The conjugation length can gradually change by changing the p-orbital overlap between the monomers. Usually a polymer is not straight and planar but has bends, kinks and can rotate around the single bond (torsion) connecting the monomers. Very strong bends or an interruption of the conjugation because of defects can interrupt the free movement of the exciton altogether. A polymer can be roughly thought of as a chain of segments with different conjugation lengths. This is depicted simplified in figure 2.1. The conjugated polymer backbone of these chain segments determines the energy (or “colour”) of the excitons and is called a

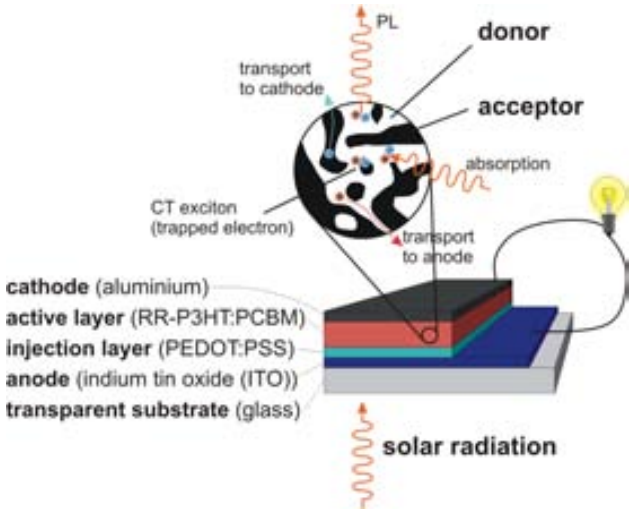

Figure 2.2: Sketch of a typical solar cell with detailed look into the active layer and the most important processes. See text for details.

chromophore. The exciton energy is the band gap energy minus the exciton binding energy. The energy of an exciton within a chromophore decreases with increasing conjugation length. An intuitive picture is that of the "particle in a box" (or a harmonic oscillator with varying force constant). In organic materials the exciton energy decreases with increasing chain length (i.e. a wider box/ weaker spring) according to experiments with oligomers [31, 32] Therefore, the conjugation length is often used as an argument, whenever changes in the exciton energy occur as is further explained in section 2.4.1.

2.2 Introduction to organic solar cell

Solar cells convert the energy of photons, typically created in our sun - hence the term *solar* cell, into electrical energy. A sketch of an organic solar cell (OSC) is shown in figure 2.2. It consists at least of a layer, in which the photons are absorbed and charges are separated, called the active layer (typically 100 nm to 200 nm thick [18]), and two electrodes to collect the opposed electrical charges. For successfully collected charges, in short, the following processes happen in an organic solar cell: The absorbed light creates an exciton in the donor polymer, which diffuses to the interface with the acceptor

material. There, the electron changes to the acceptor phase (charge transfer), separating the still bound electron and hole spatially. Then the charges break free (charge separation) and move to their respective electrode, where they are collected.

The electrodes in organic photovoltaics have two important functions. Firstly, they have to collect the charges which arrive at their interface and, secondly, they form an electric field according to the difference in their work function and thus assist the charges to reach their respective electrode. At least one electrode has to be transparent (usually the anode) in order for light to reach the active layer. Further layers can be present to enhance the absorption by a redistribution of the electric field [33] or to ease the charge transport between active layer and the electrodes (injection layer) for example to prevent the formation of surface dipoles [34].

Organic solar cells are usually not completely constructed out of organic materials, however, the active layer, the heart of the solar cell, is. This layer consists of (at least) two organic semiconducting materials, one p-type (hole conducting) and one n-type (electron conducting). Even though often the term "plastic solar cells" is coined, in fact, the most efficient organic solar cells use derivatives of fullerenes as an electron acceptor, i.e. a small molecule. While the fullerene is without real alternative at the moment, many different polymeric donor materials are tried in order to get better morphology, better conducting properties or better energy levels for efficient OSCs. The choice of the polymer is an important one, for most of the absorption happens in the polymer and the destiny of the created exciton will depend strongly on the properties of the polymer.

Important characteristics of a solar cell (also inorganic ones) are marked in the I/V-curve (photocurrent-voltage curve) of a fictitious solar cell depicted in figure 2.3. These characteristics are the open circuit voltage V_{oc}, which is the voltage between the two electrodes when no electrical current flows, and the short circuit current I_{sc}, which is the current measured when the electrodes are connected without any resistor. In both cases no power is produced by the solar cell but these values are indicative of what the solar cell is in principle capable of. This means, they can be a measure of the

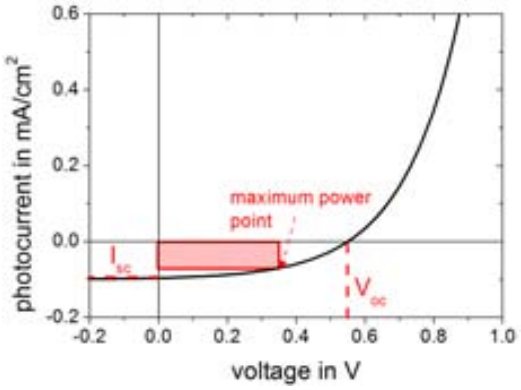

Figure 2.3: I/V curve of a fictitious solar cell with approximate I_{sc} of $0.1\,\mathrm{mA\,cm^{-2}}$ and V_{oc} of $0.55\,\mathrm{V}$

physical limits of the system [21]. The maximum power produced in the solar cell at the so called maximum power point shows how the solar cell performs under working conditions and one tries to operate solar cells as close to this point as possible. The external quantum efficiency (EQE) states how many electrons are extracted from one photon of a specific energy. This value depends on the absorption and how many of the thus created charges can be brought afterwards to the electrodes (the latter is called IQE or internal quantum efficiency). To maximise the absorption one needs a high spectral overlap between the absorption coefficient of the active layer and the solar spectrum. The solar spectrum has roughly the form of a black body emission at 5500 K and as such a big part of the total intensity lies in the infrared, while many polymers have band gaps of about 2 eV (620 nm) or higher, giving a very low spectral overlap. P3HT, for example, has a band gap of 1.9 eV and would at best collect only 30% of the solar light [17, 35]. But the lower the band gap of the polymer is, the higher the energy losses of the high energy photons are, because the exciton quickly loses the energy difference to the band gap as heat. The best compromise is assumed to be around 1.1 eV and 1.5 eV [20], but it is also possible to build dual junction solar cells, which consist in essence of two solar cells in series, one to harvest high energy photons efficiently and the other to harvest the low energy photons.

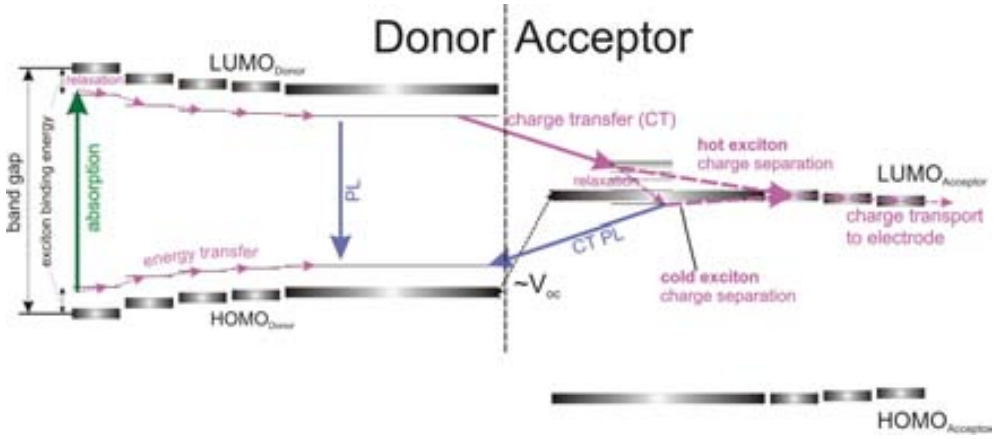

Figure 2.4: Sketch of the lowest unoccupied molecular orbital (LUMO) and highest occupied molecular orbital (HOMO) energy levels of a polymer (donor)/fullerene (acceptor) heterojunction. The sketch shows the absorption (on the left), the exciton migration through the polymer, the charge transfer, the charge separation and the movement of the electron away from the interface (on the right). More details in the text.

2.3 Organic solar cells: from absorption to charge extraction

The basic processes in organic solar cells are explained here in greater detail. First and foremost, the processes occurring from absorption until the charge separation are of interest for this thesis. Later processes concerning the transport of the charges and the injection into the electrodes will be outlined only briefly for the sake of completeness. Some of the following explained processes are depicted in figure 2.4 which shows a sketch of the energy levels within the active layer. On the left, the lowest unoccupied molecular orbital (LUMO) levels and the highest occupied molecular orbital (HOMO) levels of the donor are shown and, on the right, the corresponding ones for the acceptor.

2.3.1 Absorption and photoluminescence

During the absorption process a photon is absorbed by the polymer, elevating an electron from the HOMO to the LUMO (see figure 2.4). The HOMO-

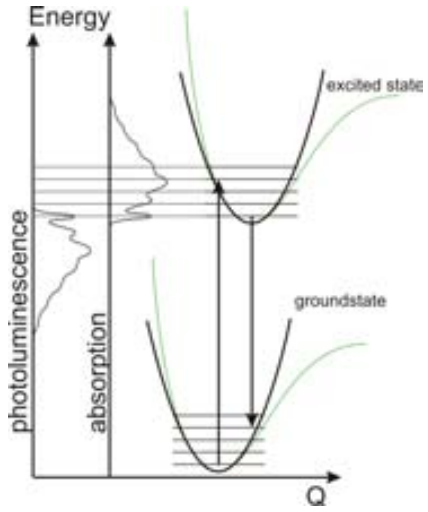

Figure 2.5: Sketch of a Franck-Condon-transition between the ground state and the first excited state. The thin (green) curve stands for the real potentials and the thicker one for the harmonic approximation. On the left, the absorption and PL spectra, which this material would have, is portrayed. Idea adopted from reference [36].

LUMO gap is also called optical band gap (or just band gap). The onset of absorption (optical gap) is at lower energies because the HOMO-LUMO gap is defined for free charges while the created singlet exciton has a binding energy which first has to be overcome to dissociate the exciton [37]. The HOMO-LUMO transition is from the well delocalised bonding π-orbital to the anti-bonding π*-orbital. The atoms in the ground state and the excited state have usually different equilibrium positions. The Franck-Condon[4] representation of absorption is illustrated in figure 2.5. It shows the electronic ground state (corresponds to HOMO) and the first excited state (LUMO) of a system, each with the vibrational energy levels according to a harmonic oscillator approximation of the configuration coordinate, which in this simple pictures corresponds to the nuclear oscillation of one specific bond. Typically the stretching vibrations of the carbon-carbon (C-C) single and double bonds with energies around 150 meV to 200 meV couple best to the electronic states of the molecule. The Franck-Condon principle states that the electronic

[4]James Franck (1882, Hamburg - 1964, Göttingen); Edward Uhler Condon (1902, Alamogordo, USA - 1974, Boulder, USA)

transition is fast ($\leq 10^{-15}$ s) compared to the nuclear motions ($\approx 10^{-13}$ s) [37] and thus, the configuration coordinate does not change during the electronic transition. This is closely related to the Born-Oppenheimer[5] approximation. This justifies the vertical transition for the absorption, which usually occurs from the vibrational ground state (0-state) to the n-th vibrational state of the first excited electrical state. The transition is written as $n \leftarrow 0$. Transitions from higher vibrational states are unlikely, because the energy of the optical phonons, to which the electronic states are coupled, is big compared to the thermal energy kT [38]. Transitions which involve the excitation of higher vibrational states are shifted to higher energies compared to the transition to the vibrational ground state.

Photoluminescence is the reverse process of the absorption. After the absorption, the system relaxes from the n-th vibrational state very fast to the 0-th vibrational state, so that usually virtually all the emission comes from the 0-th vibrational state (Kasha's[6] rule). From there, the system can go to the n-th vibrational state of the electronic ground state ($n \rightarrow 0$). Transitions to higher vibrational states are shifted to lower energies compared to the transition to the vibrational ground state.

The intensity distribution of the different transitions can be described by the Franck-Condon-factor. The intensity of a transition is proportional to the transition integral which depends on the vibronic wavefunction overlap between the initial and the final state. When the configuration coordinate of the electronic ground state and the excited state are identical (and both states have similar configurations near their respective equilibrium position), the transition between the vibrational ground states is the only one allowed as the other vibrational wave functions are perpendicular to the ground state wave function. If the configuration coordinate of the excited electronic state is shifted as shown in the example in figure 2.5, higher vibrational states get a higher transition probability and thus higher intensities in absorption and photoluminescence. This is expressed often in the Huang-Rhys[7]-factor,

[5] Max Born (1882, Wrocław - 1970, Göttingen); Julius Robert Oppenheimer (1904, New York - 1967, Princeton)

[6] Michael Kasha (*1920, Elizabeth, USA)

[7] Huang Kun (1919, Beijing - 2005 Beijing) and Avril Rhys

which is defined as

$$S = \frac{k(\Delta Q)^2}{2\hbar\omega},$$

where k is the force constant, ω the angular frequency of both electronic states, $\hbar$ the reduced Planck[8] constant and ΔQ the configuration coordinate difference between electronic ground state and the first excited state. It describes the average number of phonons created in the transition. For experimental purposes one can write this as

$$S = \sum_{n\geq 1} \frac{nI_n}{I_g} \approx \frac{I_1 + 2 \cdot I_2 + 3 \cdot I_3}{I_g},$$

where I_n is the intensity for the transition to/from the n-th vibrational state of the final state and I_g the total intensity, which is defined as

$$I_g = \sum_n I_n.$$

The Huang-Rhys factor is here of importance for a decrease of its value is often connected with an increasing conjugation length in the polymer chains [39–41].

Exciton diffusion after absorption occurs by a random walk as the exciton is neutral and, therefore, its movement is not influenced by the internal electric field caused by asymmetric work functions of the electrodes. The chromophores of the polymer are electronically coupled and after absorption the exciton can move as a whole along a polymer chain from one chromophore to the next or even to a chromophore of a neighbouring polymer chain (in crystalline materials even with roughly the same speed [28]). This happens via a Förster[9] transfer which is more efficient towards lower energies (sub-picosecond range) while it is thermically activated between levels of similar energy and a jump is relatively slow (10 ps to 100 ps) [28]. As the time constant of PL decay is in the order of magnitude of at least several tens of picoseconds [42] up to the nanosecond regime [43] an exciton is likely to arrive at a low energy chromophore before decaying radiatively. This selective

[8] Max Karl Ernst Ludwig Planck (1858, Kiel - 1947, Göttingen)
[9] Theodor Förster (1910, Frankfurt am Main - 1974, Stuttgart)

PL is in contrast to the absorption process for which all conjugation lengths contribute. This and, to a lesser degree, an often occurring relaxation process of the polymer backbone after absorption lead to a different centre of the 0-0 transition energy in PL compared to absorption. The shift between the centre of the the 0-0 absorption peak and the 0-0 PL peak is a measure of the energy loss the exciton sustains and is called Stokes[10] shift [37, 44] (note: for the system in figure 2.5 there is no Stokes-shift in contrast to figure 2.4, where relaxation occurs and the exciton migrates to a chromophore with a smaller band gap).

2.3.2 Charge transfer state and charge separation

After absorption the exciton has a certain life-time (and a corresponding diffusion length) until it undergoes either radiative (PL) or non-radiative (producing heat) recombination. If this happens, the exciton energy is lost for the power generation of the solar cell. A solar cell which consists only of the polymer would create virtually no free charges [45] because the exciton has such a high binding energy (approximately one order of magnitude greater than the thermal energy kT) and just excitons which reach one of the electrodes might break up. In order to break up the exciton before it decays and make the energy it carries accessible, an electron acceptor can be introduced to form an intermediate and more stable state on the way to charge separation. A charge transfer (CT) state, in general, is a state in which a charge is transferred from one excited molecule to the other and occurs also when doping the polymer, for example, in an oxygen atmosphere [46]. In a solar cell the expression is usually used, however, for the specific charge transfer from the donor-material to the electron-acceptor-material. The new state is no usual exciton any longer because the two charges are spatially separated, but they are still in neighbouring molecules and efficiently bound to each other by Coulomb[11] forces [26, 47]. It is usually termed charge transfer exciton/state or bound polaron pair. This CT state is so important because

[10] Sir George Gabriel Stokes (1819, Skreen, Ireland - 1903, Cambridge, England)
[11] Charles Augustin de Coulomb (1736, Angoulême, France - 1806, Paris)

it is the only known way to break up the exciton efficiently.

Virtually every exciton which reaches the donor-acceptor interface undergoes there the charge transfer, because the charge transfer process itself happens in the subpicosecond time range and is thus much faster than any other competing process [48]. The efficiency of the charge transfer is therefore to a great extent determined by the distance an exciton has to move by a random walk in order to reach the donor/acceptor interface. In order to keep this distance short, the active layer consists usually of a heterogenous blend of the donor and acceptor material, which is termed a bulk heterojunction. The phase separation of the two materials in this bulk heterojunction must at most be as large as the exciton diffusion length, which is only around 10 nm for polymers [26, 49, 50]. On the other hand, a very intimate blend of the two materials is not the best choice mostly because any free hole moving through the polymer will always be close to a free electron in the acceptor material increasing drastically the probability of their recombination (so called bimolecular recombination). Therefore, the control of the morphology is one of the most important factors in the optimisation of the active layer in order to obtain the best compromise between a low bimolecular recombination and a high charge transfer efficiency.

The LUMO-level of the acceptor material lies ideally several hundred millielectronvolts below the LUMO-level of the polymer. It is believed that the energy difference between the two LUMO levels has to be bigger than the exciton binding energy in order for the charge transfer to be efficient [26, 51, 52]. Because of the lower LUMO level the CT exciton has a considerably lower energy than the singlet exciton in the polymer, usually in the near-infrared region (e.g. 1 eV for RR-P3HT [53]). The CT state can also undergo several possible transitions. Above all, the electron and hole can recombine (geminate recombination) under the emission of light, decay non-radiatively or they can separate into two free charges - the desired case. There are two main branches for theories which try to explain how charge separation can occur, the “hot exciton theory” and the “cold exciton theory”. Directly after the charge transfer the exciton is in an excited state (“hot”, see figure 2.4). It can then make a transition to the ground state. From the ground state

it has to overcome the binding energy, which will happen with a certain probability ("cold exciton charge separation" in figure 2.4 simplified just with the electron). It is possible that, for example, the electric field between the two electrodes assists this separation [26, 54, 55] or that delocalisation of one of the charges assists in their breaking up [56, 57]. The charge transfer state is stable for several nanoseconds before it decays and the charges are lost for the charge collection [56]. Possibly, the transition from the relaxed (or "cold") state to a free electron would not be efficient enough mostly because of the still high binding energy of the CT exciton [47]. The "hot-exciton" theory states that directly after the charge transfer the still excited charge transfer exciton uses the extra energy to undergo the charge separation [57] ("hot exciton charge separation" in figure 2.4).

The open circuit voltage is believed to be determined by the HOMO(donor) - LUMO(acceptor) difference [3, 58] and therefore the efficient breaking of the exciton is achieved at the expense of the open circuit voltage [59]. The radiation observed upon the geminate recombination is also determined by the HOMO (donor) - LUMO (acceptor)-gap (and the binding energy of the CT state). This makes the charge transfer accessible to optical measurements.

After the charge separation the hole moves in the donor towards the anode and the electron moves in the acceptor towards the cathode in the internal electric field of the electrodes. Because of the misalignment of the HOMO states and the LUMO states between the two organic materials it is not very likely for the charges to change to another phase during transport. It is therefore very important that after the charge separation uninterrupted pathways exist for the hole (in the donor) as well as the electron (in the acceptor) to their respective electrodes. This emphasises even more the importance to control the morphology (a trapped electron because of a bad morphology can be seen in the sketch in figure 2.2). The further the charges are from their respective electrodes the more difficult it is to guarantee uninterrupted pathways and to avoid bimolecular recombination [26]. Additionally, the mobilities of the charges in the organic materials are very low. This is a problem because the charges need a long time to reach their electrode, which makes

the recombination process more likely. If the mobilities of holes and electrons are additionally not well balanced, one species is extracted faster than the other and a space charge builds up in the device, limiting the efficiency of the extraction of the charges [35]. Because of both the possible built-up of space charge and the bimolecular recombination the active layer has to be as thin as possible. Fortunately, conjugated polymers have a much higher extinction coefficient than silicon, making it possible to keep the active layer at a few hundred nanometres and still exhibit high absorption [26]. At the electrodes, the alignment of the work function with the energy level in the organic material and the type of contact (Schottky[12] or ohmic[13]) are important in order not to lower the open circuit voltage and in order to avoid recombinational losses. After this, the energy of the charges is at the disposal of the user as she/he sees fit.

2.4 Energy levels and decay mechanisms in organic semiconductors

2.4.1 Energy level changes

The control of the molecular energy levels is important for any optoelectronic device. The energy levels depend on the chemical structure of the molecule itself, but even the same molecule can exhibit a wide range of energies (changes of several hundred millielectronvolts [60, 61]) of the HOMO and LUMO level according to its geometrical changes and interaction with its environment. For example, the absorption and PL spectra of a molecule in a solid state are invariably red-shifted with respect to the dissolved molecule [62] (called here "solution-to-solid" shift but often called "gas-to-crystal" shift). Also under hydrostatic pressure the spectra of organic materials nearly always shift to lower energies [40, 61, 63, 64]. It is of great importance for the design of molecules and for the fabrication of devices to understand which parameters influence the energy levels of organic materials in these cases. The most

[12]Walter Hermann Schottky (1886, Zürich - 1976, Pretzfeld, West Germany)
[13]Georg Simon Ohm (1789, Erlangen - 1854, München)

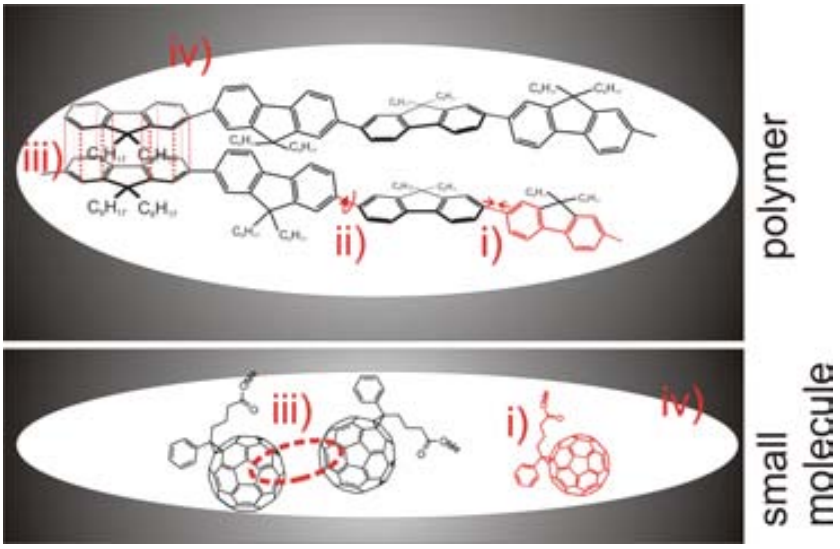

Figure 2.6: Illustration of the different parameters, which can affect the band gap of a polymer and a small molecule (without significant conformational freedom): i) the bond length, ii) the molecular conformation, iii) intermolecular/ interchain interactions and iv) the dielectric environment.

important parameters believed to influence the energy levels are depicted in figure 2.6:

The bond length ((i) in figure 2.6): Bond length changes within the molecules change the overlap of the p-orbitals and thus the delocalisation of the exciton. A shortening (lengthening) of the bond lengths could thus lead to a higher (lower) conjugation length. It was suggested that under hydrostatic pressure the resulting increased conjugation length with the shortening of the bonds is the main cause for the observed red-shift. For this, mostly the shortening of the inter-monomer bond would be important [65–67], because it is said to be relatively soft and a variation of the bond length could influence the p-orbital overlap between monomers [67, 68]. However, it was also claimed that the change in bond lengths is very small [30, 69, 70] and calculations of para-terphenyl (3P) showed that intrachain interactions, like the bond length change, play only a minor role [68]. This makes it unclear if bond length changes are enough to explain the red-shift.

Molecular conformation ((ii) in figure 2.6): The molecular conformation is influenced greatly by the interaction with neighbouring molecules or parts

of the same molecule (Pauli[14] repulsion (steric effects) and van-der-Waals[15] interaction) and the temperature. Different conformations can lead to a variation of the p-orbital overlap. This effect is especially important if rotational degrees of freedom exist in the molecule, which changes the alignment of neighbouring p-orbitals. In oligomers and polymers this is usually true for the inter-monomer bond, which then affects the planarity of the chain. A higher planarity leads to a higher conjugation length and provides thus possible contribution to the "solution-to-solid" shift [71]. The planarisation of non-planar molecules under high pressure was shown to affect the band gap considerably at low pressures [60, 67, 72], again because of an increased p-orbital overlap.

Intermolecular and interchain interaction ((iii) in figure 2.6): For this effect the π-orbital overlap of different molecules or different chromophores is important. This can be influenced by the orientation of two molecules or by their distance. Interchain interaction leads to a shift of the energy levels of the ground state along with a shift and a splitting of energy levels in the excited state as described by the molecular exciton model [73]. In this model, we may consider the interaction of two molecules or polymer chromophores having a main dipole (or transition moment). The two possible excited levels are those, in which the two dipoles are either parallel or anti-parallel. The allowed transition for absorption is from the ground state to the excited state with parallel dipoles. In the cofacial configuration (H-aggregate), the parallel state has the higher energy, in the staggered/slipped case (J-aggregate) the lower energy of the two exited states.

Another type of intermolecular interaction occurs for small molecules, like anthracene, which crystallise with two inequivalent molecules per unit cell [69]. In these cases, Davydov[16] splitting occurs leading to a red-shift.

By going from the solvent to a solid or by increasing the pressure an enhanced interchain interaction is expected. According to calculations, Davydov splitting is enhanced in anthracene crystals with decreasing intermole-

[14] Wolfgang Ernst Pauli (1900, Wien - 1958, Zürich)
[15] Johannes Diderik van der Waals (1837, Leiden - 1923, Amsterdam)
[16] Alexander Sergeevich Davydov (1912, Yevpatoria, Russian Empire - 1993, Kiev)

cular distance, which reduces the band gap [70]. But this is a very specific example and in order to explain the red-shifts for the "solution-to-solid" shift and hydrostatic pressure, aggregates seem to offer the only general explanation. For polymers, however, a staggered configuration, as in J-aggregates, might be difficult or impossible to realise for two polymer chains. A blue-shift with decreasing intermolecular distance was shown for H-aggregates in computations and the experimentally observed red-shift explained in these case by conformational [74] and bond length changes [66]. Nonetheless, for hydrostatic pressure it has been claimed that the interchain interaction can play a major role for the red-shift in polymers under pressure [61, 68] without clarifying the mechanism behind it. It was also claimed that aggregates cause the "solution-to-solid" shift. In this context it was pointed out that H-aggregates might be weakly emissive from the lower energy state[75].

One way to explain a red-shift via aggregates is to assume that the mentioned calculations are overidealised and disorder in polymer samples enables transitions to/from the lower excitated states in H-like aggregates. Temperature might also play an important role to increase the disorder and make the transitions more allowed [76]. Cornil et al. have found, that displacement of two oligomers in the cofacial configuration induces only very little oscillator strength in the lower excited level [71]. Spano et al. discussed disorder as random distribution of spatially correlated molecular transition energies [77, 78]. In their calculations even ideal H-aggregates retain absorption to the lower excited state (though less than in the isolated molecule) and only the 0-0 emission is strictly forbidden. Disorder in this picture leads above all to an increase in intensity of the 0-0 PL peak [77, 78]. With this picture in mind one can assume that in real (disordered) polymer samples, H-like aggregates have an allowed transition from/to the lowest excited state.

It was also suggested that, apart from these H-aggregates, J-aggregates exist because of the interaction of the monomers of the same polymer chain [79]. Energy changes would therefore be explained by the changed coupling between monomers. As this coupling will depend solely on the conformation of a single polymer chain, this model has to be incorporated into the intrachain model. It can help to explain the shift caused by the bond

length shift (parameter (i)) or conformation (parameter (ii)).

Dielectric constant ((iv) in figure 2.6): On the one hand, an increase in the dielectric constant (or refractive index) will lead to an increase in the polarisation energy, decreasing the HOMO - LUMO gap [37]. At the same time, more efficient screening of charges can lead to a decrease in the exciton binding energy [30, 68] implying an increase in the optical gap (onset of absorption). This means that a priori it is not even clear what effect the dielectric constant might have on the optical gap of a specific material. The interaction of the exciton with the highly polarisable solid was suggested to cause in general the "solution-to-solid" shift [62]. For hydrostatic pressure, the dielectric environment of the exciton was suggested to influence the optical gap by the stronger polarisation of the surrounding dielectric material [80].

2.4.2 Photoluminescence quenching

Additionally to the red-shift, a quenching of the PL has also been observed invariably under pressure [63]. Concerning this quenching most arguments deal with interchain interactions, which favour the formation of only weakly-emissive states after the absorption. It was suggested that shorter intermolecular distances are conducive to the formation of interchain electron-holes pairs [81, 82]. This species is no longer a Frenkel exciton but rather a form of charge transfer state and has a much lower transition probability for radiative emission. Connected with this, quenching might stem from the formation of excimers. Excimers (=excited dimers) are dimers that are stable only when one part of the dimer is in an excited state and the other in the ground state. They have a featureless long wavelength emission and long life-times, i.e. as the charge transfer state, they are likely to decay by nonradiative decay mechanisms. Their formation becomes more likely at smaller interchain distances [37, 80]. A very important quenching mechanism seems to stem from defect sites. At defects a charge transfer can occur, trapping efficiently one of the charges [74, 83]. The quenching is determined by the density of these quenching sites and the mobility of the exciton. Especially photooxidation

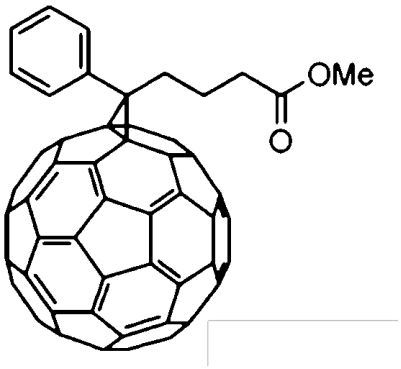

Figure 2.7: Chemical structure of Phenyl-C61-butyric acid methyl ester (PCBM)

causes a rapid increase of the density of quenching sites leading, for instance, to a decrease in PL intensity when the sample is measured in air. In contrast, under pressure the mobility of the excitons may increase because bends and kinks might disappear increasing the movement along a chain and because the increased interchain interaction aids the motion of excitons between chains [64, 80, 84]. Another possibility is that a higher dielectric function (or refractive index) leads to a lowering of the exciton binding energy [30] and thus can favour the charge separation and impeding the emissive recombination of the exciton. The formation of an H-aggregate was suggested to lead to PL quenching when, after the absorption, the exciton goes to the lowest excited state of the H-aggregate which is only weakly emissive [75].

2.5 Organic materials

2.5.1 Phenyl-C61-butyric acid methyl ester (PCBM)

Formula: $C_{72}H_{14}O_2$

Phenyl-C61-butyric acid methyl ester (PCBM, see figure 2.7) is a derivative of the buckminster fullerene C_{60} called so because of the similarity of the structure of the molecules to the geodesic domes of the architect R. Buckminster Fuller[17][85]. The side group makes the fullerene soluble in many

[17] 1895, Milton, Massachusetts, USA - 1983, Los Angeles

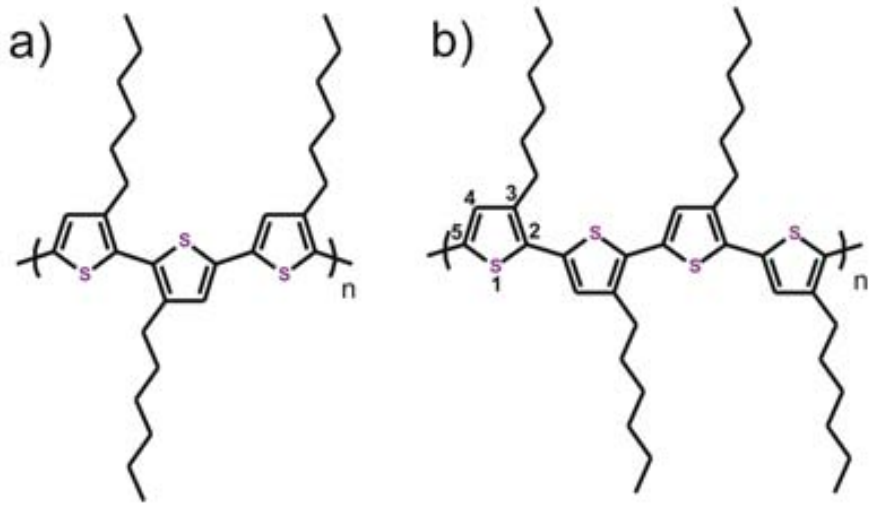

Figure 2.8: Chemical structure of Poly(3-hexyl thiophene) (P3HT): a) regiorandom (rra), b) regioregular (RR)

common solvents among them chlorobenzene and toluene. It is a very good acceptor molecule for organic photovoltaics, because of its high electron affinity and good transport characteristics. It can accept up to six electrons per molecule [54, 86] and can crystallise, showing efficient charge transport in three dimensions [87]. Additionally, bis-PCBM, the bisadduct of PCBM, was used in one experiment. The additional side group prevents crystallisation and increases the LUMO-level yielding devices with a higher V_{oc} [88].

PCBM (684430) purchased from Sigma Aldrich [89] molecular weight M_n: 911 g/mol

2.5.2 Poly(3-hexyl thiophene) (P3HT)

Formula: $(C_{10}H_{14}S)n$

Poly(3-hexyl thiophene) (P3HT, see figure 2.8) is a conjugated polymer known for its high mobilities [90, 91] and is often used as a model polymer for efficient organic photovoltaics in the P3HT:PCBM blend system. The monomer units consist of thiophene rings and an alkyl chain at the 3 position. Neighbouring rings are connected at the 2 and 5 position of the monomer and

rotated roughly 180° around the interring single bond [92]. The alkyl chain is attached in order to increase the solubility of the polymer in common organic solvents such as chloroform, toluene or chlorobenzene making it possible to process the polymer from solution using methods such as spin coating (see chapter 3.1).

The monomers of P3HT can be assembled in three different ways. The head (H) is hereby defined as the carbon atom in the 2 position and a tail (T) in the 5 position and accordingly one can have head-tail(HT), tail-tail (TT) and head-head (HH) bonds [92]. In the HH-bond case, the monomers are twisted far out of coplanarity and conjugation because of steric effects by the alkyle chains. The regioregularity is defined as the fraction of HT bonds in the polymer chain. In regiorandom P3HT (rra-P3HT) the bonding between the monomers is random and high torsion angles (roughly 50° to 70° out of coplanarity for poly(3 butyl thiophene (P3BT)) [93] appear often, while in regioregular P3HT (RR-P3HT), i.e. with mostly HT-bonds, monomers are arranged nearly coplanar (within 20° in P3BT) [93].

RR-P3HT has not only a smaller band gap because of the lower torsion angle (see section 2.1) but has, unlike rra-P3HT, additionally the capability to crystallise. The crystalline phase is very important for the optoelectronic properties of the material: The torsion angle is further reduced because of greater interchain interactions. This reduces the band gap and increases the hole mobility greatly and makes just the regioregular version of P3HT interesting for the application of photovoltaics. However, also RR-P3HT consists partially of an amorphous phase [94] making it interesting to understand the amorphous rra-P3HT as well.
RR-P3HT (445703) purchased from Sigma Aldrich [89] Regioregularity: >90 %,
rra-P3HT (510823) purchased from Sigma Aldrich [89]

2.5.3 Poly(9,9-dioctylfluorene) (PFO)

Formula: $(C_{29}H_{41})n$

Poly(9,9-dioctylfluorene) (PFO or PF8, structure in figure 2.9) is a blue

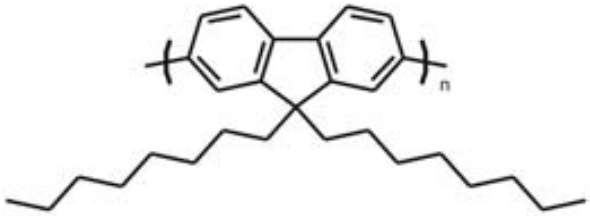

Figure 2.9: Chemical structure of Poly(9,9-dioctylfluorene) (PFO)

light-emitting conjugated polymer attracting attention because of its thermotropic liquid crystallinity at high temperatures [95] and because of its high PL efficiency, high charge carrier mobility and good processibility [96]. These traits make it a good material for organic light-emitting diodes (OLEDs). The properties of polyfluorenes depend strongly on the choice of sidechains which make the polymer soluble in many solvents but also provoke steric effects, pushing the monomers out of coplanarity.

PFO has at least three conformational phases. The α-conformation (torsion angle 135°) and γ-conformation (torsion angle 155°) and the nearly planar β-conformation or -phase (torsion angle 165°)[97]. While the torsion angle of the former two is a statistical value, the β-phase exhibits just one conformation. The higher planarity of this β-phase leads to a higher conjugation length and thus a lowering of the gap of the HOMO-LUMO transition [98]. As a result, excitons get trapped in the β-phase and most of the PL emission occurs from there even though it is a minority constituent [99] (compare also section 2.3.1).

For nearly all experiments the PFO samples were kindly provided by the groups of Prof. Jenny Nelson and Prof. Donal Bradley from Imperial College London. In the other cases, the PFO powder was provided by Sigma Aldrich (571652) [89].

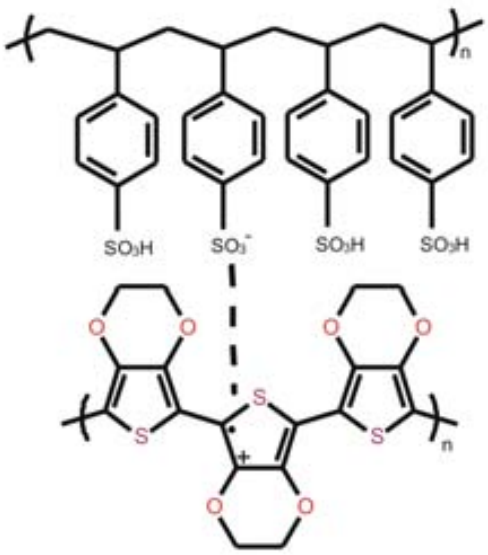

Figure 2.10: Structure of PEDOT (bottom) and PSS (top). The PSS compensates the charges in PEDOT. (according to ref. [100])

2.5.4 Poly(3,4-ethylenedioxythiophene) poly(styrenesulfonic acid) (PEDOT:PSS)

Poly(3,4-ethylenedioxythiophene) (PEDOT) and poly(styrenesulfonate) (PSS) (figure 2.10) form a PEDOT:PSS complex. PSS serves as the negatively charged counterion of the hole conducting PEDOT [100]. PEDOT:PSS is used for antistatic and conductive coatings. In organic solar cells and organic light-emitting diodes it serves also as an injection layer [101]. Because of the water solubility of PSS, PEDOT:PSS can be dispersed well in water from which it can be directly spin coated. The low solubility in common solvents for other polymers like chlorobenzene make it very attractive for the fabrication of multilayer devices from solution. For this work it was used as a sacrificial layer in the lift-off procedure of the thin films (see chapter 3.1).

PEDOT:PSS in aqueous dispersion was obtained from Heraeus under the name Clevios P Jet HC.

"This is indeed a mystery," I remarked. "What do you imagine that it means?"
"I have no data yet. It is a capital mistake to theorize before one has data. Insensibly one begins to twist facts to suit theories, instead of theories to suit facts."

Arthur Conan Doyle, **The Adventures of Sherlock Holmes: A Scandal in Bohemia**

3 Experimental Details

3.1 Preparation of samples by spin coating

All samples were prepared by spin coating in order to obtain well defined and reproducible thin films. Spin coating is a simple technique to achieve homogeneous thin films from solution. For this an excess amount of a solution is spread over the whole substrate. The substrate is then spun with a certain rotation speed for a certain time. The centrifugal forces push the liquid towards and beyond the edges of the substrate leaving a relatively thin liquid film behind. The remaining liquid evaporates (usually during the rotation process) resulting in the desired solid thin film. The parameters do not only determine the thickness of the sample, but also the time given to the molecules to reorganise and/or phase separate before the solvent evaporates. In this work usually chlorobenzene was used as a solvent for P3HT and PCBM. Toluene was used for PFO, and PEDOT:PSS was spin coated from an aqueous dispersion.

To prepare the substrates for spin coating, microscope glass slides were fragmented into roughly 25 mm by 25 mm square pieces. They were carefully scrubbed with soap and water in a first step and then sonicated in acetone and subsequently in isopropanol each for at least 15 min. The isopropanol

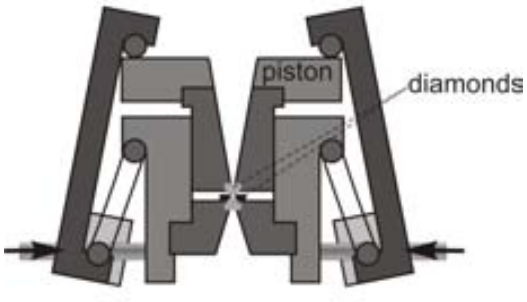

Figure 3.1: Sketch of the diamond anvil pressure cell. The cell is made out of two parts each with a diamond. The pressure is applied via the two levers.

was then blown to the edges and dried with nitrogen to prevent the deposition of unwanted solid substances in the solution ("dirt") in the isopropanol ("coffee-stain effect"). Before spin coating of PEDOT:PSS the samples were left for approx. 10 min inside a UV-oven in order to make the surface more hydrophilic. This increases the wetting of the substrate with the PEDOT:PSS dispersion considerably and facilitates the spin coating. This step had to be performed just before the spin coating of the PEDOT:PSS, for after about 30 min the hydrophilic characteristic of the substrate is slowly lost again. PEDOT:PSS was usually spin coated with 1500 rpm (rounds per minute) for 90 s and put afterwards for about 10 min on a hot stove at approx. 370 K (100 °C).

The P3HT samples (pure and blends) were usually spin coated from a solution with 20 g/l (referring to polymer concentration for blends) with 2000 rpm for 90 s to 120 s without any post-processing. Unless otherwise stated, the samples were produced with these parameters.

3.2 The diamond anvil cell

In order to apply hydrostatic pressure, a so-called diamond anvil (pressure) cell (DAC) was used (sketch in figure 3.1) [102]. In this setup the sample resides in a hole of a metal gasket, which is closed on each side by the flat face of a diamond. In order for the pressure to be hydrostatic (i.e. without shear stress) an adequate pressure medium is necessary, which has to be

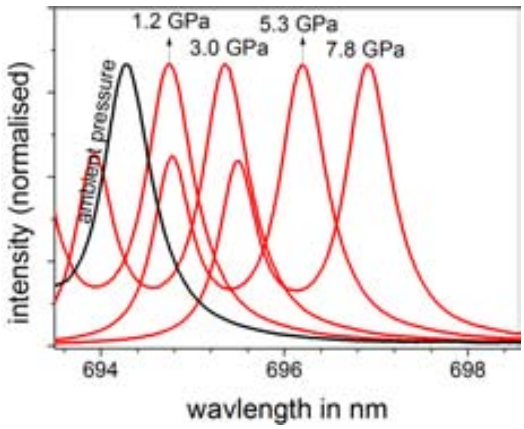

Figure 3.2: Representative examples of the shift of the ruby emission peaks with hydrostatic pressure used for the determination of the pressure; according to reference [104]

chosen according to the sample and type of measurement. The pressure transmitting medium was in nearly all cases a 4:1 methanol/ethanol mixture, which is a very common pressure medium for room temperature experiments. It stays liquid up to at least 10.4 GPa [103]. In one experiment, Helium was filled into the pressure cell, which is a more costly procedure but ensures that no chemical reaction occurs with the sample, which can be an issue for polymers under intense illumination. To increase the pressure the diamonds are mechanically pressed towards each other deforming the metal gasket in the process and applying pressure to it and, through the liquid, ultimately to the sample itself. With this setup, pressures up to 25 GPa can be reached, though we usually did not exceed 10 GPa in the experiments.

For the loading of the pressure cell with the sample, first, the gasket is indented by the diamonds to around 100 µm thickness and subsequently a hole is drilled either mechanically or with an electro-discharge-machine (easyLab Boehler microDriller). The hole diameter is usually between 150 µm and 300 µm. Then, the sample and a ruby ball are placed on any of the faces of the diamonds. The hole in the gasket, residing on the lower diamond, is filled with methanol/ethanol. The pressure cell is quickly closed trapping the liquid and the sample between the diamonds.

To calibrate the pressure in the DAC, ruby spheres were used according

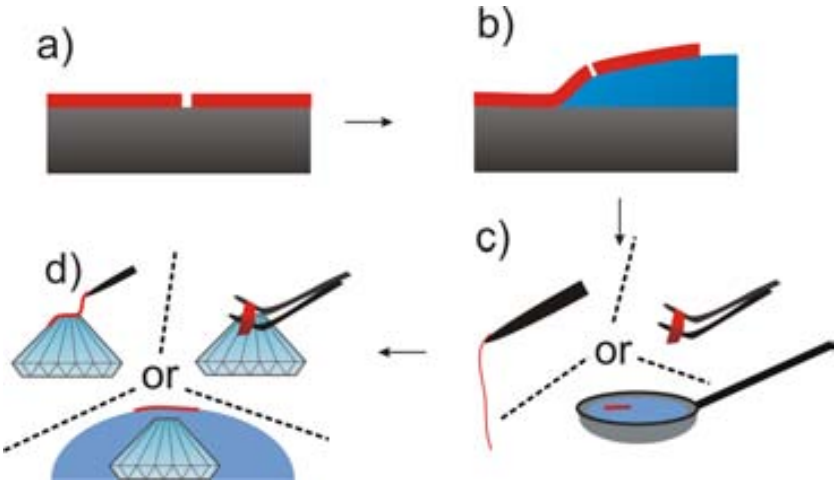

Figure 3.3: Sketch of the different steps of loading the pressure cell with the polymer sample. a) the film is cut into small pieces, b) a liquid is used so that the polymer detaches from the glass, c) the polymer is lifted from the glass, d) the polymer is put on the diamond face

to the ruby calibration by Mao et al. [104]. The PL of the ruby consists of a double peak in the red region of the spectrum as can be seen for one of our measurements in figure 3.2. The one at higher wavelength (at approx. 694.25 nm at ambient pressure and room temperature) is well characterised for its behaviour under hydrostatic pressure and shows an almost linear rigid shift towards higher wavelength of roughly 0.35 nm/GPa. Thus, for each pressure, the sample and the PL of the ruby have to be measured in order to connect the PL measurement to the inferred pressure.

The diamonds have a very high transmission for visible light and a very low photoluminescence. Therefore, the sample is accessible for optical measurements such as photoluminescence, Raman measurements and absorption measurements with very little disturbing influence of the diamonds themselves. For Raman measurements the diamond does, however, produce a strong Raman peak (see chapter 3.3) at about 165.3 meV (1333 cm^{-1}), which might make the observation of some Raman peaks impossible as this peak lies close to the peaks of organic materials that are to be investigated. This is unfortunately the case for PFO. The most pronounced peaks for P3HT, however, are at higher energies than 171 meV and are not affected.

3.2.1 Preparation of a sample for the pressure cell

The introduction of the sample into the pressure cell was not straightforward. For this reason it will be stated here in greater detail what problems arose and how they were solved or circumvented. The procedure of getting the thin film from the glass slide onto the face of one diamond is depicted in the drawings of figure 3.3. The polymer is usually precut to get a small piece which later can be put on top of a diamond (drawing (a) in figure 3.3) Usually a liquid is necessary for the lift-off. The liquid can go between the polymer and the substrate by capillary forces, and the surface tension pulls uniformly at the edges lifting the polymer off the substrate (drawing (b) in figure 3.3). This can be done either with a drop (e.g. ethanol or water) or by putting the glass slide with the polymer at a low angle into a recipient (e.g. a petri[1] dish) and fill it up very slowly (one drop at a time) with water. With the latter technique the film can also be lifted as a whole, but cutting the film while it floats would then be a challenge of its own.

After the lift-off one of the floating polymer pieces has to be introduced into the pressure cell. This was often just done with a needle (see drawing (c) in figure 3.3). For this a slightly elongated piece was "fished" out of the liquid from the long end, so that the polymer stuck to the tip of the needle but hung freely from it. (Note that the film sometimes folded up in case of very thin samples.) The free end of the polymer could then be put on top of one of the diamonds (in the experiments, the piston-side for the pressure cell, see drawing (d) in figure 3.3). A bit of liquid on the diamond can assist the polymer to unfold again, so that just a single layer is put on the diamond. Alternatively, tweezers (with a stopper to fix the spacing) can be used, so that the polymer does not fold up. It is also a good method for samples which easily break (PCBM), but one has to pay attention not to stretch the polymer film and thus change its properties.

As the biggest problem in the lifting process is the polymer sticking firmly to the tweezers or needle, it was tried successfully to do the transfer to the

[1] Julius Richard Petri (1853, Barmen, German Confederation (today's Wuppertal, Germany) - 1921, Zeitz, Germany)

diamond “contactless”. For this method the swimming sample was scooped up with a little spoon together with the water around it. The polymer was thus still freely floating. A drop of water was put around the diamond and the spoon was emptied in this drop together with the sample. After finding the sample again, which can be surprisingly difficult, one just needs to push it gently in a position over the diamond face and suck up all the liquid with a tissue resulting in the film touching down on the diamond face. As the film is not folded or pulled at during the transfer, it is probably the least damaging transfer method and always results in a single layer of the polymer on the diamond.

The biggest problem of this method is to get the sample off the glass slide used for the spin coating. Usually the polymer sticks relentlessly to the glass slide and the options of getting it off without destroying the film are very limited. The cutting can introduce the additional problem that one squeezes the polymer onto the glass along these lines, making it even harder to get any piece off. The thin polymer films are so ductile that pushing the polymer off the sample with a blade only folded it up and it stuck then to the blade. PFO is not very sticky and in the form of a thick film is also more rigid than thin films, and it was therefore easy to transfer the PFO film into the pressure cell in the described manner. For P3HT no way was found to lift P3HT off the glass. Sonicating the sample destroyed it, cooling it under the glass temperature in order to make the polymer more brittle (to prevent folding and lessen its stickiness) showed no effect.

For these challenging P3HT and PCBM samples a PEDOT:PSS sacrificial layer was spin coated first on the glass slide as described in chapter 3.1. The layer is insoluble in chlorobenzene and thus the subsequent spin coating of P3HT or PCBM in chlorobenzene is not expected to affect the PEDOT:PSS underneath. The PEDOT:PSS layer was used to assist the lift-off in a water bath, which worked perfectly even for precut samples. However, PEDOT:PSS forms a dispersion in water and isopropanol, and PEDOT:PSS is not actually solved in the water bath. As will be seen in the presentation of the results, PEDOT:PSS remained stuck to the sample even with the help of some isopropanol and a short treatment in an ultrasonic bath. This method

is therefore not perfect but was the best compromise for the presented challenge.

For all methods involving water one should carefully remove all water and allow enough time for drying, preferably in a desiccator, before closing the pressure cell.

3.3 Raman scattering

The Smekal-Raman[2] effect describes the inelastic scattering of a photon under the emission or annihilation of phonons. Apart from elastic scattering (Rayleigh[3]-scattering) the photon can also lose energy and create a phonon/phonons (Stokes-shift) or gain energy from a phonon/phonons (Anti-Stokes-shift). Raman scattering is not an absorption-emission process as the light does not need to promote an electron to an excited eigenstate, but it is sufficient that the light distorts the electron cloud while passing by, bringing the molecule to a higher energetic state (which is often called "virtual state") [105]. In this picture, Rayleigh scattering happens when the electron cloud relaxes elastically to the ground state whereas in Raman scattering the nuclei move, thus gaining or losing energy to the scattered light [105]. The energy shift is a measure of the phonon energies of the system and usually does not depend on the used laser light (with seeming exceptions when selected parts of the sample dominate the spectrum because of resonance Raman scattering [106–108]). Not all vibrations are accessible with Raman scattering but only those which change the polarisability with the movement of the nuclei. Since the energy changes are very small and the Rayleigh-scattering intensity high (about $10^6 - 10^8$ times higher than Raman scattering), the Rayleigh scattered light has to be suppressed (e.g. by edge filters) in order to observe the Raman peaks.

For the measurements a Jobin Yvon LabRam HR 800 system with two

[2]Adolph Gustav Stephan Smekal (1895, Wien - 1959, Graz); Chandrasekhara Venkata Raman (1888, Tiruchirappalli, India - 1970, Bangalore)

[3]John William Strutt, 3rd Baron Rayleigh, (1842, Langford Grove, England - 1919, Witham)

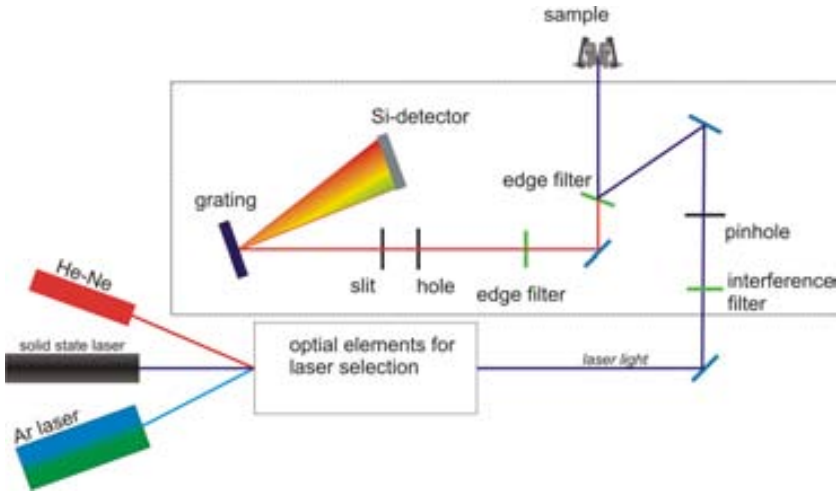

Figure 3.4: Sketch of the set-up for the Raman measurements. The light from one of the lasers is focused on the sample and the scattered light is then detected by a cooled Si charge couple device (CCD).

holographic edge filters and a liquid nitrogen cooled silicon charge couple device (CCD) detector was used. As edge filters are approximate low-pass filters only the Stokes-shift is accessible with this set-up. In figure 3.4 a sketch of the set-up and the path of the laser and scattered light is shown. Four different wavelengths from three lasers are available for Raman Spectroscopy: 2.54 eV (488 nm) and 2.41 eV (514 nm) from an argon laser, 1.96 eV (633 nm) from a Helium-Neon laser and (not shown) 1.58 eV (785 nm) from a solid state laser. Additionally, there is a solid state laser with an emission at 3.06 eV (405 nm). The light from the laser is reflected by an edge filter and focused by a confocal microscope on the sample. The scattered light is reflected into a spectrometer after being filtered by two edge filters to suppress the Rayleigh scattered light.

Usually very low light powers (for the 2.41 eV line of the Ar laser around 100 µW for PL, around 1 mW for Raman) were used in order not to damage the sensitive organic samples. In all pressure measurements and most of the others a 20x objective was used which gives a spot size of a few micrometres. The sample was measured either in the pressure cell, in vacuum in a cryostat or under a nitrogen atmosphere so as to prevent photooxidation as much as possible.

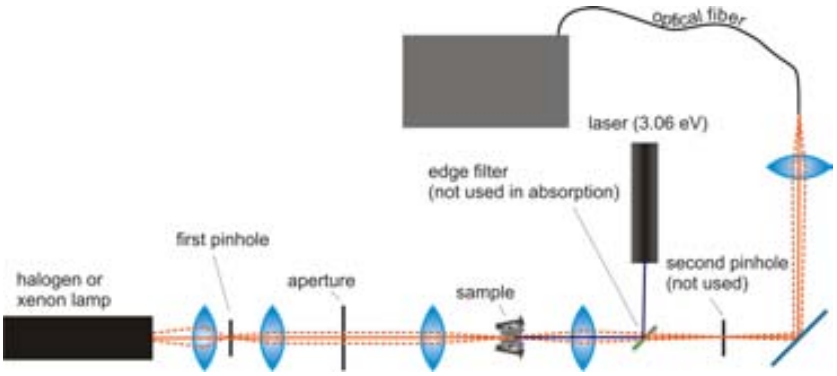

Figure 3.5: Sketch of the lab used for absorption measurements under pressure and some PL measurements.

3.4 Photoluminescence and absorption

In PL measurements a laser excites the sample and the resulting photon emission is measured usually in a backscattering configuration. The laser energy has to be chosen according to the absorption of the material but in general does not influence the resulting shape of the PL spectrum very much as the exciton relaxes after the absorption to a low energy state (see chapter 2.3.1).

The PL measurements were performed in two different set-ups. One was the Raman set-up described in the previous section and shown in figure 3.4. In order to measure the whole visible spectrum, several measurements have to be taken and stitched together, which is automatically done by the measurement software. The advantage of this set-up was that many lasers were available and the horizontal fixation of the sample on a stage or microscopic table, which facilitates the measurement with a cryostat under vacuum conditions and at low temperatures as well as the measurement in a nitrogen atmosphere. The disadvantage of the system is that the stitching of the different measurements does not work perfectly and sometimes introduces small peaks in the transition zone between two measurement windows.

A sketch of the other set-up is depicted in figure 3.5. It has just one solid state laser (3.06 eV). The light from the laser is coupled into the system by a dielectric filter, which reflects the laser light but lets through the emitted

light at longer wavelengths. The emitted light is focused into a glass fiber which leads to a single grating spectrometer with a Peltier[4] cooled silicon CCD-detector. The measurement of a spectrum consists also of a series of windows, which are not changed by the measurement software (no automatic stitching of the spectra).

For absorption measurements, the light emitted by a halogen or a Xe lamp (6263 75W Xe Ozone free) is measured in transmission once through the sample and once without a sample as a reference. For this, the light is transmitted through a pinhole, which is projected onto the sample and focused by the next lens onto a second pinhole. That pinhole should be of equal size or smaller than the image of the first pinhole in order to just select the direct light ray. That light is then coupled into the glass fiber. The second pinhole, however, was not used in the measurements, for it introduced a change in the form of the measured spectrum because of chromatic aberration.

For measurements of P3HT, the halogen lamp was preferred, as the spectrum of the Xe lamp has many disturbing high intensity peaks, especially below 1.6 eV. But as the Xe lamp has a higher intensity for high energies (noticeably over 2.5 eV it was used for measurements of PFO and PCBM.

A SOPRA GES5E ellipsometer was also used for transmission measurements with solutions and on glass slides under ambient conditions. It uses a Xe lamp and records the spectra with a CCD. The measurements were performed in air in a clean room.

3.5 Ellipsometry

Ellipsometry is a technique that measures the polarisation changes of light upon reflection on a sample. This can be used to gain insight into the properties of the sample such as composition, film thickness and the complex refractive index. Typically, linearly polarised light from a wideband light source is reflected for a well defined incident angle at the sample, resulting,

[4]Jean Charles Athanase Peltier (1785, Ham, France - 1845, Paris)

in the most general case, in elliptically polarised light, hence the name *ellipsometry*. The reflected light intensity is measured after passing through a rotating linear polariser (analiser). This makes it possible to obtain the parameters Ψ and Δ, which describe the ellipsis of the electric field vectors of the reflected light. From this the complex ratio ρ of the reflected light intensities for p-polarised light, r_p, and s-polarised light[5], r_s, can also be obtained. The relation between these parameters is described by

$$\rho \equiv \frac{r_p}{r_s} = \tan(\Psi)\exp(i\Delta).$$

Ψ and Δ form the actual raw data that is obtained in an ellipsometric measurement. Only in the case of a isotropic, homogeneous semi-infinite sample does an analytical relation to the complex refractive index $\tilde{n} = n + i\kappa$ exist (κ is called extinction coefficient). In all the other cases, an inversed method is used, for which a layer-model of the sample has to be designed to calculate the theoretical Ψ and Δ values as a function of the angle and the energy (wavelength). The parameters of the model are then iteratively modified until the best fit is achieved.

In the performed measurements, a CCD detector records the whole optical spectrum from about 1.2 eV to 5.6 eV. The measurement is usually repeated for multiple angles in order to enhance the accuracy of the results[109]. These so-called variable angle spectroscopic ellipsometry (VASE) measurements were performed with a SOPRA GES5E rotating polariser ellipsometer and a Xe lamp as a light source in a clean room.

[5] s stands for *senkrecht* meaning perpendicular in english, p stands for parallel. They refer to the polarisation of the electric field with respect to the plane of incidence, which is spanned by the normal of the sample surface and the incident light ray.

Algernon: "I hear her hair has turned quite gold from grief."
Lady Bracknell: "It certainly has changed its colour. From what cause I, of course, cannot say."

Oscar Wilde, **The Importance of Being Earnest**

4

Planarity and dielectric constant: PFO

In this chapter the measurements with poly(9,9-dioctylfluorene) (PFO) are discussed. The purpose of the investigation of PFO was to elucidate the role of planarity and the refractive index on the optical properties. This was done by the measurement of the absorption and photoluminescence (PL) of PFO films under hydrostatic pressure. Especially the red-shift of the absorption and PL under hydrostatic pressure is discussed. The main parameters which are used to explain the changes in the absorption and emission energy of the polymer are i) bond length, ii) the molecular conformation influencing bends and torsion between monomers, iii) interchain interactions and iv) the dielectric environment. This has been described in greater detail in chapter 2.4.1.

As described in chapter 2.5.3, PFO has different conformations with different planarity of the backbone. We investigated two samples of PFO, which we received from our collaborators at Imperial College London. One contained only the glassy phase of PFO and the other additionally the β-phase and is thus termed glassy+β sample. Glassy refers to the α phase, which has a higher conformational disorder with high torsion angles (around 135°) [98]. As will be seen, the γ phase, which refers to conformations with a torsion

angle around 155°, plays no role for these samples. It usually appears just through thermal cycling at around 420 K [110] . Higher planarity of the β-phase results in a higher conjugation length and thus a lower gap of the HOMO-LUMO transition than in the glassy phase. As a result, excitons get trapped in the β-phase and most of the PL emission occurs from there even though it is a minority constituent [111, 112]. This enables to compare the high pressure changes of both phases unambiguously by measuring the PL for both samples.

In order to discuss the influence of the dielectric environment on these absorption and PL spectra, the refractive index of PFO under pressure was determined with an interferometric method. The light passing through the diamond anvil cell (DAC) in the transmission measurements gets reflected multiple times between present interfaces, which is called a Fabry-Pérot[1] etalon. The reflections lead to an interference pattern in the spectrum. The interference pattern in the spectrum is dominated by the reflections between the diamond faces and the reflections inside the sample. But as the former has a much higher frequency they are easily distinguishable. An analysis of the interference maxima allows for the determination of the optical path of the PFO film (for the wavelengths of the maxima) and ultimately also of the refractive index. As the film has to be several micrometres thick in order to get many interference maxima, the film has to be clear and highly transparent. PFO is transparent in most of the visible spectrum and the scattering inside the sample was minimised by the novel sample preparation method used at Imperial College London. Not only could they control well the formation of the β-phase but also suppress the formation of crystallites in both the purely glassy sample and the glassy+β sample [113], which can act as scattering centres. This makes this the ideal polymer for both investigations.

[1]Maurice Paul Auguste Charles Fabry (1867, Marseille, France - 1945, Paris); Jean-Baptiste Alfred Pérot (1863, Metz, France - 1925, Paris)

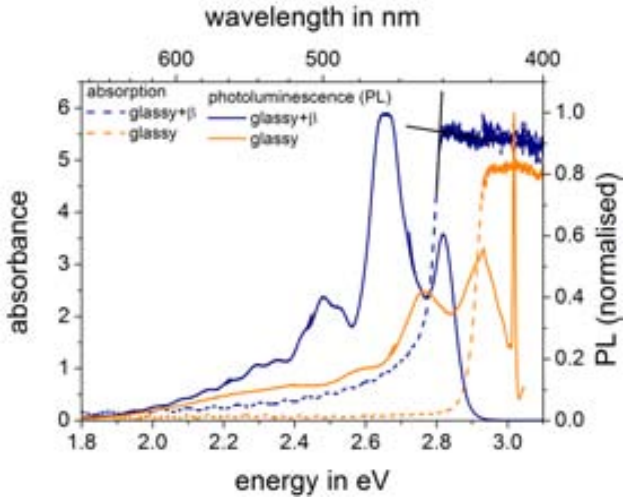

Figure 4.1: Photoluminescence and absorbance spectra for the glassy and the glassy+β sample at ambient pressure. The intersection of the straight lines (for glassy+β sample) show how the position of the absorption onset was determined.

4.1 At ambient pressure

Figure 4.1 shows the absorbance and PL spectra of both the glassy sample and the glassy+β sample for ambient pressure after spin coating. The absorbance spectra show a sharp increase at high energies above which virtually no light passes through the samples, as they are much thicker ($\approx 3\,\mu m$) than the penetration depth ($\lessapprox 200\,nm$). This absorption onset is formed by the 0-0 Franck-Condon transition, during which an electron is lifted from the HOMO- to the LUMO-level forming an exciton in PFO. The 0-1 and higher vibrational transitions, for which additionally phonons are created, lie at higher energies and influence these spectra only marginally. The absorption onset of the glassy+β sample is at lower energies than the glassy sample because of the absorption due to the β-phase [98]. Additionally, one can see an interference pattern in the transparent region caused by the Fabry-Pérot etalon of the PFO film. We will come back to the analysis of this pattern later for the determination of the refractive index. The PL spectra exhibit several well defined peaks due to Franck-Condon transitions (though some of them at longer wavelengths are again caused by the etalon). The

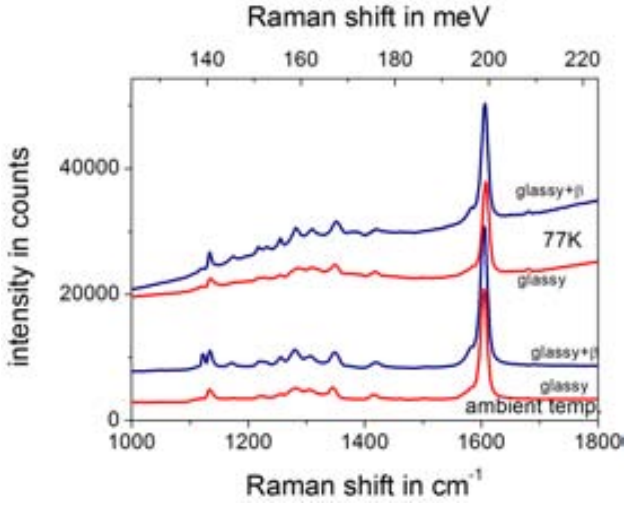

Figure 4.2: Examples for Raman measurements of PFO at ambient temperature and at 77 K.

0-0 peaks are approximately at 2.93 eV (423 nm) for the glassy sample and 2.82 eV (440 nm) for the glassy+β sample, which is indicative for the presence of the β-phase [99]. The spectra show that the glassy sample consists of pure α-phase, for no peaks attributable to the γ-phase or β-phase can be observed [97]. The Franck-Condon peaks from the glassy phase in the PL of the glassy+β sample are low in intensity or missing altogether as most excitons will be trapped in the low energy β-phase and decay there. The 0-0 PL peak lies within the absorption region, which leads to a smaller or even slightly cut (glassy sample) emission peak caused by self-absorption. The emitted photons from the 0-0 transition stem thus most probably from the surface of the sample, while the other transition peaks can stem also from parts deeper inside the sample.

For the fit of the PL spectra, it is conducive to know more about the phonons which couple to the electronic states. For this the vibrational Raman spectra of the samples were measured under vacuum conditions in a cryostat from ambient temperatures down to 77 K. In figure 4.2 the Raman spectra for both the glassy sample and the glassy+β sample are shown. Both samples have a very similar spectrum with very similar intensities of the Raman peaks. The spectrum exhibits very prominently a peak at 199 meV and a

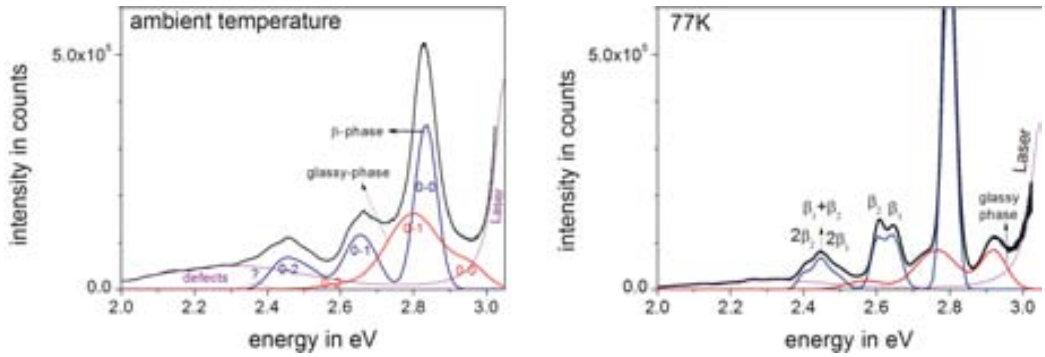

Figure 4.3: PL of the glassy+β PFO sample in a cryostat at ambient temperature and at 77 K both with fits of the Franck-Condon emission.

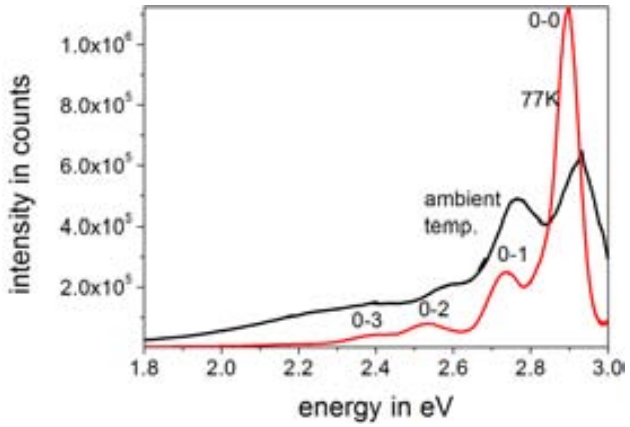

Figure 4.4: PL of the glassy PFO sample in a cryostat at ambient temperature and at 77 K

group of peaks at around 150 meV to 170 meV. The former was assigned to a symmetric ring stretching mode and the latter modes are connected to C-C stretching modes between the phenyl rings both in the same monomer and connecting two monomers [64, 114]. With lower temperatures a small shift of approx. 0.3 meV to 0.4 meV to higher energies is observed, but otherwise the Raman spectra remain mostly unchanged.

In figure 4.3 the PL emission of the glassy+β sample for ambient temperatures and 77 K are shown together with fits of the spectra. In figure 4.4 the PL emission of the glassy phase is shown at ambient temperature and at 77 K. The most obvious change in these spectra is the narrowing of the emission peaks, which in the glassy+β sample reveals a fine emission structure.

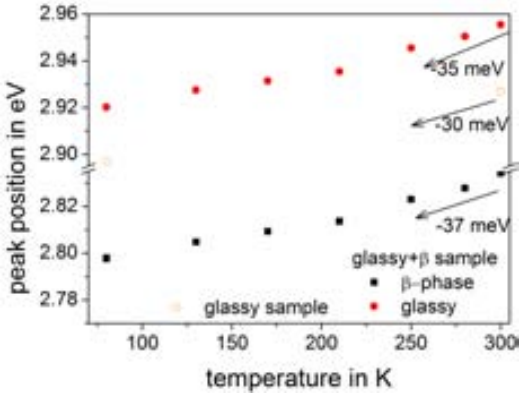

Figure 4.5: 0-0 emission peak position versus temperature for the glassy+β sample (for both the glassy and the β-phase) and the glassy sample.

The same emission is probably also present in the glassy sample, but cannot be resolved because of the broader distribution of conjugation lengths, which smears out the emission spectrum. The disorder of the torsion angle between monomers, which causes the distribution of conjugation lengths, is to a certain degree frozen-in. However, the torsional disorder is also temperature dependent. The narrowing of the emission peaks can be explained with the freezing out of the torsions of the backbone [39]. This increases the order in the polymer backbone and thus leads to a narrower energy distribution [115, 116].

For the glassy+β sample, a very good fit could be achieved, for which two Franck-Condon series were used, one for the β-phase and one for the glassy phase emission. Especially at 77 K the emission peaks from the glassy phase can be unambiguously identified in the spectrum. Probably some excitons get trapped in a low energy region of the glassy phase. It could also be an indication that bigger areas without β-phase exist in the sample so that they lie outside the diffusion length of some excitons created in the glassy phase. As the diffusion between chromophores of similar energy is assisted by thermal energy [117], this is more likely to happen at low temperatures. For the spacing between the emission peaks two main branches of the phonon spectrum are responsible. They stem from the just-mentioned stretching modes, and the best fit was achieved with an energy of 157 meV for the β_1

branch (C-C stretching modes) and 199 meV for the β_2 branch (symmetric ring stretching mode). Accordingly, the 0-1 peak is split into two peaks and the 0-2 in three peaks, for additional to the $2\beta_1$ and $2\beta_2$ peak also the combination $\beta_1 + \beta_2$ exhibits a peak. Higher orders cannot be distinguished in the spectra because of the low intensity and the disturbing interference peaks from the Fabry-Pérot etalon.

The position of the 0-0 emission peaks of the glassy and the glassy+β sample extracted from the fits is plotted versus the temperature in figure 4.5. All peaks shift approx. 30 meV to 40 meV to lower energies. Campoy-Quiles et al. estimated the expansion coefficient for PFO below the glass temperature to be approx. $1.5 \times 10^{-5}\,\mathrm{K}^{-1}$ [118]. This was not measured at cryogenic temperatures but for polymers the expansion coefficient is very little temperature-dependent for temperatures above 70 K [119]. With a temperature change of approx. 210 K this results in a 0.3 % thickness change and an approximate red-shift per thickness change between $10.7\,\mathrm{nm\,nm^{-1}}$ eV and $12.3\,\mathrm{nm\,nm^{-1}}$ eV. It will be shown later that that this is about four times the value obtained from pressure experiments. The density change with temperature is similar to what happens at low hydrostatic pressure. But while in pressure experiments the external force pushes the still vividly-moving polymer chains together, at cooling the polymer film, the rotations of the backbone are frozen out and the van-der-Waals forces can attract the polymer chains more efficiently without their movements. The pressure necessary to evoke the same thickness change in the PFO film as by the temperature is below 0.1 GPa. The results suggest that not the intermolecular distance (film thickness) is the important parameter for the red-shift but the molecular conformation, i.e. an increased planarity of the molecules, as otherwise a similar thickness change would have resulted in a similar slope for the red-shift.

Note here that in other examples a shift to higher energies is expected for cooling as has been calculated by Guha et al. [60]. This is connected with a change in the torsion potential of the molecule, which is W-shaped (the local maximum of the W being 0° torsion angle - the planar molecule). In this case, the molecules assume at low temperature a torsion angle in one of the two W-minima, while at elevated temperatures the local maximum and thus a

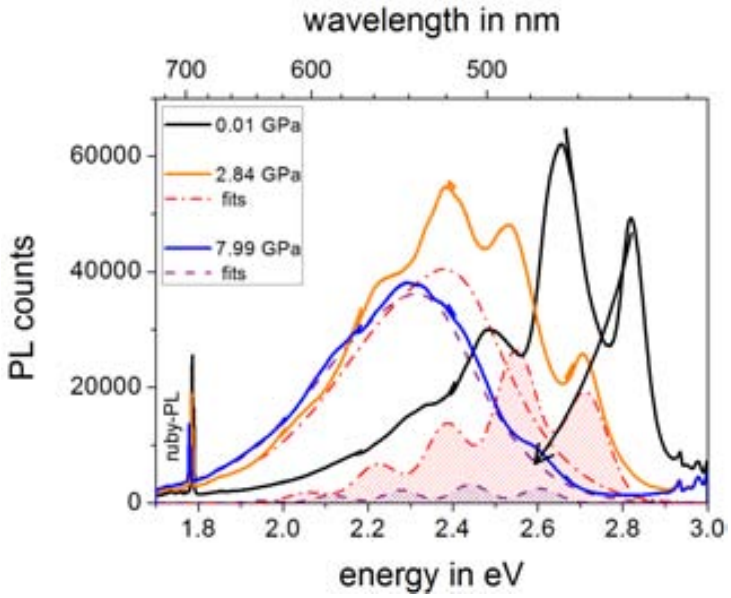

Figure 4.6: Representative spectra of the PL of the glassy+β sample under high pressure (solid lines) and their fits (broken lines). The curves with the striped area underneath represent the Franck-Condon emission fit and the other one the background emission due to defects and excimers. The arrow on the right is a guide to the eye for the shift of the 0-0 emission peak.

more planar conformation can be reached. However, these calculations were done for polymers without any sidechains [60, 67] and the torsion potential is qualitatively very different when steric effects of sidechains are introduced into the system. This is not only an important difference for these low temperature experiments but also for the high pressure experiments for which in Guha's model (without sidechains) also a planarisation under pressure occurs. This will be discussed in the following section.

4.2 PL and absorption under pressure

Figure 4.6 shows representative PL spectra of the glassy+β sample under hydrostatic pressure together with the fits. The Franck-Condon peaks red-shift and get quenched. Additionally, a strong background emission, often called "green band" [120, 121], appears under pressure, which is believed

to stem from structural defects (keto-defect) and excimer emission in the polymer [41, 64, 121]. In order to determine the energy of the transitions in PFO, a Franck-Condon series was fitted with 5 Gaussian[2] curves (for the 0-0 to 0-4 transitions) with a fixed spacing. As the two main branches of 199 meV and approx. 157 meV are smeared out and not always easily observed at high pressures, the PL spectra were fitted with an effective phonon energy of around 182 meV for the glassy and 163 meV for the glassy+β sample. The background emission was taken into account for the fit as well. For this purpose the form of the background emission was modeled for the PL spectrum at the highest pressure, for which the Franck-Condon emission is virtually entirely quenched. For all the fits this background curve was allowed to shift in energy and change in intensity maintaining its shape. This model allowed for very good fits of the experimental spectra over the whole pressure range and gave additional information about the changes of the background emission under pressure.

The fits in figure 4.6 clearly show that the Franck-Condon peaks strongly decrease in intensity while the background emission increases very fast. Within 0.5 GPa the background signal reaches its maximal intensity. As mentioned, quenching of the Franck-Condon type PL under pressure is a common phenomenon amongst organic molecules. One possible reason for this behaviour is a decrease in the oscillator strength of the Franck-Condon type emission, which results in other decay channels taking over. The strong increase in the defect/excimer emission, however, is probably mainly caused by the higher exciton mobility at smaller intermolecular distances, which increases the likelihood of the excitons being trapped at the keto-defects [64]. Additionally, the background emission may increase in intensity as excimer emission becomes more efficient at smaller interchain distances [37]. Therefore, the increase in the defect/excimer emission is a good indicator for increased interchain interaction. It is also interesting to note that the defect/excimer emission shifts under pressure to lower energies, though clearly less than the Franck-Condon emission. While it is difficult to extract exact numbers for the shift from the fit, we can at least roughly estimate that

[2] Johann Carl Friedrich Gauß(1777, Braunschweig, Germany - 1855, Göttingen)

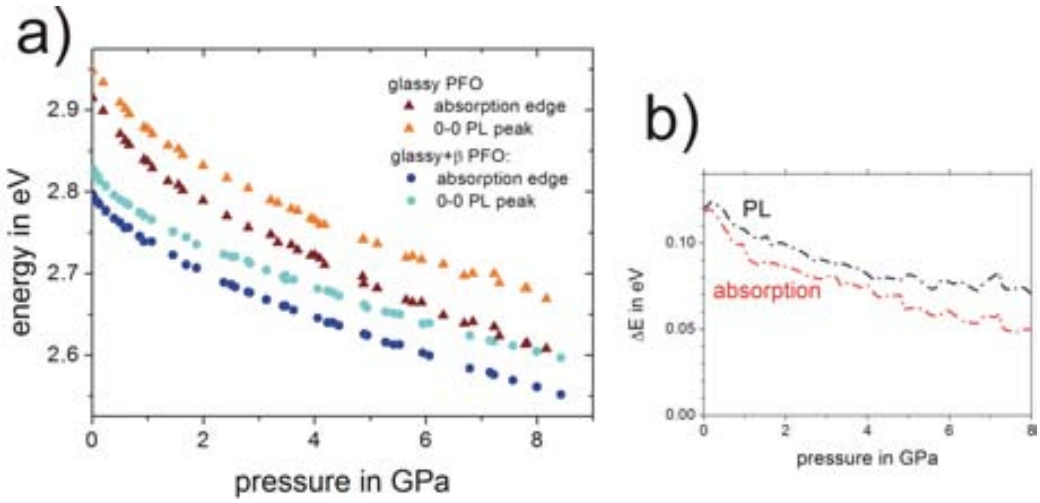

Figure 4.7: a) 0-0 emission peak position and absorption onset energy for the glassy and the glassy+β sample under hydrostatic presure; b) the energy difference between both emission peaks and both absorption onsets, which is connected to the energy change caused by planarisation

the maximum of the background emission red-shifts from 2.48 eV for ambient pressure (in accordance with ref. [121] for a low concentration of keto-defects) by approx. 140 meV to 180 meV up to 8 GPa.

Figure 4.7 shows the result of the fit of the PL spectra and of the determination of the absorption onset for the glassy and the glassy+β sample. One should note that the absorption onset is not the centre of the 0-0 absorption peak but lies at slightly lower energies. It was determined by the intersection of two straight lines marking the saturated absorption and slope as shown for ambient pressure in figure 4.1. The samples exhibit a very strong red-shift for both absorption and PL over the whole pressure range. The PL spectrum at a pressure of about 8 GPa for the glassy sample appears approx. 275 meV shifted towards lower energies as compared to ambient pressure; for the glassy+β sample approx. 225 meV. The shift of the absorption onset, especially for the glassy+β sample, is very similar to the shift of the PL. The slightly stronger shift of the absorption onset compared to the 0-0 PL emission in the glassy sample is probably partly caused by the broadening of the peaks under pressure.

In the discussion about the possible causes of the observed shift, we shall

begin with the change in bond lengths ((i) in figure 2.6). According to reference [66] the red-shift caused when shortening the inter-ring bond length is roughly 50 meV/pm in poly(para-phenylene) (PPP), supposedly explaining solely the observed red-shift. However, according to other calculations of the same group, the oligomer para-terphenyl (3P) was shown to change the bond length just by approx. 0.18 pm/GPa [68] - much less than assumed for the caused red-shift. Combining the two papers one can estimate a shift of around 9 meV/GPa or 70 meV at 8 GPa for phenyl based compounds. Because of the similarity of the inter-ring bond of the calculated molecules and of PFO it stands to reason to assume that the order of magnitude is comparable for these molecules. The shift is even likely to be smaller in PFO as it consists of fewer of these soft inter-ring bonds between monomers than PPP. We conclude that the bond length change does contribute to a certain extent, but can hardly explain the magnitude of the total red-shift observed.

The second parameter likely to cause the red-shift is the planarisation ((ii) in figure 2.6). The β-phase is already at ambient conditions nearly planar and even if further planarisation occurs, the change in the conjugation length with respect to the already extended chains is probably a minor one. Therefore, the difference between the shift of the glassy sample and the shift of the glassy+β sample shows directly the red-shift caused by planarisation in the glassy phase.

Up to 8 GPa the glassy PL shifts roughly 50 meV more than the PL of the β-phase. With an upper limit of approx. 120 meV (difference of glassy-phase to β-phase emission at ambient pressure) this means that the molecule actually does not planarise completely. It is sometimes claimed that complete planarisation happens within 1 GPa to 2 GPa [60, 67, 122, 123], while the shift which we assign to planarisation is in fact very small in the first gigapascal and seems to contradict this assumption. This is in agreement with the observation of Paudel et al. [40]. It is possible that the sidechains which prevent a planarisation at ambient pressure also impede an efficient planarisation under high hydrostatic pressure. The major difference which causes the β-phase to be more planar than the glassy phase under ambient pressure is a different conformation of the sidechains [97], which is not likely

to change under pressure. Oligomers without sidechains, as in most examples for which planarisation under pressure has been suggested, might therefore behave quite differently under pressure, which reconciles the seeming contradiction.

4.3 Refractive index and interchain interaction under pressure

In order to estimate the effect of the dielectric environment on the red-shift ((iv) in figure 2.6), we need to determine first how this parameter changes. To achieve this, the interference pattern in the transmission measurement caused by the Fabry-Pérot etalon are analysed. The light passing through the diamond anvil cell gets reflected multiple times between present interfaces. For the analysis of the polymer refractive index, the reflections between the two polymer surfaces are important. The reflections lead to an interference pattern in the spectrum, which gives a maximum for

$$M\lambda_M = 2nd,$$

where λ_M is the wavelength of the maximum with index M, n the refractive index at λ_M and d the thickness of the film. In order to have many and well resolved maxima, the optical path has to be much longer than the wavelength of visible light, i.e. several micrometres.

In the transmission measurement, only λ_M is measured, but with the help of a known refractive index for ambient pressure (here measured with ellipsometry) one can determine the indexation M and the thickness d as well. As during the pressure changes the interference peaks move, one has to pay great attention not to lose the indexation. The remaining problem under pressure is that only the wavelength-dependent optical path nd is known for each pressure. So it is usually necessary to know how the thickness changes as well. While for many inorganic materials even the assumption of virtually no change in thickness might get a reasonable approximation, for soft matter one always has to take the thickness change into account. We will therefore

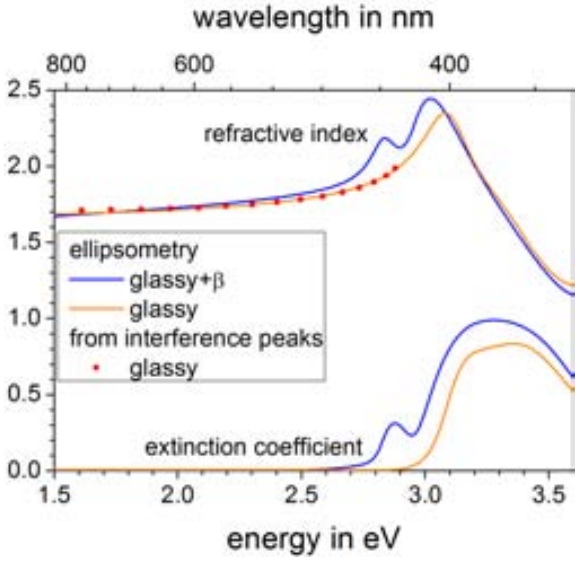

Figure 4.8: Refractive index and extinction coefficient for the glassy sample and the glassy+β sample as determined by ellipsometry. For the glassy sample the refractive index determined by the Fabry-Pérot analysis is shown as well.

first determine the optical path and then the thickness change.

In order to determine the optical path under high pressure the two samples were measured as a reference with ellipsometry under ambient pressure[3]. In figure 4.8 the resulting refractive index and the extinction coefficient for the glassy and the glassy+β sample are presented. The refractive index has an asymptotic behaviour for longer wavelengths, with virtually no difference between the two samples. The behaviour close to the band gap, on the other hand, is clearly different due to the additional β-phase in the glassy+β sample, which causes the small peak of the 0-0 absorption at 2.88 eV (430 nm) in the extinction coefficient and the corresponding increase in the refractive index of that sample. The difference in the extinction coefficient and in the refractive index are relatively small, showing that the β-phase is, as expected, a minority constituent.

For the measurement of the etalon interference maxima a glassy sample was used in order to get the widest possible transparent region. The glassy+β

[3]data from the same samples taken from reference [113]

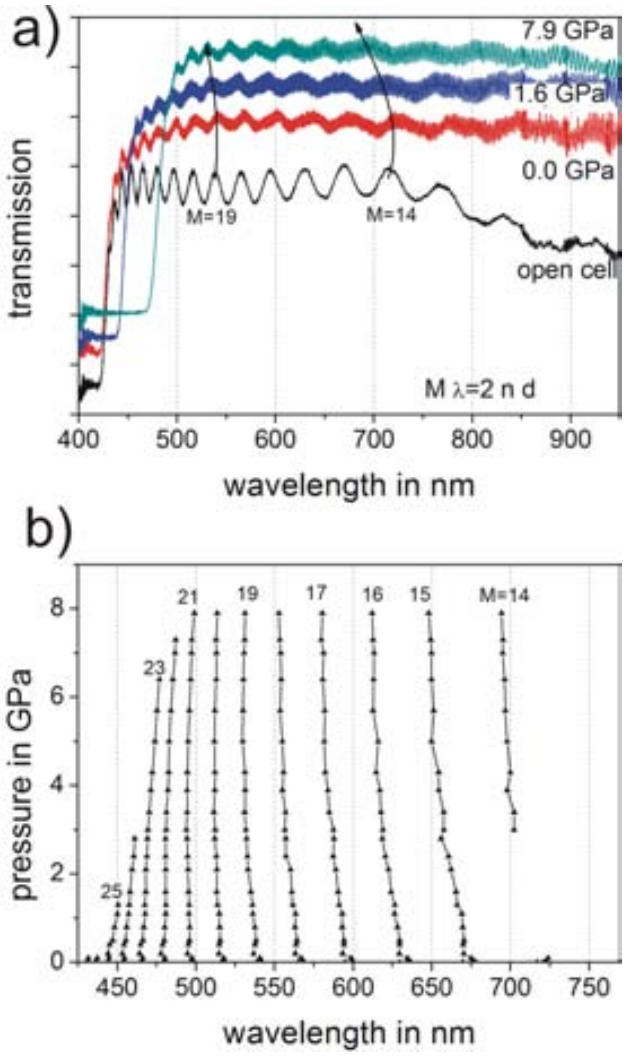

Figure 4.9: a) Representative transmission measurement of PFO with interference pattern. The high frequency oscillation stems from reflections between the diamond faces, the low frequency oscillation stems from the reflection between the polymer surfaces. b) Movement of interference maxima (from the polymer surfaces) with pressure.

sample will most probably have a very similar change of the refractive index in the transparent region under high hydrostatic pressure. The measurement requires a much higher control of the experimental conditions than for the previous absorption and PL measurements. As the low refractive index contrast between polymer and the alcohol pressure medium results in a very weak reflection at the interface, it is important to have a very smooth surface in order to optimise the signal. Since the sample thickness can change slightly laterally, it was of paramount importance to remain with the focused light spot exactly on the same position of the sample; otherwise the small lateral thickness changes will introduce misleading shifts of the interference peaks. First, the piece of the glassy sample was measured with the nearly closed pressure cell in air. Then, the alcohol was introduced and the pressure cell was closed. As the sample did not move, the spot position was virtually unchanged.

Figure 4.9 (a) shows representative transmission spectra for this glassy PFO sample. The graphs show the already discussed shift of the absorption onset and, in the transparent region, the shifts of the interference peaks (marked with arrows). The high frequency oscillation stems from the diamond surfaces which are at the beginning of the experiment approximately 100 µm apart. With the help of the ellipsometry data we determined the indexation of the interference maxima and the thickness d at the spot size (2924 nm). The evolution of the position of the indexed maxima with pressure is shown in figure 4.9 (b). The maxima far away from the absorption region move constantly to shorter wavelengths, while close to the band gap they are "pushed" away towards longer wavelengths, as the band gap redshifts.

For a quantitative analysis of the optical path an estimate of the change in the thickness d is necessary. A very simple but efficient method is to observe with a camera the change in the lateral dimensions. The changes in the width of a soft material like a polymer are easily detectable with an optical microscope. As throughout the determination of the refractive index this method assumes an approximately isotropic behaviour of the optical and mechanical properties of the polymer under hydrostatic pressure.

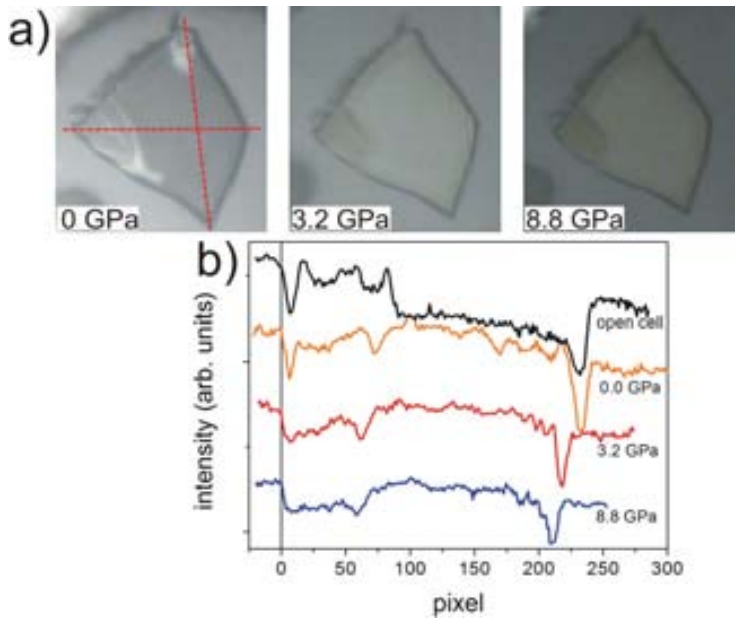

Figure 4.10: a) Representative photographs of a PFO piece under hydrostatic pressure; b) brightness profiles of a diagonal in the photos used to determine the exact size of the polymer piece (shifted for clarity)

Figure 4.10 (a) shows three representative photos taken of the polymer piece inside the pressure cell at different pressures. On the lower left, the ruby crystal for the pressure determination can be seen. The lines mark the diagonals which were measured to estimate the area and thus the density change of the piece from the geometrical mean value. With the assumption of isotropic behaviour the change in area directly gives the change in thickness and volume as well, and the density change is simply the reciprocal volume change.

The curves in figure 4.10 (b) are profiles of the intensity/brightness of the photos along one of the diagonals. The outer transition from the dip to a constant brightness was defined as the border of the polymer piece. Figure 4.11 (a) shows the estimated (normalised) thickness change of the PFO sample under hydrostatic pressure. To fit the data, the Murnaghan[4] equation of state was used

[4]Francis Dominic Murnaghan (1873, Omagh, Ireland - 1976, Baltimore, USA)

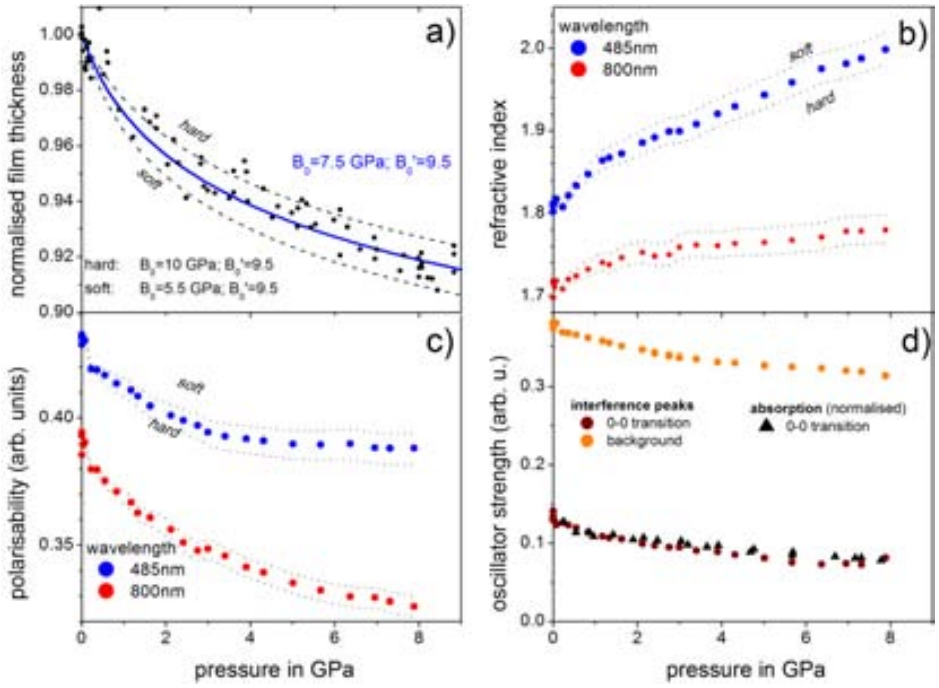

Figure 4.11: Various parameters for PFO versus pressure. a) normalised thickness, b) refractive index, c) polarisability and d) oscillator strength

$$d(p) = d_0(1 + B_0'/B_0 p)^{-1/(3B_0')},$$

where p is the pressure, B_0 is the bulk modulus at ambient pressure, B_0' its derivative and d_0 the thickness at ambient pressure (set to 1 in the graph). We estimated the free parameters to be B_0 =7.5 GPa and $B_0' = 9.5$, which fit the measured points well and are in accordance with typical values for polymers [124, 125]. The hard and soft limit marked by the dotted lines were chosen as a confidence band. The total thickness change up to 8 GPa is about 8 %.

As mentioned before, nd can be calculated from the positions of the interference peaks λ_M (as shown in figure 4.9 (b)) and with the known thickness change it is now possible to calculate the refractive index from the transmission data. Figure 4.12 shows the measured refractive index of PFO for various pressures up to 7.9 GPa. The refractive index shifts to lower energies and increases with pressure.

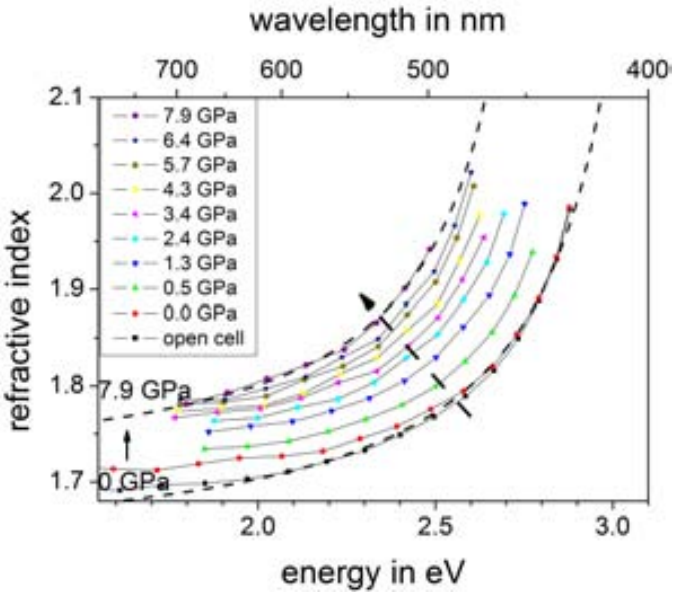

Figure 4.12: Examples for the change of the refractive index of PFO under hydrostatic pressure as determined by the transmission measurement; the dashed lines are Sellmeier fits for 0 GPa and 7.9 GPa.

In order to understand in greater detail the roles of the band gap shift and the density increase on the measured n values, we have analysed the data using the Sellmeier[5] equation describing the refractive index based on the Lorentz[6] oscillator model, with one oscillator representing the 0-0 transition centred around the band gap and one constant background for the transitions at higher energies (an oscillator at infinity). This resulting Sellmeier equation reads:

$$n^2 = 1 + \frac{B_1}{C_1 - \lambda^2} + B_2,$$

where B_1, B_2 and C_1 are fitting parameters. For a reliable fit, C_1, which is the square of the 0-0 transition wavelength, had to be fixed. For this purpose, the refractive index of the ellipsometry measurement of the glassy sample (figure 4.8) was fitted with the Sellmeier equation. We obtained a value of 389 nm (3.19 eV) for the 0-0 transition wavelength. For the mea-

[5]Wolfgang von Sellmeier (born 19th century, German Confederation)
[6]Hendrik Antoon Lorentz (1853, Arnhem, Netherlands - 1928, Haarlem)

surements under pressure it was assumed that the 0-0 absorption transition shifts parallel to the 0-0 PL transition (figure 4.7), leaving B_1, B_2 as the fitting parameters. The dashed lines in figure 4.12 are fits for 0 GPa and 7.9 GPa. The form of the curve stays almost the same under high pressure and the two main effects are the shift of the band gap to longer wavelengths (connected to C_1) and the increase in high frequency components (B_2).

In figure 4.11 (b) the refractive index obtained from the fit is plotted versus pressure for two wavelengths, one very close to the band gap (485 nm (2.56 eV)) and one far away (800 nm (1.55 eV)). While the former has a constant strong shift because of the influence of the shifting band gap, the latter changes just about 0.08 up to 7.9 GPa. Additionally to the refractive index, the polarisability can be estimated from the Lorentz-Lorenz[7] equation.

$$(n^2 - 1)/(n^2 + 2) = \rho P,$$

where P is the polarisability (or proportional to it to be exact). The polarisability, on the other hand, depends, according to the Lorentz-oscillator model, on the oscillator strength of the optical transitions. With the same model as for the Sellmeier equation one can write

$$P \propto \frac{f_0}{1239.84^2(1/\lambda_0^2 - 1/\lambda^2)} + f_1,$$

where λ_0 is the centre of the 0-0 transition and f_0, f_1 are fitting parameters proportional to the oscillator strength of the transitions. λ_0 is the same as $\sqrt{C_1}$ from the Sellmeier equation and was fixed in the same manner for the high pressure fits. The values of the fits for the polarisability are shown figure 4.11 (c) and for the oscillator strength in figure 4.11 (d). The decreasing oscillator strength results in a strong drop of the polarisability, which counteracts the increase in the refractive index caused by the strongly increasing density. Altogether, this results in only a very small increase of the refractive index in the transparent region.

This behaviour is completely different from that of inorganic materials

[7]Ludvig Valentin Lorenz (1829, Helsingør, Denmark - 1891, Frederiksberg)

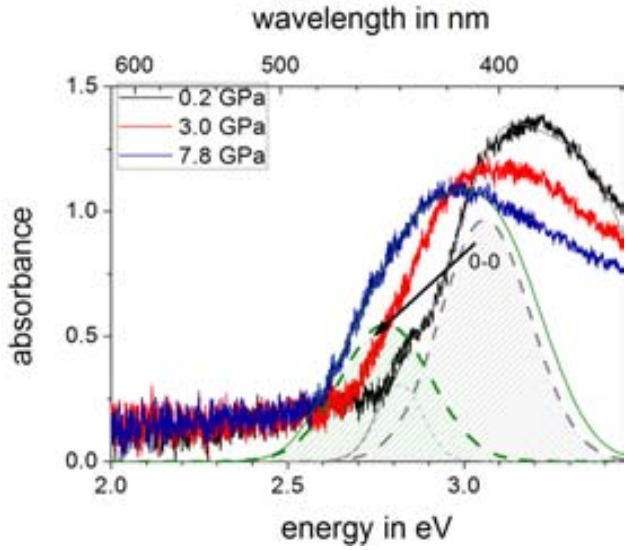

Figure 4.13: Examples for absorbance for a thin layer of PFO under hydrostatic pressure. The fit for 0.2 GPa and 7.8 GPa are shown as a thin solid line. The Gaussian function for the description of the 0-0 transitions from these fits are shown as the dashed thick lines.

for which the oscillator strength commonly increases with pressure (e.g. in GaAs [126]). This is especially surprising as the oscillator strength[8] in these cases is inversely proportional to the band gap; i.e. for the observed redshift in polymers an increasing oscillator strength would be expected, unless the matrix element for electron-photon interaction overcompensates the decreasing band gap. We therefore tested, whether this decrease in oscillator strength can be seen in a lower absorbance value as well. For this purpose we measured the transmission of a much thinner PFO film, which was fabricated by spin coating from a toluene solution (8 g/l) on glass, in order to have non-saturated spectra and thus quantify the absorption. Some examples of the absorbance with the corresponding fits with Gaussian functions are shown in figure 4.13. Since the sample is thin no interference peaks can be seen this time, and it is possible to see a slight broadening of the spectrum. In order to make the fit more reliable, the width of the peaks and the

[8]The oscillator strength is written as $f = |M|^2/(m_0\hbar\omega)$, M is the matrix element for electron-photon interaction, m_0 the free electron mass and $\hbar\omega$ the energy of the transition [126].

distance between the peaks were kept constant and the Gaussian peaks were again assumed to shift parallel to the 0-0 PL transition (figure 4.7). The absorbance is proportional to the thickness and the absorption coefficient. The absorption coefficient is proportional to the oscillator strength of the transition. Therefore, to compare the oscillator strength with the absorption measurement, the area of the 0-0 transition peak in the absorbance was divided by the thickness of the sample. The resulting values (normalised to the f_0 value at the lowest pressure) are shown together in figure 4.11 (d). Even though the two curves were obtained in a very different way, they coincide nicely, which gives strong confidence in the performed analysis.

We continue the discussion with the effect of the dielectric environment ((iv) in figure 2.6) on the PL spectra. The small increase in the refractive index from 1.7 to 1.78 can affect both the polarisation energy (leading to a red-shift in the PL) and the exciton binding energy (leading to a blue-shift). For PFO very different values for the exciton binding energy at ambient pressure have been reported: 0.3 eV from reference [127] and 0.5 eV to 0.7 eV from reference [128] from experimental studies and a very high calculated value of 1 eV from reference [129]. The exciton binding energy is proportional to $\epsilon^{-2} \approx n^{-4}$ [130] which for our measurement results in a change in the exciton binding energy of roughly 20% for a pressure of 8 GPa. Disregarding the calculated value of reference [129], we estimate a change in exciton binding energy between 60 meV and 140 meV. However, the same change in the global refractive index resulting from the pressure increase can be easily achieved by mixing the polymer with materials with a higher refractive index. For different polymers this has been done and no big shift of the polymer PL compared to the pure polymer was observed [131] (see also chapter 6.2). This can indicate that the red-shift caused by the polarisation energy and the blue-shift caused by a decreased exciton binding energy cancel each other out. This can be understood because the mechanism of the polarisation of the environment due to the exciton is very similar for both effects and might be identical in terms of strength and their dependence on the refractive index. For the pressure measurements, we have a very different reason for the increase of the refractive index but this interpretation is still compatible

with our experiment. This could mean that both the reduction of the band gap due to the polarisation energy increase and the reduction of the exciton binding energy might be in the order of magnitude of 100 meV. Independent of the exact value no net shift of the absorption onset or PL emission due to the refractive index is expected.

The strongly increased density and the increase of the defect/excimer emission, which was mentioned before, give strong evidence for an enhanced interchain interaction ((iii) in figure 2.6), the last parameter which will be discussed. From the measurements one cannot directly infer the magnitude of the PL shift due to interchain interaction. However, it is reasonable to argue that interchain interaction causes the so far unexplained part of the red-shift, i.e. approx. 155 meV). This is in the same order of magnitude (140 meV to 180 meV) observed in the defect/excimer emission red shift (vide supra). Moreover, this estimate of the red-shift caused by interchain interaction is in accordance with the assumption of Schmidtke et al. [61] that interchain interaction is responsible for a big part of the observed red-shift in poly(9,9-di-n-octylfluorene-alt- benzothiadiazole) (F8BT) (140 meV out of 460 meV). As excimers are an interchain species, it is a very interesting notion to assume that the defect/excimer emission, commonly shifts by the same amount as the Franck-Condon emission shifts because of interchain interaction.

As the refractive index seems to change the HOMO-LUMO gap very little, and interchain interaction in turn seems to be a very important factor, the comparison of the PL and absorption spectra of PFO in a toluene solution and a solid film can give additional insight into the effect of the two parameters. In contrast to a film, in solutions the molecules are mostly isolated from each other and interact only with the solvent molecules. The refractive index of toluene is, with a value of 1.5, much lower than that of the solid PFO film. Figure 4.14 shows the PL and absorption of a dilute PFO solution in comparison to the one of the glassy thin film. For normalisation of the absorption with the absorption coefficient of the glassy film[9] measured with ellipsometry the maximal slope of the curve (which is at around 3.1 eV)

[9] Absorption coefficient is $\alpha = \frac{4\pi\kappa}{\lambda}$, where κ is the extinction coefficient measured with ellipsometry and λ the wavelength in vacuum.

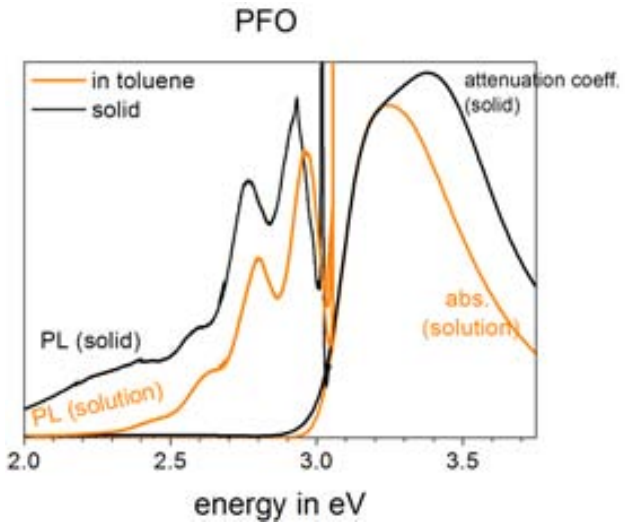

Figure 4.14: PL and absorption spectra of PFO in a toluene solution and as a solid film

was used as a normalisation criterion in order to best visualise a rigid shift between the curves. The solid film has a slightly broader absorption than the solution, but the absorption onset is otherwise at the same energy. In PL the difference is more clearly noticeable. The PL shift from the solution to the glassy solid is about 30 meV to 40 meV to lower energies. The small shift means probably that none of the parameters discussed in this chapter efficiently changes the band gap of the material (or less likely: they cancel each other out), including increased interchain interaction.

Costa et al. observed for PFO in methylcyclohexane (MCH) the emission peak at approx. 3.00 eV, i.e. shifted by 60 meV to higher energies compared to the solid glassy film while they observed the β-phase emission in solution unshifted at 2.82 eV [132]. This rules out that the "solution-to-solid" shift stems from interchain interaction or the change in the dielectric constant as this should affect both conformations in a similar manner. As the inter-ring bond length probably does not change, the most likely explanation for the small shift is that a very slight planarisation occurs when going from the solution to the solid film. At first it might seem unlikely that interchain interaction has virtually no effect on the emission spectrum, but should be so important under high pressure. However, the defect/excimer - emission was

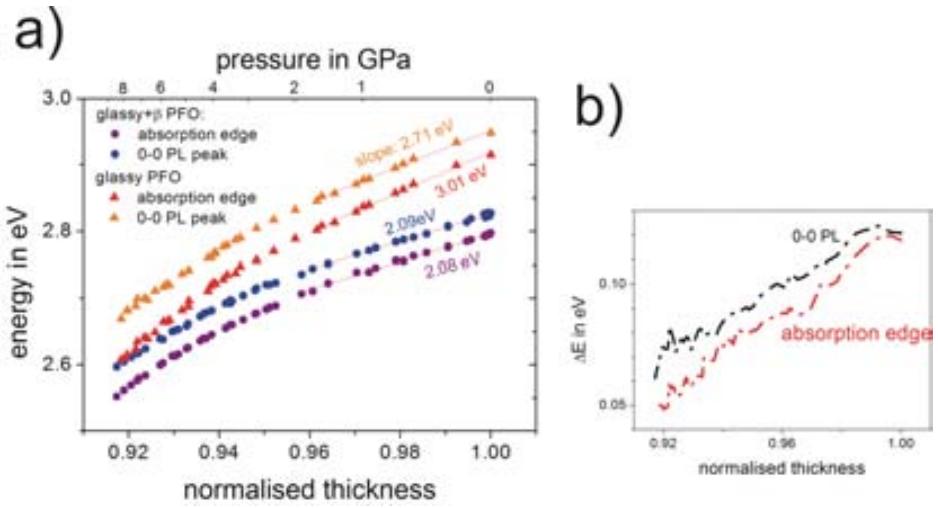

Figure 4.15: (a) 0-0 emission peak position and absorption onset energy for the glassy and the glassy+β sample under hydrostatic presure plotted versus the film thickness; (b) the energy difference between both emission peaks (compare with figure 4.7)

already used as a good indicator of enhanced interchain interaction and both in the solution and the solid film at ambient pressure this defect/excimer emission is very low, which suggest little or no interchain interaction, while a slight increase in pressure enhances the transfer of excitons to other chains. This shows that interchain interaction is relatively unimportant at ambient pressure in spite of the close proximity of the polymer molecules and only becomes truly important under pressure. The latter assumes a low order and can be different in highly crystalline materials like RR-P3HT, as will be discussed in the next chapter.

4.4 Dependence on interchain distance

The fast change of the band gap and the refractive index for up to 2 GPa is raising the question of whether a more efficient mechanism is active in the low pressure region. The fast decrease has been specifically used to justify and quantify planarisation [122]. Usually, the so called pressure coefficients give the shifts per gigapascal and therefore the samples show for low pressures

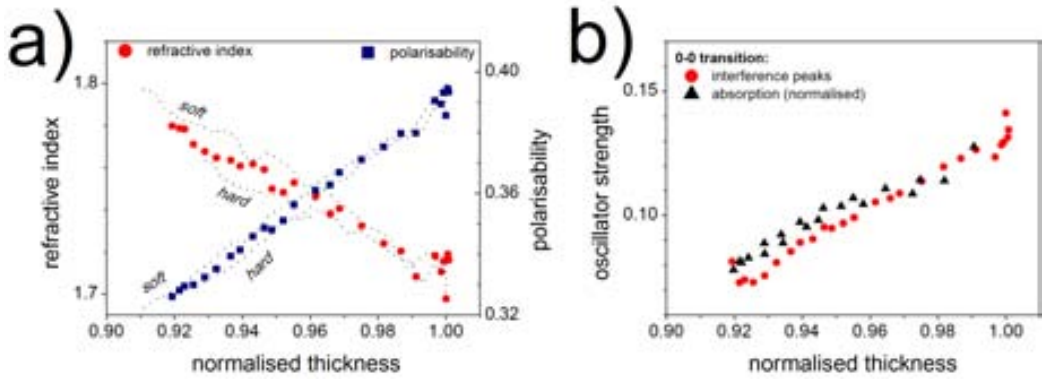

Figure 4.16: Various parameters for PFO under pressure plotted versus normalised thickness: (a) refractive index and polarisability (both for 800 nm) and (b) oscillator strength

a higher pressure coefficient than for high pressures. However, this can be detrimental for the physical understanding of the observed effects.

In figure 4.15 the data of figure 4.7 is plotted not versus the pressure but versus the normalised thickness representative for the interchain distances. The energy changes become now linear for low pressures with the glassy sample just having a steeper slope than the glassy+β sample. A near-linear behaviour can be also seen in figure 4.16 for the change of the refractive index, polarisability and oscillator strength. This shows that the strong changes for very low pressures just mirror the fast reduction of the intermolecular distances. This dependence can clarify the cause for the initial shift. This makes it, for example, less likely that the bond length change - with a more linear dependence with pressure [68, 72]- is responsible, while planarisation is very likely to depend more on the intermolecular distances. But again there is no indication - like a change in slope for the glassy sample - that the planarisation is completed after approx. 1.5 GPa. The deviation from the linear behaviour at pressures beyond approx. 3 GPa (or 0.95 normalised thickness) shows that at very short interchain distances the interchain interaction causes an even stronger shift. Although the possibility cannot be excluded that at higher pressures a possible anisotropy of the PFO film becomes more apparent, which would have caused a higher inaccuracy in the estimated intermolecular distances.

	glassy	glassy+β
total shift	275 meV	225 meV
bond length	70 meV	70 meV
planarisation	50 meV	—
interchain interaction	155 meV	155 meV
dielectric environment	—	—

Table 4.1: Estimates of each contribution to the total shift of the photoluminescence of the glassy and the glassy+β shown in figure 4.7

4.5 Chapter conclusions

Summarising the most important results of this section, we have measured the absorption and photoluminescence of two phases of PFO with different planarity under hydrostatic pressure of up to 8 GPa. Apart from the red-shift of the transitions we analysed the interference pattern in the transparent region of a glassy phase PFO sample and estimated the density change under hydrostatic pressure using a Murnaghan equation of state. From this, we obtained the absolute value of the refractive index, the change in polarisability and the change in the oscillator strength of the 0-0 absorption transition for hydrostatic pressure up to 7.9 GPa.

From this it was discussed how the parameters influence the optical gap of the polymer. The red-shifts attributed to the different parameters are summarised in table 4.1. This emphasises the interchain interaction as the most important parameter. It was also shown that planarisation occurs just incompletely even at the highest pressure, which was suggested to be caused by the disturbing influence of the sidechains.

Newton:"Ich ertrage Unordnung nicht. Ich bin eigentlich nur Physiker aus Ordnungsliebe geworden."

Friedrich Dürrenmatt, **Die Physiker**

5

Intermolecular interaction: P3HT and PCBM

In this chapter we investigate the optical properties of the pure materials of poly(3-hexyl thiophene) (P3HT) and of phenyl-C61-butyric acid methyl ester (PCBM) in diluted solution and in thin films both under ambient conditions and under hydrostatic pressure. In solution the molecules are isolated from each other, while in the thin film under pressure, the molecules are forced to be in close proximity to each other. This series of experiments thus allows for the investigation of the materials under increasing intermolecular interaction. The effect of order on the interchain interaction in the crystalline phase will be discussed with the help of two types of P3HT. This chapter is also important for organic solar cells, for which both P3HT and PCBM are often used. In this sense, the chapter presents the basis for P3HT:PCBM blends, a model organic solar cell system, which is the topic of the following chapter.

The two types of P3HT, which will be discussed in this chapter, are regiorandom P3HT (rra-P3HT) and regioregular P3HT (RR-P3HT). From a chemical point of view the two polymers are almost identical. The different properties they exhibit arise from the *regular* head-to-tail connexions between monomers in RR-P3HT in contrast to rra-P3HT, resulting in stronger steric

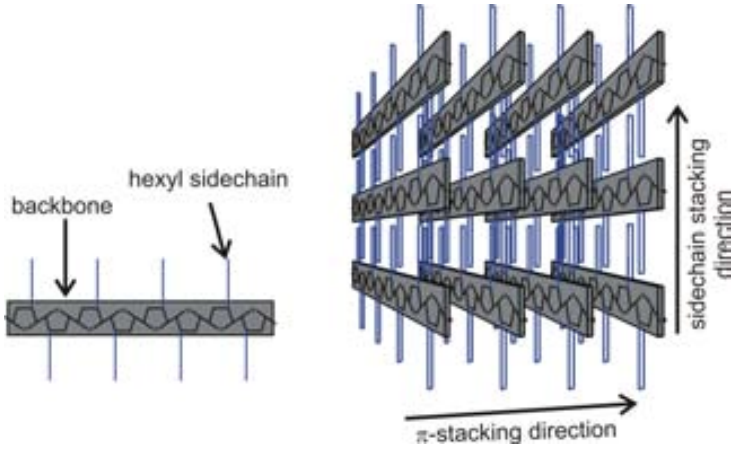

Figure 5.1: Sketch of the stacking in the crystalline phase of P3HT. Inspired by [133]

effects of the sidechains for rra-P3HT (see chapter 2.5.2 for details). Amorphous films of rra-P3HT are characterised by high torsion angles between the monomers of roughly 50° to 70° [93]. RR-P3HT, in contrast, forms a semi-crystalline film. In the crystalline phase the polymer chains are well aligned with the neighbouring chains in ordered stacks, which leads to a very planar backbone conformation and strong interchain interaction [134]. Figure 5.1 shows a sketch of how the crystalline phase looks like. The strongest π-orbital overlap of the neighbouring polymer backbones is in the π-stacking direction of the crystal. Perpendicular to this direction the chains also order along the direction of the sidechains.

PCBM is included here for two reasons: Firstly, it is one of the most commonly-used acceptor materials, and the similar fullerene bisPCBM, the bisadduct of PCBM, and PC70BM, a fullerene derivative with a ball of 70 instead of 60 carbon atoms, are nowadays most often found in high efficiency organic solar cells. Secondly, the spherical geometry of the C_{60} ball does not allow for any planarisation. This means that optical changes have to be explained by variations in bond length, intermolecular interaction or the dielectric constant. We investigated the properties of the pure materials using Raman, absorption and PL measurements at ambient conditions, at low temperatures and at high pressures.

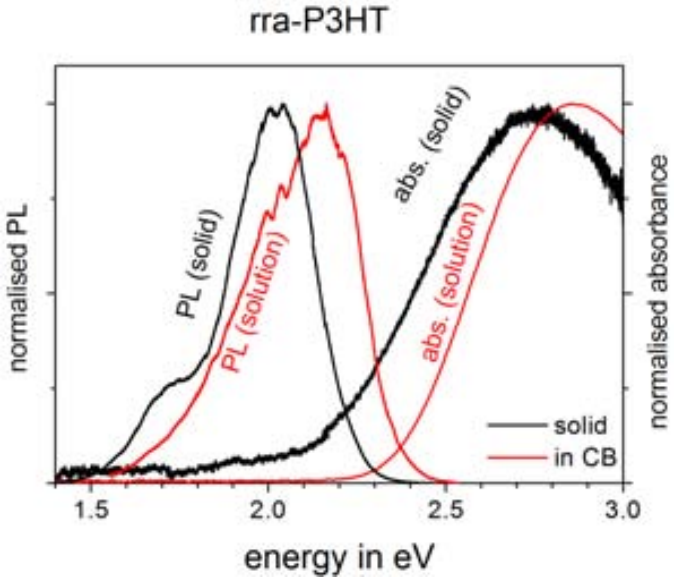

Figure 5.2: PL and absorption spectra of rra-P3HT in a chlorobenzene solution and as a solid film

5.1 From solution to solid film (ambient pressure)

We now immerse ourselves in the specifics of absorption and photoluminescence of P3HT in solution. As the molecules do not interact with each other, the solutions are a good way to study intramolecular effects. Both inter- and intramolecular effect can be studied by the "solution-to-solid" shift in the spectra.

In figure 5.2 the absorption and emission spectra of rra-P3HT of highly diluted solutions in chlorobenzene and those of a thin film are shown; in figure 5.3, the corresponding spectra for RR-P3HT. Both absorption spectra of the solutions are completely featureless and even the PL spectra consist of broadened peaks of the Franck-Condon series (see chapter 2.3.1 for an introduction to PL and absorption). In solution, rra-P3HT has the maximum of absorption at approx. 2.86 eV, the absorption onset at 2.37 eV and the 0-0 emission peak at 2.21 eV. The absorption onset was determined by the intercept of straight lines describing the low energy slope of the absorption

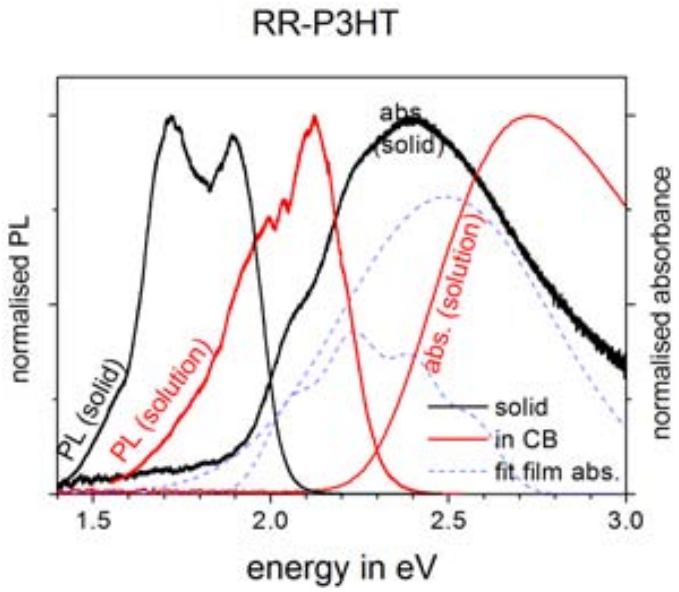

Figure 5.3: PL and absorption spectra of RR-P3HT in a chlorobenzene solution and as a solid film. For the solid film absorption, a fit is shown, separating the contributions from the crystalline and the amorphous part of the film.

and the low energy background signal. RR-P3HT has the maximum of absorption in solution at approx. 2.73 eV, the absorption onset at 2.27 eV and the 0-0 emission peak at 2.12 eV.

The very similar shape of the absorption and emission spectra of both materials in solution indicates that the differently attached sidechains do not change the optical properties considerably. The absence of clearly visible peaks in the spectra is due to the broad distribution of conjugations lengths, i.e. the isolated polymer chains in the solution can twist and bend freely and assume a wide range of different conformations with different conjugation lengths. The energy difference between the two types of P3HT (about 100 meV) is best explained with a different effective conjugation length. In solution the red-shift of RR-P3HT with respect to rra-P3HT shows thus that the steric effects of the sidechains in RR-P3HT are clearly less, and more conformations closer to planarity are assumed. This shows already in solution the higher potential of RR-P3HT for higher order and more planar conformations, which is even more pronounced in the film.

The overall shape of the rra-P3HT spectra is virtually the same for the solid film compared to the solution. In contrast, for the RR-P3HT film the emission peaks become narrower and the absorption shows distinct peaks at the low energy side. Comparing the film to the solution in rra-P3HT, there are red-shifts of 200 meV in the absorption onset and between 100 meV to 130 meV in the absorption maximum and PL (PL 0-0 emission at 2.09 eV). For RR-P3HT, the red-shifts are much greater. The absorption onset and absorption maximum are shifted between 320 meV to 350 meV to lower energies compared to the solution. The PL is shifted by 220 meV (0-0 peak at 1.90 eV).

When considering the film, rra-P3HT stays amorphous [135] and retains thus most of the characteristics it had in solution, which shows that very little order is gained in the solid state. As a result, the energy shifts are quite low. The shift of the absorption onset is probably bigger because of the broadening of the entire spectrum, which does not affect the apparent maximum. In contrast, RR-P3HT forms a semicrystalline film. The crystalline phase is not only more ordered, but consists of chains with a very planar conformation and thus with a very high effective conjugation length [135]. Thus, the low energy absorption probed with the absorption onset stems from the crystallites explaining the big "solution-to-solid" shift observed for RR-P3HT . In the PL spectra mostly the emission of the crystallites is seen. In a similar way as the β-phase in PFO (see chapter 4.1), the crystallites act as low energy traps. The clearly resolved and strongly red-shifted emission peaks are a manifestation of the formation of this well ordered phase with a much narrower distribution of conjugation lengths.

Planarisation [71, 134], the increasing dielectric constant [62] and the formation of aggregates [75] were all suggested to cause the observed "solution-to-solid" shift in polymer samples. Planarisation occurs certainly in RR-P3HT and contributes thus to the "solution-to-solid" shift. The increase in the dielectric constant cannot be discarded as a reason but is unlikely because the similar change in the dielectric constant from solution to the solid for PFO did not produce a large "solution-to-solid" shift (chapter 4). The formation of aggregates due to interchain interaction is worth to be discussed in

more detail. Strong interchain interaction in RR-P3HT is already evidenced by the usually much weaker photoluminescence of RR-P3HT than that of rra-P3HT [134]. This can be explained by any interchain mechanism introduced in chapter 2.4.2, such as excimer formation and interchain electron hole pairs or the formation of disordered H-aggregates. The PL spectra of RR-P3HT were quantitatively explained by assuming disordered H-aggregate formation [76]. The disorder makes the 0-0 emission from the lowest excited state possible, which in the ideal H-aggregates is forbidden [77, 78]. The emission from the lower excited state of these aggregates would lead to a red-shift in the film with respect to the solution. This is in agreement with the only weak "solution-to-solid" shift in PFO which showed little interchain interaction at ambient pressure (see chapter 4.1). In P3HT it is thus likely that additional to the planarisation, interchain interaction plays a significant role in the "solution-to-solid" shift.

In the absorption spectrum, the low energy peak at 2.07 eV is connected to the absorption by the crystalline phase [136, 137] and the other peaks to the vibronic replica in the Franck-Condon series. Thus, most of the low energy part of the absorption spectrum stems from the crystalline phase which does not exist in solution. The shape of the high energy absorption of the amorphous part of RR-P3HT is probably similar to rra-P3HT [138]. In order to estimate the absorption of amorphous RR-P3HT with a simple model, the crystalline absorption was fitted with a Franck-Condon series with a Huang-Rhys-factor describing the intensity distribution (see chapter 2.3.1). The amorphous part was modeled with one Gaussian curve, which is enough to fit the broad rra-P3HT film absorption (centre: 2.76 eV, full width at half maximum (FWHM) 0.70 eV). This model disregards any high energy absorption the crystalline phase might have and, therefore, higher energies (beyond 2.8 eV) were excluded from the fit. The resulting fit is presented also in figure 5.3. The Gaussian peak describing the absorption of the amorphous phase of RR-P3HT is at 2.49 eV and has a width of 0.70 eV. The Huang-Rhys-factor of the Franck-Condon series describing the crystalline part is 1.47. The Huang-Rhys-factor is slightly higher than what has been reported before (0.95 in a film from methylene chloride and 0.8 from tetrahydrofu-

ran [139]) but those spectra have accordingly a stronger 0-0 absorption peak. It is also possible that the Huang-Rhys-factor is slightly overestimated because the formation of H-aggregates might lower the intensity of the 0-0 absorption peak [76], which has not been taken into account. The believable Huang-Rhys-factor and the similar width of this amorphous RR-P3HT phase absorption compared to the rra-P3HT absorption give confidence in the analysis.

Our analysis shows that the maximum of the amorphous phase of RR-P3HT is shifted compared to the respective solution by about 230 meV to lower energies. This shift is about twice that of rra-P3HT and means that, contrary to the solution, the solid film of RR-P3HT is very different from its regiorandom counterpart: In addition to the formation of the crystalline phase, the amorphous phase exhibits higher conjugation lengths compared to rra-P3HT. This is an important result because it clarifies how films of RR-P3HT and rra-P3HT can be compared: Many of the qualitative properties of an amorphous phase can be expected to be very simliar (small interchain interaction, good miscibility with small molecules, form of distribution of conjugation lengths etc.), but quantitatively there can be some differences which are important when doing an analysis. Tsoi et al. [108] have tried, for example, to determine the volume percentage of the ordered (crystalline) phase in RR-P3HT blends in a Raman study, assuming that the amorphous phases of RR-P3HT and rra-P3HT are identical in terms of their Raman properties. According to our analysis, this must lead to quantitatively wrong results as the amorphous phase in RR-P3HT exhibits higher conjugation length and thus a smaller Raman shift than rra-P3HT[1]. As in this thesis rra-P3HT was also used to understand the properties of the technologically more important RR-P3HT, this result recommends also caution not to overstretch the analogy of the two phases.

Finally, the case of PCBM is discussed. The absorption and PL spectra in solution and thin film are shown in figure 5.4. The absorption of PCBM occurs mostly in the ultra-violet region of the spectrum, but has a very long

[1]This connexion between the Raman shift of the symmetrical C=C stretching mode and the conjugation length will be explained in chapter 5.4.

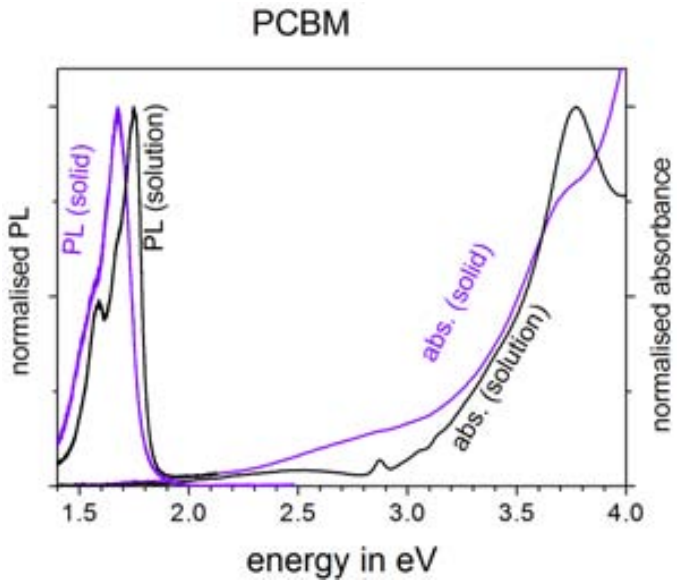

Figure 5.4: PL and absorption spectra of PCBM in a chlorobenzene solution and as a solid film

tail into the visible region. The small, broad peak at around 2.4 eV observed in solution stems from a symmetry forbidden transition to the lowest excited singlet state as both have an even parity[2]. The low energy onset of this peak (approx. 1.9 eV) can thus be seen as the optical gap of PCBM. When going from the solution to the film the absorption peak shifts from about 3.77 eV to 3.68 eV (taking into account the steep background which seemingly shifts the peak slightly to higher energies). Additionally, the spectrum broadens considerably, which is associated with the dispersion of electronic states in the solid due to structural disorder [140, 141]. In the visible region, the absorption of the film has a broad absorption peak at around 2.8 eV, which has also been described in the literature [141, 142]. This broad absorption might stem from clustering or crystallisation of PCBM, which is confirmed by the absence of this peak in the solution, where no appreciable absorption of clusters/crystals is expected. A possible explanation is that the symmetry forbidden transitions of isolated molecules are becoming weakly allowed because of intermolecular interaction, which lowers the symmetry in the solid

[2]Light couples to the higher vibrational states with odd parity [140].

film [141].

The PL spectrum shows a very sharp onset at around 1.75 eV in solution, which is shifted approx. 80 meV to lower energies (to 1.67 eV) and broadened for the solid film. This emission is associated with the transition from the first excited singlet state to the odd parity vibrational states of the ground state (the 0-0 emission is forbidden) [140]. It is noteworthy that PCBM has an approximate Stokes shift of 0.2 eV. Usually for small molecules, the Stokes shift is very small or nonexistent if no conformational freedom exists in the chromophore [143] like in PCBM. In the case of PCBM, the Stokes shift stems from the phonon energy of the odd vibrational states, which shifts both PL and absorption away from the forbidden 0-0 emission and away from each other. The red-shifted spectra compared to the solution have been observed before [141, 142]. As no planarisation is possible in the ball-like molecule, the shift is probably connected to the intermolecular interaction in the PCBM film. The stronger intermolecular interaction in the solid might allow for a greater delocalisation of the exciton wavefunction over several PCBM molecules, lowering thus the band gap. For this to be effective, the local order is very important, i.e. small intermolecular distances and crystalline environment favouring delocalisation.

5.2 Low temperatures

Lowering the temperature can provide a mechanism to bring chains closer when reducing the temperature by freezing out their rotational degrees of freedom and low energy vibrations, allowing the van-der-Waals forces to pull the molecules towards each other more effectively. In the experiments of this section, the molecules are brought a little bit closer in this manner by cooling down the samples to cryogenic temperatures. P3HT and PCBM were spin coated on small pieces of Si and introduced into a cryostat, which was evacuated before cooling. The samples were cooled down with liquid nitrogen to 77 K. In figure 5.5 (a) the PL spectra of RR-P3HT and rra-P3HT are shown at 77 K and room temperature. The most obvious changes when decreasing the temperature are a narrowing of the emission peaks and a slight shift to

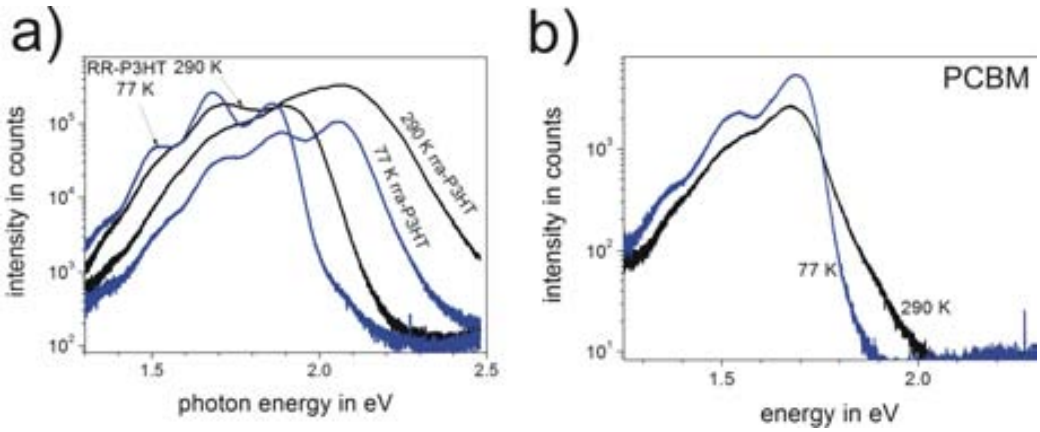

Figure 5.5: PL at ambient temperature and at 77 K of a) RR-P3HT and rra-P3ht and b) PCBM

lower energies. The 0-0 peak of RR-P3HT shifts on cooling from 1.90 eV to 1.86 eV, the 0-0 peak of rra-P3HT from approx. 2.11 eV to 2.05 eV. The narrower emission peaks can be explained by a higher order, the energy shift by more planarity at low temperatures. This is similar to the measurement of PFO in chapter 4.1, which exhibited a shift of 30 meV to 40 meV on cooling. The peaks of PCBM (figure 5.5 (b)) also get narrower but no blue-shift is observed. This corroborates the explanation, that planarisation is responsible for the shift, as PCBM molecule cannot planarise.

A closer distance between chains could also lead to enhanced intermolecular interaction at low temperatures. For PCBM this does not seem to occur probably because the molecular rotations and vibrations do not prevent the molecules from their approaching each other significantly. In polymers this is different because of the great conformational freedom and, at least for P3HT, it seems likely that enhanced interchain interaction is also a reason for the red-shift as we discussed before for the "solution-to-solid" shift. Especially in the case of a red-shift due to interchain interaction, it is interesting to estimate the thickness change of the film. We estimate a 0.3 % thickness change with cooling to 77 K like in the case of PFO, whose expansion coefficient at room temperature was given as $1.5 \times 10^{-5}\,\mathrm{K}^{-1}$ [118]. The red-shift with cooling is much higher than the shift induced by pressure for a similar thickness change (vide infra). This confirms that the reasons for the red-shift

Figure 5.6: Photographs of a P3HT sample in the pressure cell taken in reflection.

at low temperatures is different from that observed by applying pressure and cannot be described only by the change of the interchain distance (sample thickness).

At low temperatures it is much more obvious that the emission consists of only one Franck-Condon series both for RR-P3HT and rra-P3HT. The same spacing of approx. 170 meV to 180 meV coincides with the energy of the main stretching modes in the molecule as measured with Raman (this will be shown in chapter 5.4), which indicates that mostly these modes couple to the electronic states. The low temperature measurements are thus also useful to get a better understanding of the emission spectra, which is important for the fits in the following section for the pressure experiments.

5.3 PL and absorption under pressure

For the measurements under hydrostatic pressure the samples were introduced with the pressure transmitting medium (methanol/ethanol) into the diamond anvil cell. The samples showed little degradation under illumination with the laser, which indicates that little or no oxygen was in the pressure cell and the samples did not react significantly with the alcohol. The absorption of the intense laser light can produce locally considerable heat and at very low pressures it can happen that one burns holes into the film. This is usually not a problem for the measurements after some pressure (>1 GPa) has been applied once, possibly because of an improved thermal contact between the sample and the diamond afterwards.

Figure 5.6 shows photos of a RR-P3HT sample inside the pressure cell taken through the same 20x lens as used for the PL measurement. The outer part is the gasket. In the upper part of the photo a little bit of the diamond can still be seen, while the rest is covered by the polymer. In the upper right part the ruby is located (marked with an arrow). It is located on the other diamond face and is therefore out of focus in this image. Under higher pressure, the hole shrinks and the polymer film often gets slightly crumpled. The polymer can be identified by its red colour, though often in the beginning of the experiments it appears green probably because of interference effects between the diamond and the polymer film.

Figure 5.7 shows some representative PL spectra of (a) RR-P3HT and (b) rra-P3HT under high hydrostatic pressure. In both cases a strong red-shift, an enormous loss in PL intensity and a broadening of the emission peaks is observed. This behaviour is quite similar to the one observed for PFO, but, in contrast to PFO, no background emission appears with pressure. This indicates that no new efficient emission channels like defect emission or excimers are formed (they would lead to more qualitative changes in the emission spectrum as in the case of PFO). In the graphs, one spectrum for decreasing pressure is shown for each sample, while the others are from the first pressure increase. The similar curves for similar pressures indicate that in both samples no permanent change is observed after the first pressure increase, i.e. no permanent (dis)ordering of the polymer or the creation of nonradiative traps is caused by applying pressure.

The spectra are difficult to analyse quantitatively, for the emission peaks are broad and weak and additional peaks are superimposed on the PL spectra (two peaks are marked in figure 5.7 (b) by vertical arrows). These peaks are weak for pure materials under ambient conditions but the very low PL intensity under pressure gives these signals an increasing weight, and thus they can significantly change the spectrum. They are probably connected to Raman scattering of the diamonds and the stretching modes of P3HT. The energy of these Raman modes changes only weakly with pressure (see chapter 5.4), which explains that the peaks remain stationary throughout the experiments. Additional disturbing influences are a high energy tail of

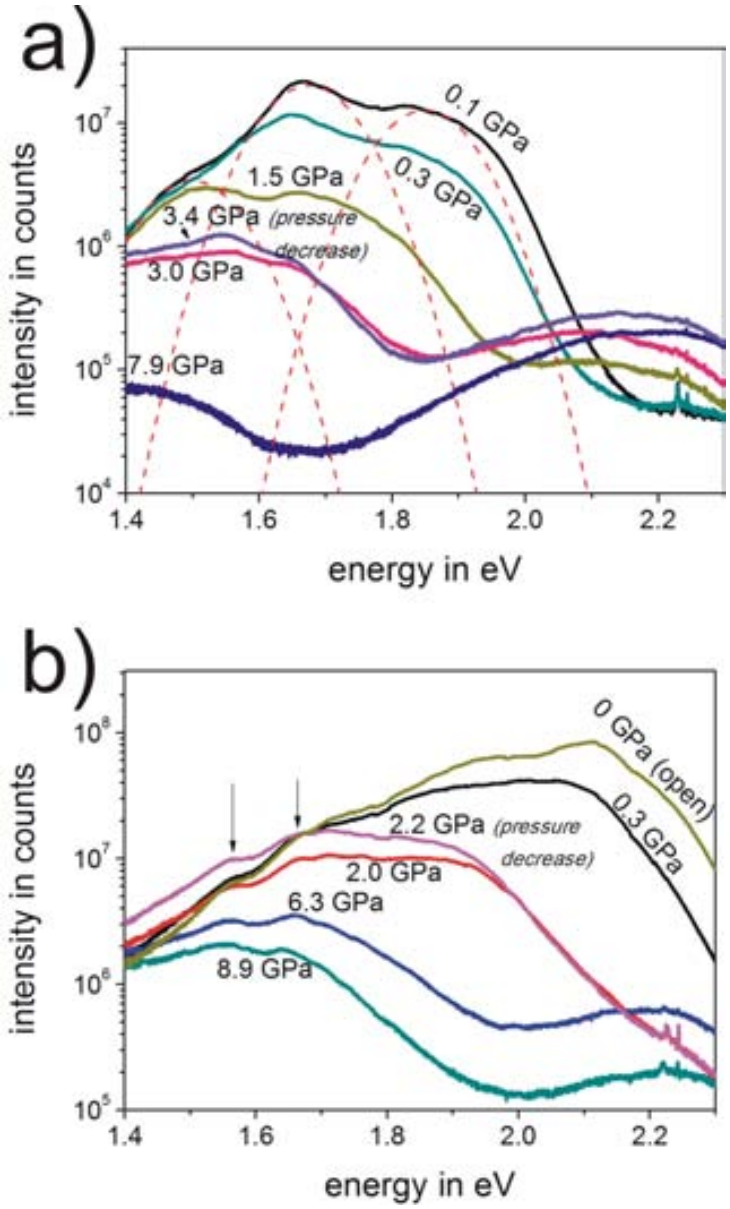

Figure 5.7: Representative PL spectra of (a) RR-P3HT and (b) rra-P3HT under pressure. The dashed lines in figure (a) correspond to the Gaussian curves of the Franck-Condon fit for 0.1 GPa.

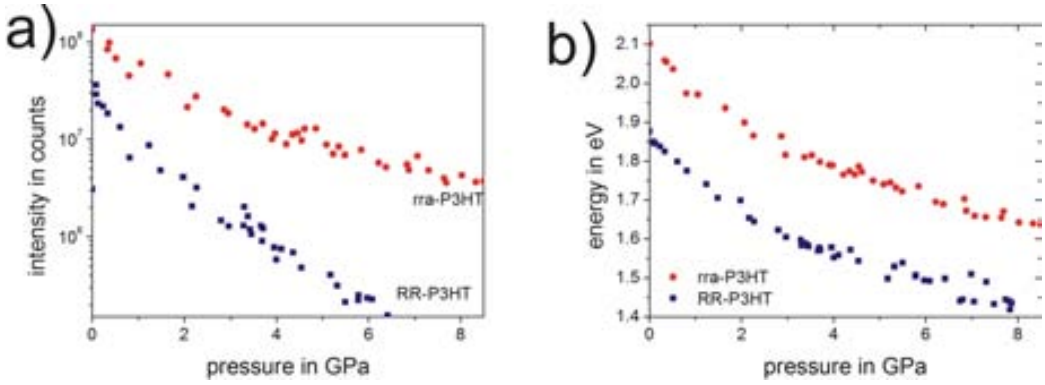

Figure 5.8: (a) Intensity of the polymer emission and (b) 0-0 PL position of RR-P3HT and rra-P3HT versus pressure

the polymer PL and a peak at around 2.1 eV. The latter is caused by the involuntarily introduced PEDOT:PSS layer (see chapter 3.2.1). The peak appears only for samples fabricated with a PEDOT:PSS sacrificial layer and can therefore be ascribed neither to the sample (P3HT or PCBM (shown later)) nor to the pressure medium.

To obtain a meaningful fit with a Gaussian series under these conditions, some of the parameters of the peaks have to be fixed and/or correlated. Using the ambient pressure measurement as a reference, the inter-peak spacing was set to 175 meV and all peaks were set to have the same width. Where necessary, an additional Gaussian curve was used in the fit for both the PEDOT:PSS emission and for the high-energy tail. An example of a fit for RR-P3HT at 0.1 GPa is shown as dashed lines in figure 5.7 (a).

The results of the fits, the total area of the Franck-Condon series (i.e. the emission intensity) and the position of the 0-0 emission peak, are plotted versus pressure in figure 5.8 for RR-P3HT and rra-P3HT.

The intensity of the PL of both polymers (figure 5.8 (a)) decreases similarly in an almost exponential manner. RR-P3HT has a lower intensity at ambient pressure as mentioned before and shows a stronger PL quenching under pressure. Structural defects in the P3HT polymer chain can be traps for the charges and offer a non-radiative decay channel for excitons. If increased exciton mobility under pressure facilitates the trapping of excitons at these defects, this can lead to a quenching of the PL [74]. Additionally, as

already suggested to explain the lower PL intensity for RR-P3HT at ambient conditions, the formation of only weakly emissive interchain states like excimer states or interchain electron hole pairs could be formed more efficiently for smaller interchain distances and explain the quenching. All these effects are likely to be stronger in the crystal phase, for which interchain interaction is already higher at ambient pressure because of the well ordered polymer chains.

The emission spectra of the two polymers shift in a very similar manner (figure 5.8 (b)). RR-P3HT from approx. 1.88 eV to 1.43 eV and rra-P3HT from 2.10 eV to 1.65 eV, i.e. both shift almost parallel roughly 450 meV to lower energies from atmospheric pressure up to 8 GPa. Having in mind the analysis of glassy and glassy+β PFO in chapter 4, on the one hand, one might expect planarisation in rra-P3HT under pressure to produce a stronger shift of the PL of rra-P3HT, but, on the other hand, interchain interaction would be expected to cause a stronger shift of the PL of the crystalline RR-P3HT phase. But as we had discussed already for the red-shifts of the PL spectra of PFO in the last chapter, a comparison of the PL shifts with respect to pressure can be misleading.

For most parameters (with the exception of the bond length change) it is conducive for the understanding to compare the energy shifts with respect to the interchain distance. This is more difficult for P3HT than it was for PFO (see chapter 4.4) as RR-P3HT forms two separate phases (crystalline and amorphous) with different compressibilities. While the amorphous phase can be assumed to be approximately isotropic, the compressibility of the crystal depends strongly on the direction of the unit cell of the crystal. For the interchain interaction inside the crystal the interchain distance perpendicular to the thiophene rings (along the π-stacking direction, see figure 5.1) is the most important. We took the change of this interchain distance from the x-ray measurement from Mårdalen et al. [144] for poly (3 octyl thiophene) (P3OT). According to that work the interchain distance δ depends on the pressure p like

$$\delta(p) = (\delta_0 - \delta_1) \exp\left(\frac{\kappa}{\delta_1/\delta_0 - 1} p\right) + \delta_1,$$

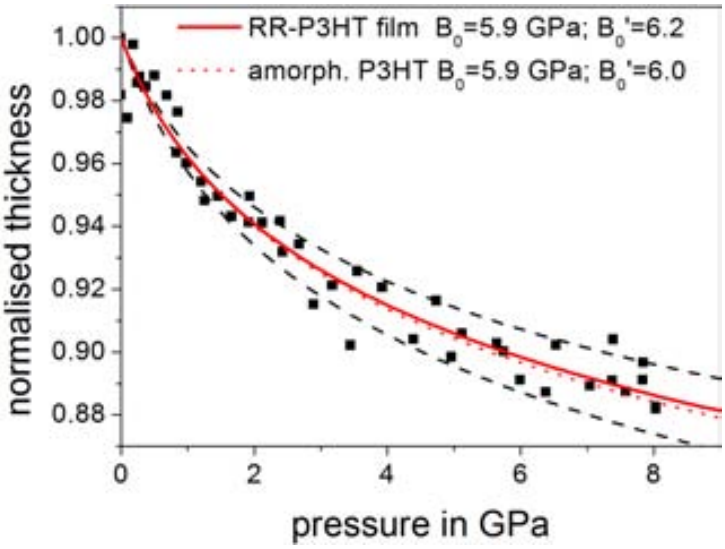

Figure 5.9: Estimated thickness change of a RR-P3HT film with pressure. The red lines correspond to fits using the Murnaghan equation.

where $\delta_0 = 0.38\,\text{nm}$ is the interchain distance at ambient pressure, $\delta_1 = 0.344\,\text{nm}$ the saturated interchain distance and $\kappa = 0.039\,\text{GPa}^{-1}$ the compressibility at ambient pressure. The interchain distance changes according to this formula by 9.1 % at 8 GPa. This value is higher than for the PFO sample (about 8 %). To confirm the higher compressibility of P3HT and to obtain the bulk modulus for the amorphous phase of P3HT, as for PFO in chapter 4.3, photos were taken from a thick (drop cast) RR-P3HT film under hydrostatic pressure and the compression of the polymer film was used to estimate the bulk modulus. The result of the estimated thickness change with pressure is shown in figure 5.9. The fit gives a bulk modulus $B_0 = 5.9(6)\,\text{GPa}$ and $B_0' = 6.2(6)$ following the Murnaghan equation (compare chapter 4.3). The total thickness change at 8 GPa is then estimated to be 11.4 %.

This proves that P3HT is more compressible than PFO and shows that the interchain distance (thickness) of the mainly amorphous film is reduced faster than in the crystalline phase. The crystalline phase can thus be seen as hard agglomerations in a soft amorphous matrix. In order to obtain the bulk modulus of the amorphous matrix the crystallinity has to be estimated. From the fit of the RR-P3HT absorption (figure 5.3) we estimated the 0-0

absorption peak, which stems from the crystalline phase, to have an almost 3 times lower absorbance value than the amorphous phase of RR-P3HT. With an approximately 3 times higher extinction coefficient for the crystalline phase of RR-P3HT than for rra-P3HT[3], we estimate that our samples have a crystallinity of about 10 %. A crystallinity of P3HT (regioregularity 92 %) around 10 % was found by Malik et al. [94]. Other groups measured values between 10 % to 20 % [145, 146]. Much higher crystallinities (higher than 40 %) have been reported [138, 147], but as our material has a low regioregularity (above 90 % [89]) and the sample has not been annealed, a low crystallinity is more likely. Combining the bulk modulus of crystalline RR-P3HT [144] with the approximate 10 % crystallinity of the RR-P3HT samples, the bulk modulus of the amorphous phase of RR-P3HT, also used for rra-P3HT, was estimated to be $B_0 = 5.9\,\mathrm{GPa}$ and $B_0' = 6.0$. As in chapter 4.3, the interchain distance is assumed to be reduced like the thickness of the sample since the applied pressure is hydrostatic and the volume change depends mostly on the reduction of intermolecular distances.

Figure 5.10 shows the same plot as in figure 5.8 (b) but versus the normalised interchain distance, using the bulk modulus of amorphous P3HT for rra-P3HT and the values from Mårdalen et al. [144] for the crystalline RR-P3HT. We use the compressibility of crystalline P3HT rather than that of RR-P3HT because the PL is expected to come from the crystalline phase. This plot gives an almost perfect line over the whole pressure range for rra-P3HT. And also RR-P3HT shows a very linear behaviour for interchain distances over 0.93. If the different emission energy between rra-P3HT and RR-P3HT at ambient pressure is mostly caused by the difference in the planarity of the molecules (the chain being virtually planar in the crystal) rra-P3HT could shift potentially up to 220 meV more than RR-P3HT. The very linear shift shows, as in the case of PFO (chapter 4.4), that any possible planarisation happens gradually in the whole pressure range contrary to reports

[3]Estimated from ellipsometry data for RR-P3HT from Dr. Mariano Campoy Quiles, not shown. They indicate an extinction coefficient of 0.6 for the 0-0 peak of the crystal. Assuming a crystallinity not higher than 50 % this results in an extinction coefficient of at least 1.2. The amorphous rra-P3HT has a maximum extinction coefficient of 0.4 (figure 6.2 (a)).

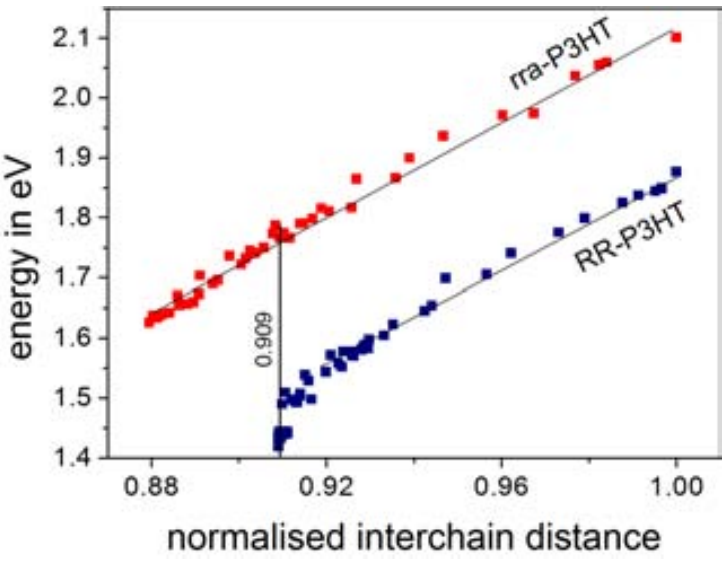

Figure 5.10: 0-0 PL position of RR-P3HT (crystalline phase) and rra-P3HT versus the normalised interchain distance. The black lines are linear fits of the data. Compare to figure 5.8 (b) where the data is plotted versus pressure.

of planarisation within 1 GPa to 2 GPa for other systems [60, 67, 122, 123]. However, the Raman measurements presented in the next section strongly suggest that no planarisation as in PFO occurs in rra-P3HT. While steric effects impede the planarisation of rra-P3HT molecules at ambient pressure, in the case of PFO the molecule is capable of forming more planar conformations (β-phase) and high order (liquid crystals) under certain conditions. This makes it likely that planarisation in rra-P3HT is in general more costly in energy or impeded by steric effects and thus not significant under pressure.

The red-shift of both materials down to a normalised interchain distance of about 0.93 is almost parallel, but then RR-P3HT exhibits a non-linear behaviour for very short interchain distances. Initially, the crystal is still very compressible but at higher pressures, it is likely that the Pauli repulsion between the very close molecules in the crystal becomes important and decreases the compressibility. As simultaneously the PL of RR-P3HT continues to shift strongly with higher pressure, this leads to this stronger shift of the RR-P3HT PL with normalised interchain distance. For PFO we observed a similar but weaker deviation from linearity at short interchain distances.

For the measured pressure range, this does not happen in rra-P3HT as the packing of the polymer chains is lower.

This stronger shift compared to rra-P3HT is most likely caused by interchain interaction which is more effective in the ordered crystal at short distances than in the disordered phase. Therefore, one can estimate from the different shift with the interchain distance how much *more* the PL of the crystalline phase of RR-P3HT red-shifts because of interchain interaction than the one of the amorphous rra-P3HT. At a normalised interchain distance of 0.909, which corresponds to 8 GPa for RR-P3HT crystals and 4.5 GPa for rra-P3HT, the PL of RR-P3HT has shifted the full 450 meV, while the PL of rra-P3HT has shifted approx. 330 meV[4].

The linear and almost parallel shift at longer interchain distances shows that in both materials the effect of interchain interaction is very similar and almost independent from the packing of the material. This means additionally that the effect of higher order in the crystals does not show up, to this point. One should keep in mind for this comparison that the morphologies of the two films are very different, the packing of amorphous films is lower and the interchain distance is actually not as well defined in the amorphous material as in the crystalline phase.

We can now estimate the different contributions which lead to the total PL shifts observed in the pressure measurements. Assuming a similar red-shift due to bond length change as for PPP of 9 meV/GPa [66, 68] (compare chapter 4.2), the PL in the crystalline phase shifts 70 meV because of a pressure induced shortening of bonds and the PL of rra-P3HT only 40 meV. This means, that at least 90 meV of the red-shift of RR-P3HT is caused by interchain interaction. The real value is probably much higher as interchain interaction is likely to cause a red-shift in rra-P3HT as well. This value shows therefore mostly that interchain interaction causes a major shift under pressure in RR-P3HT making it believable that interchain interaction can be almost entirely responsible for the red-shift in both P3HT samples.

[4]Assuming even softer rra-P3HT, as one would get assuming 30 % crystallinity in a RR-P3HT film, the PL shift of rra-P3HT would be slightly lower. The thickness change of 0.909 would be reached for 4.2 GPa giving an approximate shift of 320 meV. This does not change the qualitative argument, which is given here.

	RR-P3HT crystal	rra-P3HT
total shift	450 meV	330 meV
bond length	70 meV	40 meV
planarisation	—	0 meV
interchain interaction	380 meV	290 meV
dielectric environment	—	—

Table 5.1: Estimates of each contribution to the total red-shift of the PL of rra-P3HT and the crystalline part of RR-P3HT after a change of intermolecular distance to 0.909, which corresponds to 8 GPa for RR-P3HT crystals and 4.5 GPa for rra-P3HT.

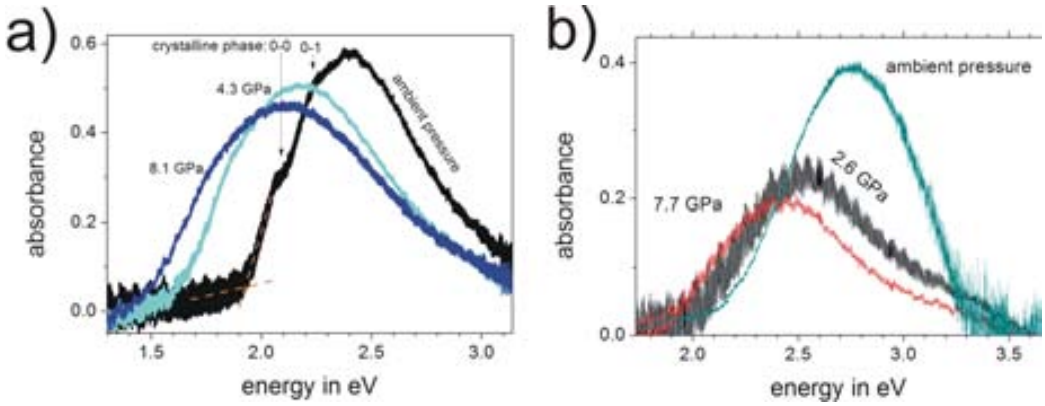

Figure 5.11: Representative absorbance spectra for a) RR-P3HT and b) rra-P3HT under pressure

A tentative assignment of red-shifts to the different parameters is shown in table 5.1, with interchain interaction as the major contribution accounting for 380 meV in RR-P3HT crystals and 290 meV in rra-P3HT.

Before emission occurs, the exciton usually undergoes many transitions. Therefore, the PL of the material gives a picture of just a few sites with low energies or from states which have no or very low transition probabilities for absorption (e.g. excimers). In absorption, chromophores of all conjugation lengths contribute to a similar degree to the spectrum giving the opportunity to further characterise the polymer systems and the origin of the shifts.

The absorption spectra of RR-P3HT and rra-P3HT under high pressure are plotted in figure 5.11. The spectra broaden considerably and even RR-P3HT has a featureless spectrum at elevated pressures. The spectra also

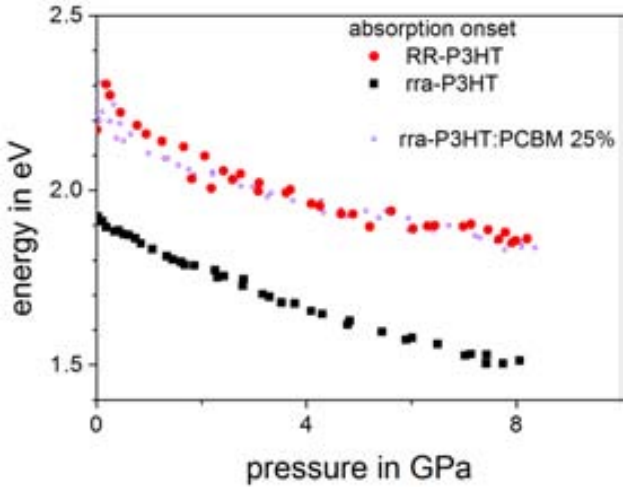

Figure 5.12: Absorption onset of RR-P3HT and rra-P3HT under pressure

shift considerably to lower energies but maintain a high absorption at high energies probably from transitions to electronic states of higher energy, which were previously outside the measured spectral range. As a fit of the data with a series of Gaussians would be very unrealiable, the energy shift was determined with the absorption onset.

The shift of the absorption onset for RR-P3HT and rra-P3HT are shown in figure 5.12. The absorption onset for rra-P3HT is estimated to be between 2.25 eV and 2.3 eV and shifts to 1.85 eV (400 meV to 450 meV) up to 8 GPa. The absorption onset of RR-P3HT shifts from 1.92 eV to 1.49 eV (430 meV). This means, that both materials have a very similar shift and they are also comparable to the shift observed before in PL. This confirms the magnitude of the shift of the energy levels of P3HT observed in the PL measurements.

The determination of the absorption onset for rra-P3HT samples at low pressures is not very precise. The scattering of the data points in the low pressure region is mostly caused by changes in the background and a strong interference signal because of the reflection at the faces of the diamonds of the pressure cell. Therefore, additionally, the fit of the blend of rra-P3HT and 25 % PCBM is shown beforehand (it will be discussed in more detail in the following chapter) to give more confidence to the extracted absorption onset. The quality of the spectra of the blend is higher and we believe the

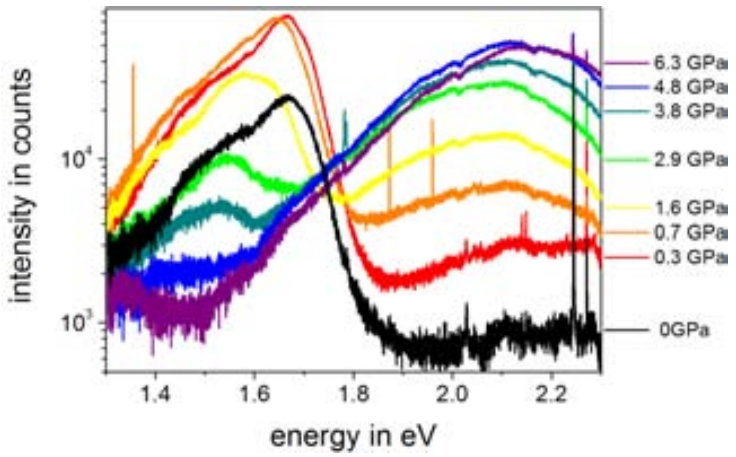

Figure 5.13: Representative PL spectra of PCBM under pressure

absorption onset to be comparable in the two cases. Both show, indeed, very similar values and very similar shifts.

The maximum of absorption cannot easily be determined, but it is a rather safe observation that it shifts also considerably, at least 300 meV. This observation is important because it shows that the shifts do not just occur for the longest conjugation length as probed by PL and the absorption onset, but occurs for all chromophores in a similar manner. As interchain interaction is probably the major contribution to the red-shift, this shows that even in these regions of higher disorder, interchain interaction occurs. It is difficult to quantify this, not only because the shift of the maximum of absorption is difficult to determine, but also because in chain segments with high torsion angles and low conjugation length, planarisation can play a significantly more important role than for higher conjugation lengths.

Apart from the polymer samples, also the PCBM PL was measured under high hydrostatic pressure. The film was spin coated from a chlorobenzene solution on PEDOT:PSS. Some representative spectra under different pressures are shown in figure 5.13. The emission at lower energy stems from PCBM and the one appearing at high pressures at high energies stems from PEDOT:PSS. It is the same emission seen in the P3HT measurement (figure 5.7) and just appears under high pressure. It is therefore clear that this emission cannot be a property of either P3HT or PCBM and the only

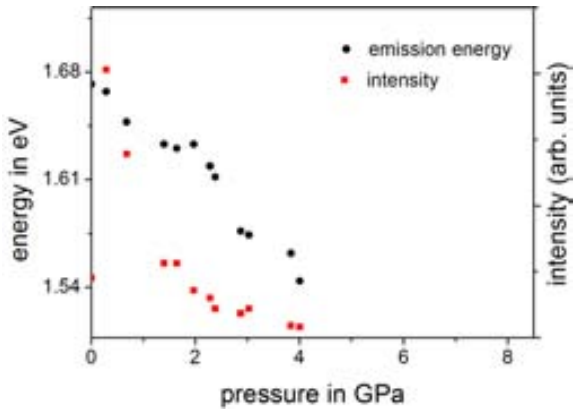

Figure 5.14: High energy onset of emission and PL intensity for PCBM under pressure

common element is PEDOT:PSS, except for the diamond and the pressure medium, which have virtually no PL. Fortunately, for none of the pure materials this PEDOT:PSS emission was much of a problem, either because of their stronger intensity or - as in the case of PCBM - a very different emission energy. Even though the PEDOT:PSS emission made the analysis of the data difficult, it is also a very interesting observation on its own account. We are not aware of any report about an increase in polymer PL under pressure. It is also curious that the PL emission energy does not shift to lower energies. PEDOT:PSS is not a very usual polymer, though. It consists of the negatively charged PSS molecule which acts as a counterion for the holes transported in PEDOT. Possibly the ionic character of this material causes this different behaviour.

We come back to the more ordinary pressure behaviour of the PCBM PL. The emission of PCBM is very weak and strongly quenched under high pressure. After 3 GPa the PCBM PL almost disappears. A fit was avoided because of the noisy signal and the changing shape of the emission. The emission of the highest energy emission peak loses in relative strength. A rough estimation of the centre and height of the highest energy emission peak is shown in figure 5.14. Above pressures of 4 GPa no peak could be identified. Qualitatively the result looks very similar to the polymer results shown so far: a monotonous near-linear red-shift and an exponential decay of the emission

intensity. The shift up to 4 GPa is approx. 130 meV and is thus nearly as much as PFO after 4 GPa (170 meV) and clearly less than P3HT (310 meV). As planarisation cannot occur for PCBM, either the compression/ deformation of the buckyball or the intermolecular interaction has to explain the shift. The former cannot be ruled out, but the bonds have been described as very rigid [148] and even in phenyl- or thiophene-based polymers mostly the inter-ring bond was reported to change [67]. It seems therefore very unlikely that this effect is stronger in a very rigid structure such as PCBM than in the polymers. Furthermore, the experiments of the solution/thin film comparison showed that the intermolecular interaction shifts the PL spectrum 90 meV to lower energies. The high pressure experiments are increasing the interaction even further and an additional shift of a similar magnitude seems reasonable. So even for PCBM, intermolecular interaction seems to be the main reason for the red-shift.

The red-shift of PCBM seems weaker than for the polymers, but in terms of the red-shift with thickness change this might be different. For C_{60} many very different bulk moduli have been reported [148]. A thickness change of roughly 4 % after 4 GPa seems to be reasonable for PCBM. This would make the red-shift for PCBM stronger than for PFO (glassy PFO shifts 110 meV) and comparable to P3HT (RR-P3HT shifts 160 meV). As the molecules are very different, a comparison cannot be made as straightforward as just suggested. But it shows that "weak" is a very relative term and has to be seen in the appropriate context.

5.4 Raman studies under pressure

The effect of stuctural order and pressure on the polymer vibrations was investigated by means of Raman scattering. Raman probes the properties of the molecules on a local level giving, for example, information about the backbone conformation [65]. It is also important for the understanding of the PL spectra of P3HT as the coupling of the electronic states to the vibrational stretching modes determines the spacing between the emission peaks or absorption peaks of the polymer (similar to the case of PFO in chapter 4).

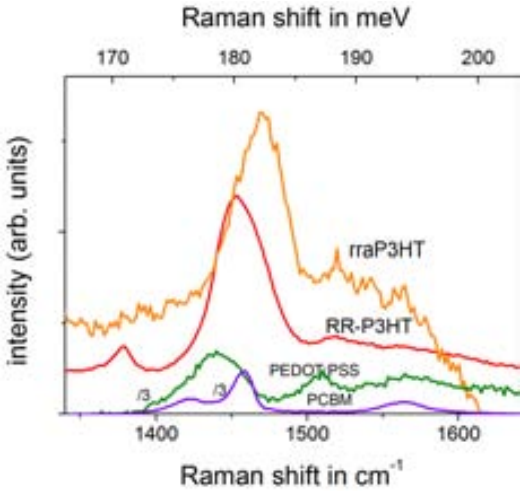

Figure 5.15: Raman spectra of RR-P3HT, rra-P3HT, PCBM and PEDOT:PSS, measured with an excitation energy of 2.54 eV. The background was removed for clarity. The spectra were normalised to the main peak height.

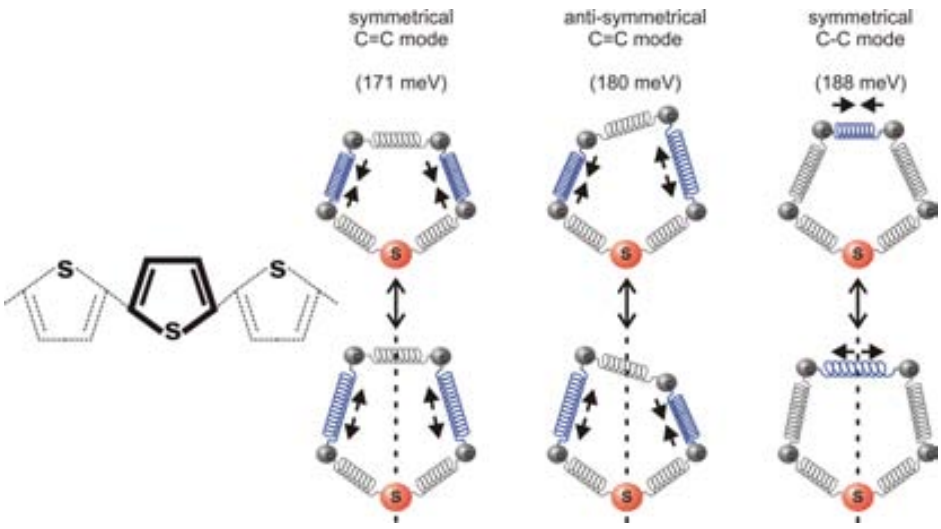

Figure 5.16: Sketch of normal vibrational modes in a thiophene molecule (without H-atoms).

Figure 5.15 shows the Raman spectra of RR-P3HT, rra-P3HT, PCBM and PEDOT:PSS. These were taken with a laser excitation of 2.54 eV. The PL background, which is especially high in the rra-P3HT sample, was removed for clarity. In order to better understand the vibrational modes of P3HT, which give rise to the depicted Raman peaks, a spring-model sketch of a thiophene molecule (without H-atoms) is shown in figure 5.16. The two double bonds have a symmetric and an anti-symmetric normal mode. This symmetry is considered with respect to a rotation of 180° around the vertical dashed line or by mirroring at the plane perpendicular to the page through the dashed line. Because of the sidechain and the interaction between monomers the symmetry is broken and the normal modes are more complex, but essentially the vibrations stem from the modes drawn here for a single thiophene molecule. The P3HT main peak at around 180 meV (1450 cm^{-1}) is attributed to the symmetric stretching vibration of the double bonds of a thiophene ring. The antisymmetric stretching mode of these double bonds becomes manifest in the much smaller peak at around 188 meV (1516 cm^{-1}). The carbon single bond stretching mode of the thiophene ring has an energy of approx. 171 meV (1380 cm^{-1}) [149, 150]. For rra-P3HT this mode also exists and splits into a double peak [108]. In this measurement, however, the strong PL signal does not permit the observation of that mode. The measurement shows that the symmetric C=C energy is to a certain degree sensitive to the planarity of the polymer chain, which affects also the conjugation length, as the Raman peak lies at lower energies for RR-P3HT [151]. The reason for the sensitivity for the planarity of the chain could be connected to a different interaction between the vibrations of neighbouring monomers with different torsion angles between the monomers.

For measurements with 2.54 eV and 2.41 eV (Ar-laser lines), the Raman intensity of P3HT is very strong, because the laser energy lies in the absorption region (see figure 5.3) and resonant Raman scattering occurs. This means that Raman scattering signal increases by many orders of magnitude for vibrations of a chromophore with an electronic transition in approximate resonance with the laser energy [105]. As a result, dispersion in the Raman measurements with the excitation energy occurs, as can be seen in figure 5.17,

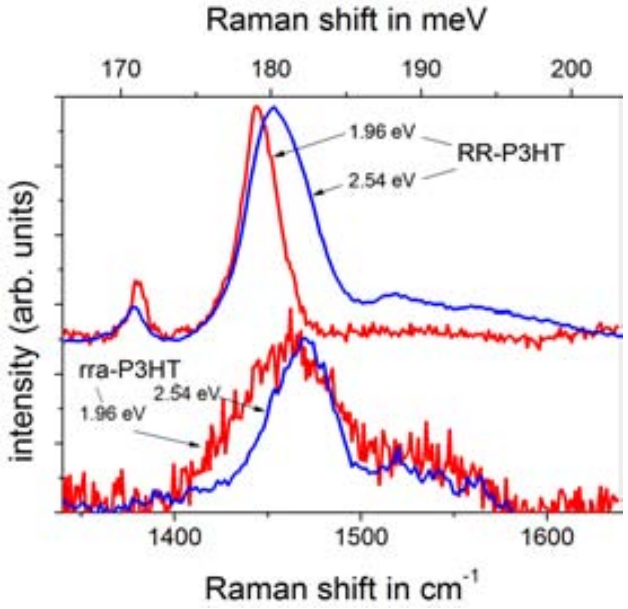

Figure 5.17: Raman spectra of RR-P3HT and rra-P3HT with two different excitation energies: 2.54 eV and 1.96 eV. The background was removed and the spectra (shifted vertically for clarity) normalised to the peak height.

where the Raman spectra for RR-P3HT and rra-P3HT with excitation energies of 2.54 eV and 1.96 eV are compared. As rra-P3HT is out of resonance with the 1.96 eV laser light, all conjugation lengths - also the higher ones - are equally probed. As a result the symmetric C=C peak is very broad for rra-P3HT. In the case of RR-P3HT, which is barely in resonance, predominantly the higher conjugation lengths are probed, and as a result the peak is shifted to lower energies.

Additionally, also the polymer PEDOT:PSS and PCBM were measured under the same conditions (figure 5.15). The Raman peaks of both PEDOT:PSS and PCBM are very weak for green/blue lasers compared to P3HT and play no role in the interpretation of pressure experiments as long as P3HT is present. The Raman peaks of PCBM seen in figure 5.15 are caused by tangential vibrations of the fullerene ball: The so called "pentagonal pinch" mode at around 181 meV (1458 cm^{-1}) corresponds to the tangential displacement of the carbon atoms around each of the pentagons of the fullerene ball [140]. For PEDOT:PSS the main peak at 178 meV

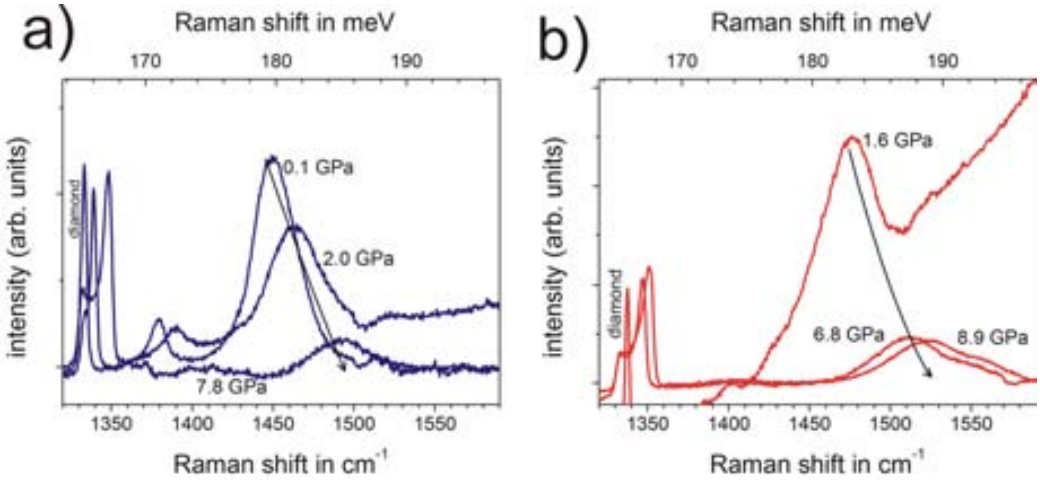

Figure 5.18: Representative Raman spectra of a) RR-P3HT and b) rra-P3HT under pressure; measured with an excitation energy of 2.41 eV

(1434 cm^{-1}) belongs to a C=C double bond stretching mode in the PEDOT molecule [152].

The Raman spectra of the pure polymers were studied also under pressure. Figure 5.18 shows some representative Raman measurements for both RR-P3HT and rra-P3HT under high hydrostatic pressure. The graphs were not normalised to their peak height but shifted in intensity according to their background signal in order to make the comparison easier. The Raman modes broaden under pressure, lose in intensity and strongly shift to higher energies. These are characteristics invariably observed for stretching modes of polymers under pressure [61, 65, 153]. The shift to higher energies is connected with the anharmonic potential of the bonds. The closer the molecules get, the stiffer the bonds become [80]. Therefore, C-C single bonds and C=C double bonds show a similar shift to higher energies in most polymers (often called "hardening" following the common spring model of bonds). In general, the peaks were fitted with Gaussian curves in order to determine their position, while the background from the PL tail observed at high energies in the Raman data was fitted with a polynomial function (usually cubic). As shown above, the higher the planarity of a chain section is, the higher in energy are its stretching vibrations. The resulting Raman peak is a superposition of the peaks of vibrations corresponding to chain sections of different planarity

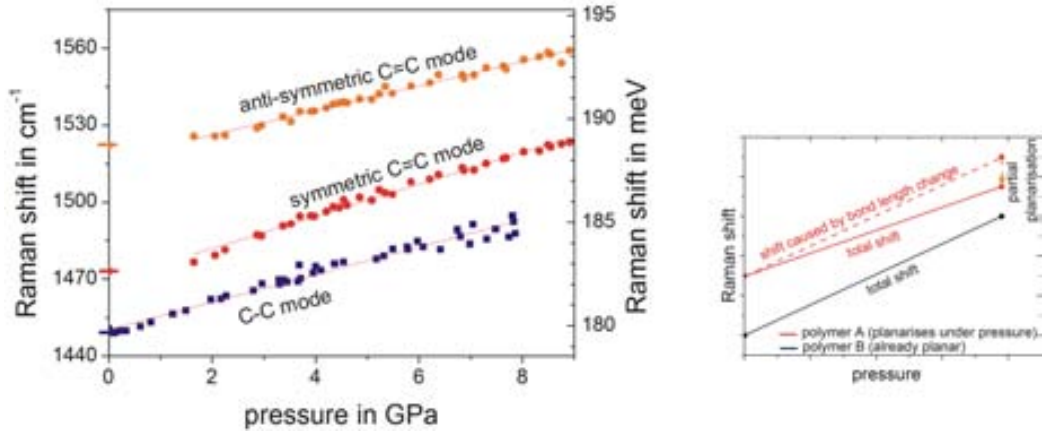

Figure 5.19: left panel: Energies of Raman peaks of RR-P3HT and rra-P3HT versus pressure; right panel: visualisation of how planrisation might affect the Raman shift (see text for details)

and, as a result, different conjugation lengths (even under the here observed resonance conditions). This broadens the Raman peaks and gives them usually a peak shape close to a Gaussian curve. The symmetric double bond mode is clearly asymmetric in shape and for a successful fit a split-Gaussian function was used (different width for left and right side of the peak).

The result of the fit for RR-P3HT and rra-P3HT are plotted versus pressure in the left panel of figure 5.19. The shift is almost linear and very similar in both polymers. The symmetric C=C peak of rra-P3HT shifts from 182.6 meV to 188.2 meV from ambient pressure to 7.8 GPa (approx. 5.6 meV) and for RR-P3HT from 179.7 meV to 185.0 meV (approx. 5.3 meV). The distance between the symmetric C=C peaks remains almost constant (increase of approx. 8 %). Even though most of the shift is not connected to a change in the planarity but shortening of the bond length [80], the relative change between the two materials can still be used to infer changes in the conformation which can affect the peak position.

For example, if polymer *A* were to planarise (higher conjugation length) under high pressure compared to an already planar polymer *B* then both materials would have a very similar shift due to the shortening of the bonds[5],

[5]This assumption is just likely to be true for chemically very similar polymers as for both P3HT types

but polymer *A* would exhibit superimposed a shift to lower energies due to the planarisation (see figure 5.19). Thus, a smaller *total* shift to higher energies could be caused by planarisation.

This argument was similarly used for poly para phenylene (PHP) under pressure. PHP shows no Raman shift for the first 2 GPa because the hardening and the strong planarisation cancel each other out [65]. But in the case of rra-P3HT and RR-P3HT this does not seem to be the case. From the almost constant distance between the two symmetric C=C peaks one can infer that the planarity is affected in both materials in a very similar manner. A possible planarisation in rra-P3HT over the whole pressure range would probably be visible in a decrease of the distance of the two symmetric C=C peaks as in RR-P3HT the polymer chains are already more planar (especially in the crystalline phase). If anything, the slight increase in the peak distance suggests an ordering in RR-P3HT or a *dis*ordering in rra-P3HT.

5.5 Chapter conclusions

In conclusion, this chapter has shown the importance of the conformation of the molecules but especially of the interchain/-molecular interaction when going from isolated molecules with all rotational degrees of freedom to restricted and interacting molecules in a solid film at high pressures. The "solution-to-solid" shift showed that RR-P3HT and rra-P3HT are similar in solution but form very different films. Strong and very similar shifts of the PL and the absorption in RR-P3HT and rra-P3HT were observed under pressure and discussed in detail considering mostly planarisation and interchain interaction as the reasons. The stronger red-shift of the PL with intermolecular distance for RR-P3HT were identified to stem mostly from the increased interchain interaction under pressure. In the previous chapter we could just assume that the unexplained part of the shift is caused by interchain interaction, in this chapter the comparison between the crystalline and the amorphous phase allowed for much clearer evidence and a much more direct determination of the order of magnitude of the red-shift due to interchain interaction. The evidence for a strong red-shift in PL and

absorption caused by interchain interaction was used to justify that most of the red-shift can be explained this way. Also the small molecule PCBM was measured and showed a considerable red-shift under pressure thus confirming the importance of intermolecular interactions.

These experiments of the pure materials raise the question of how this behaviour will change in a blend of P3HT with PCBM and especially of the then created charge transfer state. The charge transfer state energy depends on the energy difference between the LUMO (PCBM/acceptor) and the HOMO (P3HT/donor). It is interesting to see if any possible change in the charge transfer energy can be explained by the changes in the pure materials. This will be discussed in the following chapter.

He would be Montag-plus-Faber, fire plus water, and then, one day, after everything had mixed and simmered and worked away in silence, there would be neither fire nor water, but wine. Out of two separate and opposite things, a third.

Ray Bradbury, **Fahrenheit 451**

6 Effects of mixing on structure and energy levels

The active layer of efficient solar cells up to now usually consists of electron donor and acceptor blends. Blending of appropriate organic semiconductors opens up the possibility for the exciton to undergo a transition to a charge transfer (CT) state, an important intermediate state on the way to charge separation and charge collection at the electrodes (see chapter 2.3.2 for more details). The properties of the charge transfer, such as energy and decay mechanisms, may depend strongly on the morphology of the blend, but also the single components might show very different properties than the ones observed in pure materials. The mixing is studied in this chapter by the blends of P3HT and PCBM, a widely used model system for solar cells [25].

The results of the last chapter, in which P3HT and PCBM were discussed in pure films, are the basis for this chapter. The observed changes of the emission and absorption of the single components upon mixing give information about how the interaction of the two molecules changes conformational and morphological properties of the single components compared to the pure films. Pressure measurements of the blend combine the studies of pure materials under pressure from the last chapter with the studies of the PCBM concentration dependence in the blend. The observed changes in the

PL of the CT state upon mixing and under high pressure give the opportunity to investigate how the CT state energy and its decay can be influenced. This information is important in order to understand the underlying mechanism governing the charge transfer and subsequent charge separation processes.

In this chapter we will discuss the PCBM concentration dependence of the PL intensities and energies of P3HT and the CT state. For the pressure study of the CT state, two blends with different PCBM concentrations were measured. For most of the blends, rra-P3HT was used as the charge transfer state PL has a high intensity and lies in the energy range detectable with a Si detector, but implications for the blends with semi-crystalline RR-P3HT will be also discussed.

6.1 Clustering of PCBM

Beyond the solubility limit of PCBM in a polymer, the formation of PCBM clusters[1] is likely to occur for spin coated samples. The size and crystallinity of these clusters might influence, among other things, the delocalisation and mobility of the exciton or electron. Therefore, it is important to study for which concentrations PCBM clusters form and whether they are crystalline.

In order to know when a crystalline phase of PCBM is formed in rra-P3HT:PCBM blends, we performed differential scanning calorimetry (DSC) measurements[2]. DSC is a technique that allows to determine the energy necessary for heating a sample at a constant rate. This is done by comparison of the sample in a pan with a reference (empty pan), which is heated at the same time and maintained at approximately the same temperature during the heating and/or cooling process. Most especially, DSC is used to determine exothermic and endothermic phase transitions, which can be identified as peaks in the heating-temperature-curves. Their onset marks the transition temperature, their area the energy necessary for the phase transition.

[1]The term “cluster” instead of the more common “aggregate” is used to avoid confusion with the term indicating the delocalisation of electronic states (H-/J- aggregates).

[2]The DSC measurement and analysis was performed by Anne A. Y. Guilbert in the research group of Prof. Jenny Nelson at Imperial College London in a cooperation with our group.

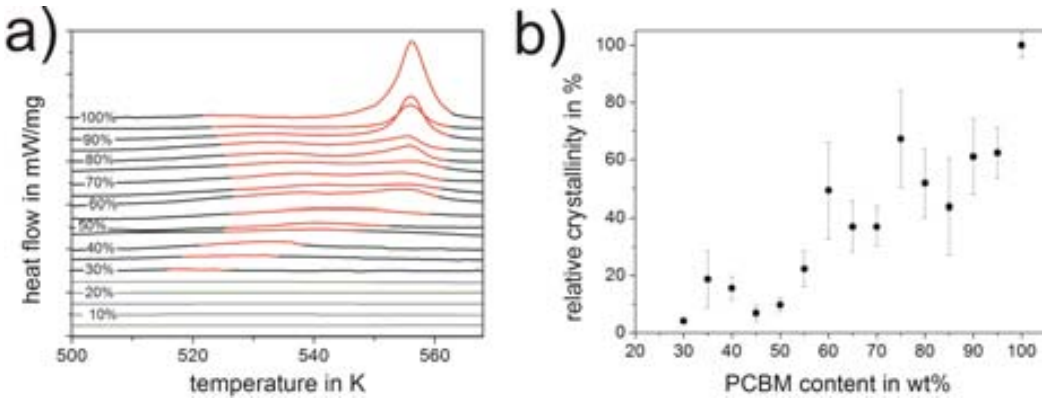

Figure 6.1: DSC measurements of rra-P3HT:PCBM blends for different concentrations of PCBM (a) heating curve showing the melting peak of PCBM (marked red); the heating curves are shifted in y-direction for clarity, (b) relative crystallinity of PCBM

Figure 6.1 (a) shows the heating curves of rra-P3HT:PCBM blends for different PCBM concentrations at a heating rate of 20 K/min. As rra-P3HT is amorphous it does not exhibit any melting peak. Therefore, the observed peaks correspond to the melting of the crystalline PCBM phase. A film of pure PCBM was taken as a reference sample, and the energy for the phase transition was determined. The energy for the phase transition in the blends was then compared to that of the reference sample, yielding the relative crystallinity[3] of the blend sample taking into account the absolute amount of PCBM which is heated in each case.

Figure 6.1 (b) shows that the first crystals can be detected at concentrations of about 30 % PCBM. After this, an approximately linear increase in crystallinity is observed. This does not mean necessarily that below that value PCBM is solved in the rra-P3HT matrix as it is possible that at lower concentrations small amounts of almost amorphous or nanocrystalline clusters form [154, 155], which might be difficult to detect with DSC. This value gives, however, an upper limit for the solubility of PCBM in rra-P3HT. This is in accordance with results by Yin et al. who have reported that PCBM is miscible in the amorphous phase of RR-P3HT up to 20 % PCBM [156].

[3]Even the pure PCBM film is just partially crystalline and the measurement does not give the total crystallinity.

As stronger intermolecular interaction can be expected in the crystalline phase, one can also expect that exciton and/or electron delocalisation/ mobility inside the clusters increases at around 30 % PCBM [56]. This might be accompanied by a change of the optical properties as well, e.g. a shift of the absorption peak in PCBM and the formation of the aggregate peak at 2.9 eV (compare chapter 5.1).

In order to see how the optical properties in such a blended film change, an ellipsometric study[4] was performed on rra-P3HT:PCBM spin coated on a Si substrate for different concentrations of PCBM. The data was fitted employing the Bruggeman[5] effective medium approximation. The approximation describes the complex dielectric function of the blend film combining the complex dielectric functions of its components [109]. The single components are thought of as small (compared to the wavelength) spherical inclusions behaving like the bulk material in terms of their optical properties (no size effects, no interaction between materials). The effective dielectric function of the whole film depends, therefore, mostly on the dielectric function of the single components and on the concentration in volume percent. In the figures and discussion, we refer to the concentration by weight percent as determined during the preparation of the solutions. In the first approach, the fit was performed with the concentration as a free parameter and with fixed dielectric functions based on the measurements of the samples of pure rra-P3HT and PCBM.

Figure 6.2 (a) shows the absorption coefficient[6] for the samples with different PCBM concentrations according to this model. The peak at around 2.8 eV is caused by rra-P3HT, and the strong increase in the ultra-violet region is attributed to PCBM. This property is identical to the absorption of the pure materials as presented in chapter 5.1. As no changes in the materials were allowed, just the intensities change in this model. Consequently, the PCBM peak remains for all concentration at the same position. This is al-

[4]The analysis of the data was performed by Dr. Mariano Campoy-Quiles.

[5]Dirk Anton George Bruggeman (dutch physicist, PhD 1930 in Utrecht)

[6]The absorption coefficient is $\alpha = \frac{4\pi\kappa}{\lambda}$, where κ is the extinction coefficient (the imaginary part of the refractive index) measured with ellipsometry and λ the wavelength in vacuum.

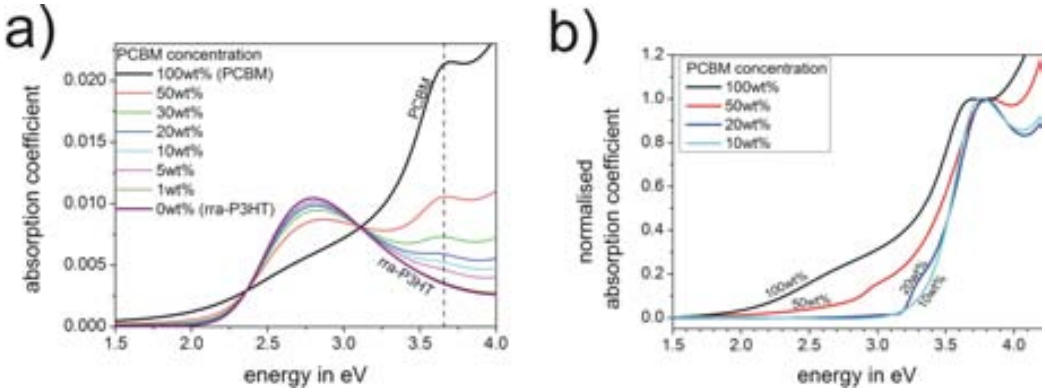

Figure 6.2: Analysis of ellipsometric measurement with the Bruggeman model showing the absorption coefficient of (a) the film assuming dielectric constants as in the pure materials (b) of PCBM when allowing for its dielectric constant to change (fixed concentrations).

ready a good approximation of the real dielectric function, but there remain discrepancies between this model and the experimental data.

In order to improve the fit, we assumed that the dielectric function of (at least) one of the materials did change with blending. Most likely, the dielectric constant of PCBM is different in small clusters or when solved in the P3HT matrix (for which case, strictly speaking, the Bruggeman model is not valid, but it often works nonetheless). Therefore, in the following fit just the parameterised dielectric function of PCBM was allowed to change (the volume concentrations were fixed from the previous fit). The resulting normalised absorption coefficients of PCBM for several concentrations are shown in figure 6.2 (b). For all the blends, the peak at around 3.78 eV remains almost unshifted. This is almost the same position as found in a dilute solution. For pure PCBM, the same peak is shifted to 3.68 eV.

Up to 20 % PCBM no broad absorption peak at 2.9 eV, indicating intermolecular interaction, can be observed. Only for the highest concentration in the blend, 50 % PCBM, there are indications that this absorption peak is formed. Below the concentration for which PCBM crystals were detected by DSC, the absorption coefficient is probably only weakly influenced by PCBM clustering. As mentioned, it is also possible that small clusters have a low crystallinity. This would indicate that a crystalline phase has to be present

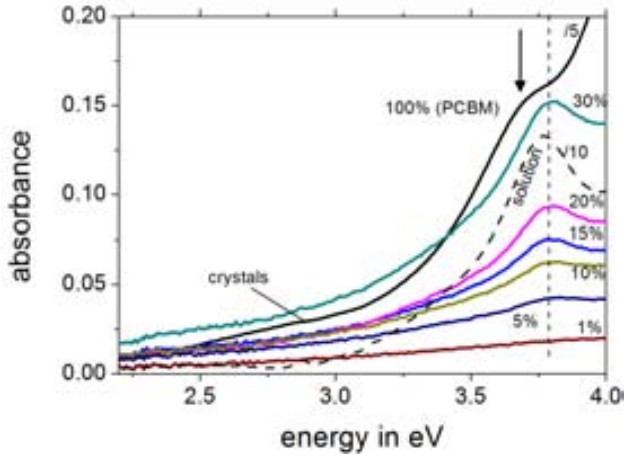

Figure 6.3: Absorbance spectra of PCBM:PMMA films on glass with different concentrations of PCBM, normalised to PCBM concentration. The arrow marks the absorption peak position for the pure PCBM film, the dashed vertical line for the blends.

for an effective intermolecular interaction between PCBM molecules and formation of this peak[7]. The absorption peak at 3.78 eV is obviously not very sensitive to clustering or crystallisation of PCBM even for these relatively high concentrations of PCBM.

In order to investigate whether signs of clustering can be observed below the crystallisation concentration, absorption measurements of PCBM blends with the polymer poly(methyl methacrylate) (PMMA) were performed. In rra-P3HT:PCBM blends the peak at 2.9 eV would be difficult to detect in absorption measurements because of the strong absorption of rra-P3HT. In contrast, PMMA is transparent and has no conjugated electron system for PCBM to interact with, which makes the analysis possible. Even though PCBM might not show the same miscibility behaviour in PMMA as in rra-P3HT, it can help to give indications concerning the clustering of PCBM in an amorphous polymer matrix.

The absorbance spectra of the blends are shown in figure 6.3. The absorption caused by PCBM is very low and can just be seen clearly from 5 % PCBM on. The characteristic absorption peak of PCBM is at approx. 3.79 eV

[7]This will be even clearer later when measurements of pure bisPCBM are presented for which this peak is absent (figure 6.12).

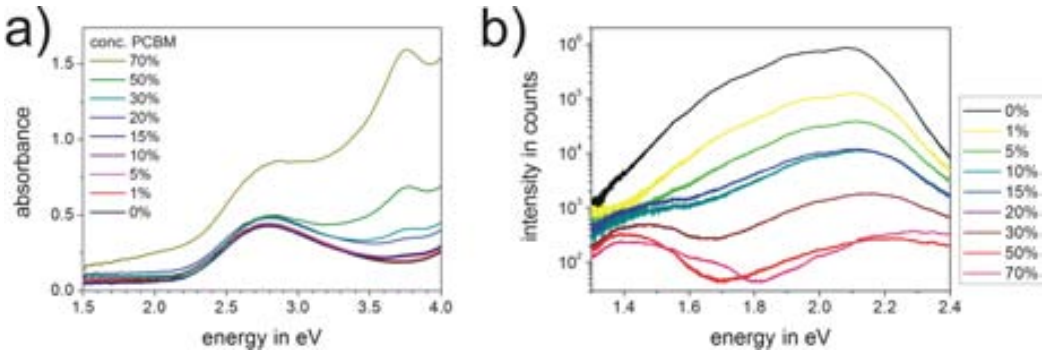

Figure 6.4: rra-P3HT:PCBM for different PCBM concentrations: (a) absorbance spectra; (b) PL spectra

for the blends, which agrees well with the energy of the peak in rra-P3HT blends obtained by the ellipsometry analysis. For higher PCBM concentrations up to 30 % PCBM this peak remains at the same energy and the low energy tail remains also mostly unchanged, i.e. no significant intermolecular interaction was observed. This corroborates the result from the ellipsometry and DSC measurements that any possible clusters below 30 % PCBM do not show significant signs of crystallisation. The PCBM behaves optically as completely dispersed in the PMMA matrix.

The samples were thermally annealed in order to see whether this can induce clustering and crystallisation of the PCBM molecules, which would then lead to an increase in intensity of the 2.9 eV absorption peak. The samples were put on a hot stove at about 400 K (130 °C) for approx. 25 min. The changes in the absorption spectra are almost negligible (and therefore not shown). Probably even at the highest concentration of 30 % no crystallisation could be induced.

6.2 Influence of PCBM concentration on P3HT and on the charge transfer state

We shall continue the discussion about PCBM clustering and crystallisation in this section by investigating the effects of this on the polymer phase and the CT state. It will be interesting to see which changes occur with in-

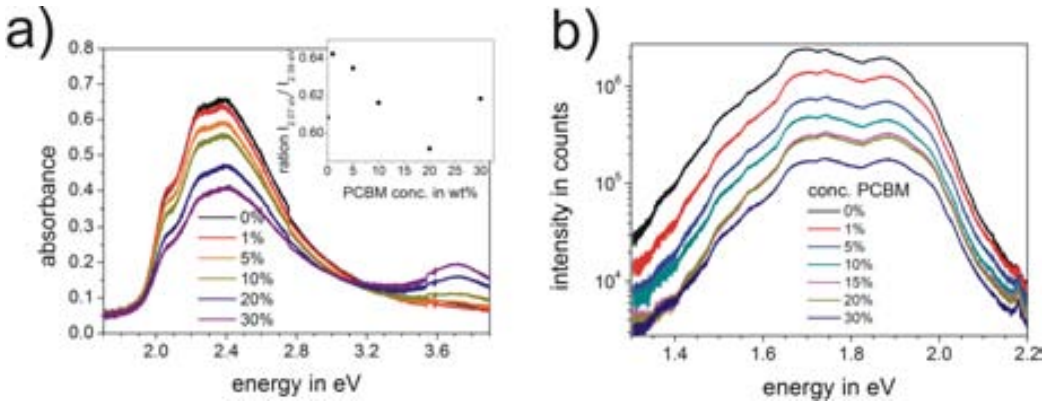

Figure 6.5: RR-P3HT:PCBM for different PCBM concentrations: (a) absorbance spectra with the inset showing the ratio between the absorbance at 2.07 eV and 2.39 eV; (b) PL spectra

creasing PCBM concentration and whether they can be attributed to the dissolved PCBM molecules, to clustering or to crystallisation of PCBM. For this purpose, the systems RR-P3HT:PCBM and rra-P3HT:PCBM were studied in absorption and PL. Additionally to the two PCBM blends, rra-P3HT:bisPCBM blends were measured in PL. bisPCBM has one additional sidechain compared to PCBM, which enhances its solubility in common organic solvents [157]. Its HOMO and LUMO levels are shifted up in energy by about 100 meV to 130 meV [22, 158] compared to PCBM. These differences might influence the morphology and CT state properties in the blends.

Figure 6.4 (a) shows the absorption spectra for rra-P3HT:PCBM for different concentrations of PCBM. The absorption is mostly a superposition of the absorption of the single components. The polymer absorption peak at around 2.8 eV is qualitatively the same as in the pure material. Confirming the ellipsometry measurements in rra-P3HT:PCBM blends, the absorption peak at around 3.76 eV remains stationary up to 70 % PCBM.

The absorbance spectra of RR-P3HT:PCBM for different PCBM concentrations are shown in figure 6.5 (a). In contrast to the other blends with a polymer concentration of 20 g/l, for these samples, the *total* concentration was fixed to 20 g/l. This does not change the concentrations in the film, but affects the film thickness and results in a decreasing P3HT absorption peak

with increasing PCBM concentration. Apart from the intensity changes, very few changes happen with the mixing of RR-P3HT and PCBM. Above all the absorption peak at 2.07 eV is visible even at high PCBM concentration and the ratio between the intensity at 2.07 eV (absorption by crystals) and the intensity at 2.39 eV (absorption predominantly by amorphous phase) is changing very little and not systematically (inset to figure 6.5 (a)), which even shows that PCBM is not impeding the crystallisation of RR-P3HT during spin coating. This is understandable as the mobility for PCBM will be pretty high in the solvent compared to P3HT and PCBM would thus not disturb the polymer chains approaching each other.

The high crystallinity is surprising when compared to results in the literature. For the same blend, a much lower crystallinity has been reported compared to the pure film [108]. A possible reason for the discrepancy is the use of relatively low concentrations in our experiments, which allows the molecules to phase separate better during the drying process. The sample is thus better comparable with annealed samples which show almost the same crystallinity of RR-P3HT as in the film of pure RR-P3HT [108].

The PL spectra for RR-P3HT:PCBM blends in figure 6.5 (b) show a strong decrease in the PL intensity of over one order of magnitude with increasing PCBM concentration. This PL quenching is caused by the formation of CT states, which are not visible in absorption measurements. This observation shows for this sample that the two components are well mixed, thus ensuring a charge transfer for most excitons at high PCBM concentrations. Intercalation of PCBM inside the crystalline phase of RR-P3HT is not possible as there is insufficient space between the sidechains [159] and so the intimate mixing occurs only in the amorphous phase. Thus, the quenching caused by the charge transfer competes with the migration of the exciton to the crystalline regions. Once the exciton is in a more crystalline area, it is likely to decay radiatively. Because also the crystal absorbs light and because not all excitons close the crystalline phase will be captured by PCBM, this explains why even at high PCBM concentrations the polymer still exhibits a certain PL emission.

The situation is different in the amorphous rra-P3HT for which very in-

timate blends with PCBM are possible [156, 160]. The strong intermixing becomes obvious in the PL spectra of rra-P3HT:PCBM in figure 6.4 (b). In these blends the PL is quenched much more efficiently than in the RR-P3HT blends. The remaining emission is at higher energies and stems probably from high energy sites in the polymer. The low energy emission stems from the CT state (around 1.4 eV for 50 % PCBM). In RR-P3HT this peak is not visible in our accessible spectral range. Tvingstedt et al. showed with electroluminescence (EL) measurements that the CT state in RR-P3HT:PCBM has an energy of around 1.0 eV [53]. Since the acceptor molecule is the same, one may expect that the difference in the CT energy reflects the difference between the donor(P3HT) HOMO levels (see sketch of energy level in figure 2.4). If we assume that bimolecular recombination occurs between the PCBM and the *crystalline* phase of RR-P3HT, and that the HOMO-LUMO gap in RR-P3HT is symmetrically reduced compared to rra-P3HT, one can expect the CT peak of RR-P3HT:PCBM to lie approx. 100 meV lower than the one for rra-P3HT:PCBM (about half the difference between the 0-0 emission peaks of the pure polymers). However, the difference between the CT state energies is much bigger than this. EL measurements give often lower energies than CT emission after photoexcitation because EL comes only from low energy sites [161]. Additionally, the interface itself plays an important role. The order of the polymer at the interface can significantly influence the charge transfer state [24]. In this case, it might be that PCBM induces greater disorder in rra-P3HT than in the crystalline phase of RR-P3HT, thus increasing the band gap in the polymer and the energy of the CT state.

The intensity of the CT emission is small: for 50 % PCBM, it is almost 4000 times smaller than that of the pure polymer (for a comparable absorption by the polymer). Assuming that almost all excitons undergo the charge transfer, one realises that the radiative recombination would be an almost insignificant decay channel of the CT state, if it did not serve us to gain so much information about the CT state properties. It has been reported using transient absorption measurements that about 70 % of the CT states undergo a geminate recombination to the ground state in this system [162]. This seems unreasonably high and probably fails to take into account other

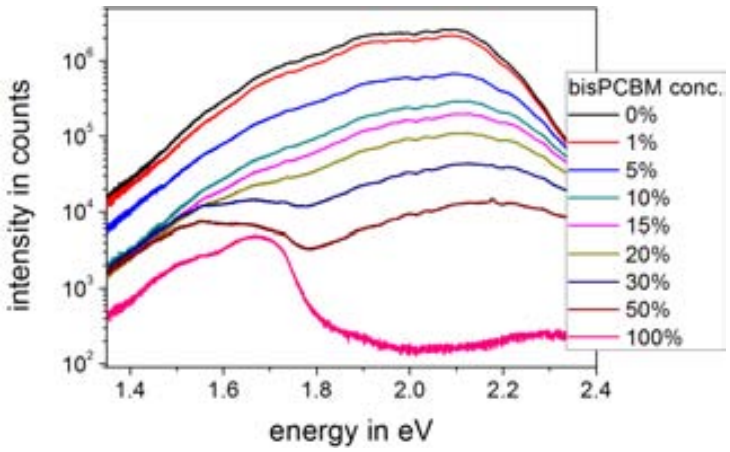

Figure 6.6: PL spectra of rra-P3HT:bisPCBM for different bisPCBM concentrations

decay channels. At high PCBM concentrations (70 %), another peak appears in the spectrum at about 1.7 eV, the emission energy for PCBM (compare figure 5.4). For rra-P3HT:PCBM, it is likely that at such high concentrations of PCBM, the absorption of PCBM is very significant and not all PCBM emission is quenched by the polymer because the pure PCBM phase forms areas that are bigger than the exciton diffusion length.

The PL spectra of rra-P3HT:bisPCBM blends for different bisPCBM concentration are shown in figure 6.6. The spectra are very similar to the one of the rra-P3HT:PCBM blends, but in the bisPCBM blends the concentrations at which the fullerene PL appears (visible at around 1.7 eV) is much lower (at most 20 %). This might be connected to the different isomers of bis-PCBM present, each with different HOMO and LUMO levels. This can lead to energetic disorder in the bisPCBM phase and concomitant trapping of the exciton at low-energy isomers. As a result, bisPCBM PL in films with bisPCBM clusters would be very inefficiently quenched.

For the quantitative analysis of all the spectra, the pure polymer samples were fitted with a series of Gaussian peaks. Within each series, the Gaussian peaks have equal width and equal spacing between the peaks of around 170 meV to 175 meV. A peak at high energies probably connected to emission from high energy chromophores in the polymer was necessary for a good fit.

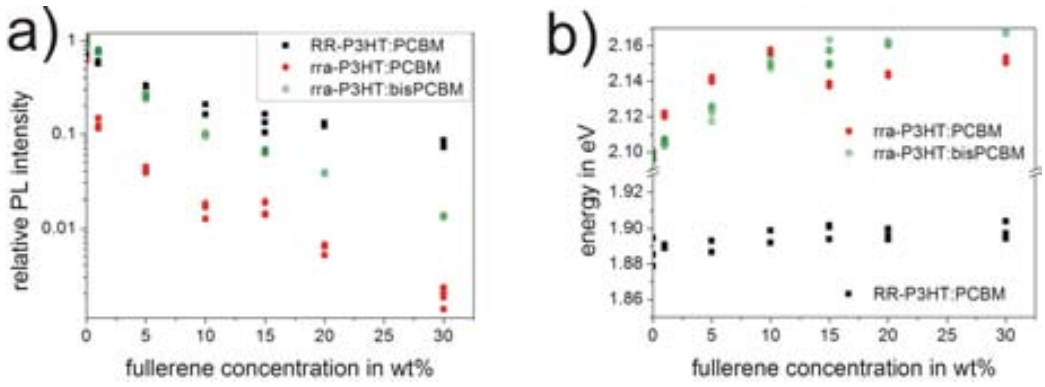

Figure 6.7: Results of PL fits for RR-P3HT:PCBM, rra-P3HT:PCBM and rra-P3HT:bisPCBM blends for different concentrations: (a) the normalised integrated intensity of the polymer PL, (b) the energy of the 0-0 transition peak of the polymer PL.

For blends, it was assumed that the form of the polymer emission remains unchanged. This means that the area-ratios of the peaks and the distance between the peaks remained fixed. This assumption is not obvious, for a higher disorder in blends might slightly change the relative peak intensities (Huang-Rhys factor), but as the fits work well in the high energy region (0-1 and 0-0 emission peaks), this effect seems to be small. The emission of the PL as a whole was allowed to shift and it was necessary to allow for a change of the width of the peaks. A fit just with this Franck-Condon-like emission cannot explain well the low energy region of the spectra of the rra-P3HT samples because of the increasing importance of the charge transfer emission. Therefore, an additional Gaussian peak in the low energy region was introduced to account for the CT peak.

For bisPCBM blends, the bisPCBM, emission was taken into account by modeling the emission in pure bisPCBM films. Just the area of this emission was allowed to change. Even with this strong restriction, a clear distinction between CT peak and bisPCBM emission was not possible for low bisPCBM concentrations because CT PL, bisPCBM PL and polymer PL all overlap. Therefore, the CT state will just be discussed for the concentration of 50 % at the end of this section.

Figure 6.7 shows (a) the intensity ascribed to the pure polymer emission.

The polymer PL intensity in rra-P3HT:PCBM blends decreases by almost 3 orders of magnitude up to fullerene concentrations of 30 %. This is a much stronger decrease than for the RR-P3HT:PCBM and rra-P3HT:bisPCBM blends. The intensity decrease for rra-P3HT:PCBM blends is especially strong for the first percent of PCBM. This shows how efficiently the smallest amount of PCBM quenches the PL of the polymer. As mentioned, the higher PL intensity in RR-P3HT:PCBM is a result of the stronger phase separation (with pure P3HT crystals).

For rra-P3HT:bisPCBM, the likeliest explanation for the weaker PL quenching with increasing bisPCBM concentration is, that at very low concentrations clustering of the bisPCBM molecules occurs. This is in agreement with a recent study by Guilbert et al. about RR-P3HT blends with multiple adduct fullerenes [163], which shows the greater tendency of bisPCBM to form clusters after spin coating. This clustering might be enhanced by a better solubility of bisPCBM in chlorobenzene, giving the molecules more time to diffuse and accumulate into clusters during the drying process. However, it seems that this clustering happens because of the kinetics of the drying process during spin-coating rather than complete immiscibility of bisPCBM and rra-P3HT, for at higher concentrations still very efficient PL quenching occurs.

Two other reasons for the less efficient PL quenching should be taken into account as well: Because of the higher molecular weight of bisPCBM a fraction of 0.2 fewer[8] bisPCBM molecules are in the blend for the same concentration by weight. However, this cannot explain quantitatively the lower quenching. A less efficient charge transfer might also cause less PL quenching, but as the charge transfer is a very fast process, without any competing processes, even a much slower CT transition than for rra-P3HT:PCBM blends (but still fast compared to the exciton diffusion) would leave the charge transfer efficiency virtually unaffected.

Concerning the 0-0 emission energy, one can see in figure 6.7 (b) that for the rra-P3HT blends the emission energy (centre of gaussian peak of the fits) shifts approx. 60 meV to higher energies up to a fullerene concentration

[8]PCBM has a molecular weight of 911 g/mol, bisPCBM of 1102 g/mol.

of about 15 %, after which this shift seems to saturate. Contrary to that, the RR-P3HT blends show no appreciable shift with PCBM concentration (the approx. 10 meV to 20 meV blue-shift is in the order of the scatter of the data points). This can just be explained by a strong intermixing between the rra-P3HT and the PCBM molecules. There are two possibilities as to why this shift occurs in rra-P3HT blends but not in the RR-P3HT blends. One is that the PCBM introduces conformational disorder in the polymer backbone [164], leading to a lower conjugation length. The other possibility is that because of the good mixing of the two components, the charge transfer becomes a competing process to the exciton migration to low energy chromophores. This means, that the polymer itself exhibits the same distribution of conjugation lengths as in the pure polymer sample, but the chromophores with the highest conjugation lengths do no emit any longer because most excitons undergo a charge transfer first [42]. As the crystalline phase of RR-P3HT does not contain any fullerene, probably neither effect would lead to a shift in RR-P3HT PL. It should be possible to distinguish between these two theories in absorption experiments.

For this purpose we revisit the absorption data shown for rra-P3HT:PCBM in figure 6.5 (a). A Franck-Condon fit of the absorption peak showed very little changes (not shown), suggesting that the polymer absorption does not shift as a whole to higher energies. However, a fit of a featureless absorption in this manner is not very precise and a disturbing influence of PCBM molecules would affect most probably more the chromophores of the highest conjugation lengths, which are the ones responsible for the PL. Therefore, the low energy absorption onset was determined by the intercept of the straight lines describing the low energy slope of the absorption and the low energy background signal. This can be seen in figure 6.8 (a) for two curves, one for 0 % and one for 50 % PCBM. The resulting position of the absorption onset versus the PCBM concentration is shown in figure 6.8 (b). The absorption onset shifts approx. 50 meV to higher energies for PCBM concentration up to 50 %, which is almost the same shift as observed in the PL. We note that scattering caused by PCBM clustering would appear to shift the edge to *lower* energies. This shift clearly indicates that there really

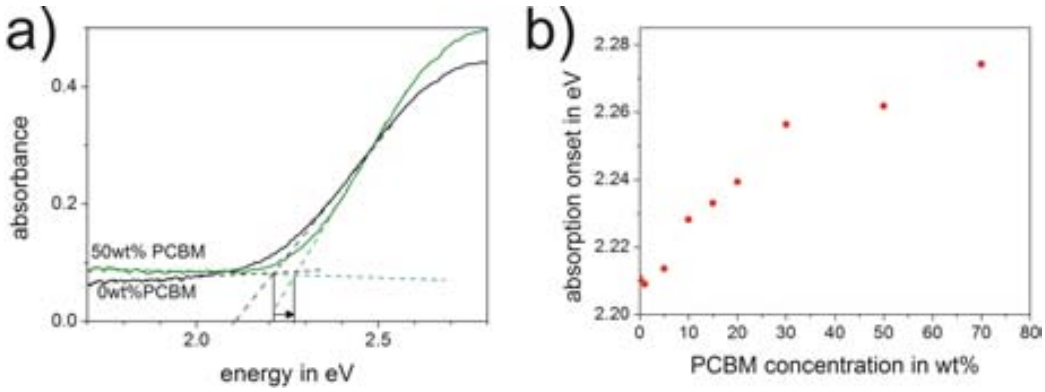

Figure 6.8: (a) Two rra-P3HT:PCBM absorbance spectra showing the determination of the absorption onset of rra-P3HT, (b) absorption onset of rra-P3HT as a function of the PCBM concentration

is a change in the absorption and that the change in the PL is mostly caused by a change of the low energy chromophores. The more gradual shift in the absorption onset energy in contrast to the strong initial increase in the PL is probably just caused by the lower sensitivity of the measurement method because of a lower selectivity of contributing chromophores.

The analysis of the PL measurement indicates that the blue-shift in the polymer PL saturates at around 15 % because the solubility limit of fullerenes in rra-P3HT is reached and clusters start to grow at a faster rate. Fullerenes which are in clusters cannot contribute to any increase in disorder. This is, at least, a lower limit of the solubility as it is possible that the saturation is reached only for the disordering effect, not of the solubility of PCBM in the rra-P3HT matrix.

The dependence of the CT emission intensity on PCBM concentration can give information about the efficiency of charge separation. In this context it can also give information about the formation of clustering. The CT emission intensity in the PCBM blends increases to its maximum value for very low PCBM concentrations, as seen in figure 6.9 (a), and for PCBM concentrations between 15 % and 50 % decreases again. This can be seen best by the solid line representing the average value of the measurements for each concentration. The initial increase has to exist as the CT emission is 0 at 0 % PCBM. It gives confidence into the fit that it can qualitatively show this, even though

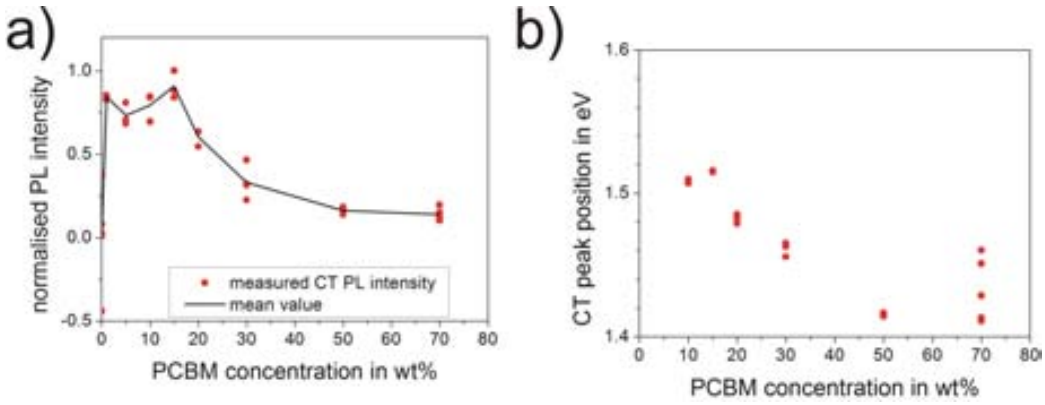

Figure 6.9: Results of the fits of the PL of rra-P3HT:PCBM blends: (a) integrated intensity of the CT state and (b) its emission energy

the very strong polymer PL overlaps with the CT PL (the pure rra-P3HT emission is about 500 times stronger than the most intense CT emission of the blends) and it is possible that for low PCBM concentrations the value is overestimated. The initial increase of the CT emission intensity can be clearly attributed to the, at first, very efficient formation of the CT states (compare to the concomitant efficient PL quenching shown in figure 6.7 (a)), which should be linear with PCBM concentration for sufficiently dispersed PCBM molecules. In the experiment, no further increase happens between 1 % and 15 % PCBM even though the polymer PL is further quenched. For even higher PCBM concentrations the CT intensity decreases strongly. This is not an effect of less light absorbing P3HT molecules in the blend as the absorption of the P3HT is very similar in all blends (figure 6.4 (a)). It instead means that less CT states decay radiatively for higher PCBM concentrations.

There are various decay mechanisms for a CT-state (see figure 6.10): charge separation (with the transition rate k_{CS}), radiative geminate recombination to the ground state (k_{GR}) and back transfer to the polymer triplet state (nonradiative geminate recombination, $k_{triplet}$) [26, 165]. The triplet CT state, from which the transition to the polymer triplet state occurs, can form because of only weak electronic coupling in the CT state [26]. The question is which of these decay channels can gain or lose in strength with increasing PCBM cluster size. At this point the available data is not suffi-

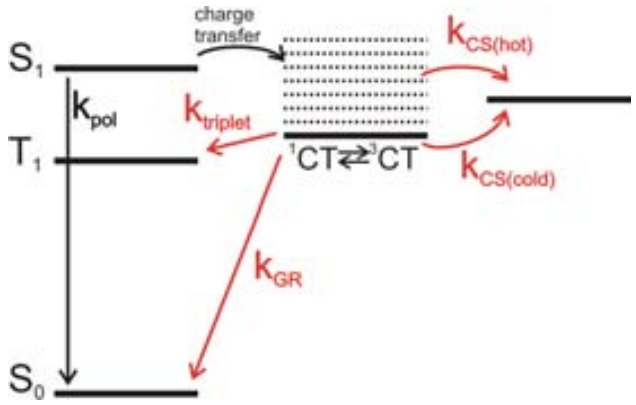

Figure 6.10: Sketch of the decay channels of the CT state. Transition rates of the transition to polymer triplet state ($k_{triplet}$), of radiative geminate recombination to the polymer ground state (k_{GR}) and of charge separation of a hot ($k_{CS(hot}$) and cold ($k_{CS(cold)}$) charge transfer state. Also shown are the charge transfer itself and the recombination of the exciton in the polymer with the transition rate k_{pol}. Based on [26, 165].

cient to exclude any of these channels. But it seems most reasonable that, above all, the efficiency of the charge separation changes with the size of the clusters [161].

The charge separation can be described well with the Onsager[9] theory [166]. According to this theory, the exciton dissociates when the electron-hole distance exceeds the dissociation distance (or capture radius) for which the binding energy equals the thermal energy kT. Even if the mean distance between hole and electron is smaller than the dissociation distance, the CT exciton can break up with a certain probability [26]. The electron is more likely to escape the interface than the hole because of its higher mobility. But for single PCBM molecules or very small clusters the electron cannot escape as long as the cluster is smaller than the dissociation distance [161], which is in the range between 4 nm [26] and 15 nm [21]. (The outer ball diameter of a fullerene molecule is 1.0 nm [140]). But for growing clusters the cluster size exceeds the dissociation distance and charge separation is possible, even if the electron still cannot move very far. The size of the PCBM cluster [21] and the local mobility [57] have been suggested to greatly assist the charge

[9]Lars Onsager (1903, Kristiania, Norway - 1976, Coral Gables, Florida, USA)

separation process. Additionally, the increasing dielectric constant will lower the dissociation distance [166] allowing even more electrons and maybe even holes to escape the interface. Therefore, a growing cluster size with a possible greater delocalisation of the electron can make it more likely for the CT state to overcome its Coulomb attraction and thus lead to an increased charge separation rate [56].

The intensity drop from 15 % to 50 % PCBM can, thus, be explained best with a low increase of formation of CT states (as can be estimated by the PL quenching in figure 6.7) accompanied by an increasing amount of clusters for which charge separation is possible and becomes more likely with growing size.

The increased probability for a charge separation lowers the probability for all the other decay channels, including the observed radiative geminate recombination. This is probably true for both the hot exciton and the cold exciton picture of charge separation (see chapter 2.3.2 and figure 6.10). Assuming that the change in the CT PL is representative for the quenching of these other decay channels, one can estimate how much more efficient the charge separation becomes. The CT peak intensity drops roughly 75 % for an increase in PCBM concentration from 15 % to 50 %. This means that 75 % of the initially formed CT states (which is almost equal to the number of initially formed excitons in P3HT) undergo the charge separation. This is just a rough estimate, but shows the great importance the size of the clusters probably has for the charge separation. This result agrees well with the suggested begin of the formation of clusters at about 15 % PCBM, deduced from the blue-shift of the polymer PL.

For the energy of the CT state, a very different behaviour is seen than for the polymer emission. Figure 6.9 (b) shows the energy of the CT emission for rra-P3HT:PCBM blends represented by the Gaussian peak. At PCBM concentrations below 10 % the emission is unfortunately too weak for a precise determination of the peak position[10]. The position of the CT emission shows a clear red-shift of 100 meV for PCBM concentrations increasing from 10 %

[10] In these cases, the CT peak was fixed to 1.51 eV in order to still estimate the emission intensities.

to 50 %. The red-shift for increasing PCBM concentration has been observed before in PF8DTBT:PCBM by Loi et al. [167] and in PF10DTBT:PCBM[11] by Veldman et al. [56] and was attributed to the change of the dielectric constant of the medium with increasing PCBM concentration.

Veldman et al. estimated the Gibbs[12] free energy change with the charge transfer and explained thus most of the observed shift [56]. The dependence of the CT state energy with the average dielectric constant $\langle \epsilon_\mathrm{r} \rangle$ is according to this

$$E_\mathrm{CT}\left(\langle \epsilon_\mathrm{r} \rangle\right) = E_0 - Z\left(1 - \frac{1}{\langle \epsilon_\mathrm{r} \rangle}\right)\left(\frac{1}{r^+} - \frac{1}{r^-}\right) - \frac{Z}{\langle \epsilon_\mathrm{r} \rangle}\left(\frac{2}{R_\mathrm{CC}}\right),$$

where E_0 a system dependent energy and $Z = e^2/\left(8\pi\epsilon_0\right)$, e being the electron charge and ϵ_0 the vacuum permittivity. R_CC is the centre-to-centre distance of the ions, r^+ the effective radius of the cation (charged P3HT) and r^- the effective radius of the anion (charged PCBM) [56], which are model dependent parameters[13] [168]. The first part of the right hand side of the equation takes into account the solvation energy of the ions in the dielectric environment, i.e. the lowering of the energy levels by the polarisation energy, and the second part the Coulomb attraction of the ions, i.e. the binding energy of the CT state [168]. The dependence of the CT state energy on the dielectric environment might be stronger than for Frenkel excitons because the electron and the hole are spatially separated. In their estimation, Veldman et al. show that the change of the polarisation energy with the dielectric constant outweighs the reduction of the exciton binding energy. This would give an approximately linear shift with the PCBM concentration. Assuming a dielectric constant of rra-P3HT of 3.0 [169] and of PCBM of 4 [170] and their respective densities of about 1100 kg/m^3 [171] and 1500 kg/m^3 [155], the dielectric constant is expected to change approximately from 3.08 to 3.42

[11] PFnDTBT stands for poly[2,7-(9,9- dialkylfluorene)-alt-5,5-(4',7'-di-2-thienyl-2',1',3'-benzothiadi- azole)] , n being the number of carbons of the alkyl substituents. This means it contains both a fluorene part and a thiophene part.

[12] Josiah Willard Gibbs (1839, New Haven, Connecticut, USA - 1903, New Haven)

[13] r^+ =0.45 nm, r^- =0.56 nm [56] and R_CC =2.0 nm were used, but the energy change with the dielectric constant is not very sensitive to these values.

with an increase in PCBM concentration from 10 % to 50 % and a concomitant CT red-shift of 70 meV.

Instead of only the global dielectric constant, as suggested by Veldman et al. [56], the local dielectric environment could be more important. In this case one would have to consider more the change of the dielectric environment within a few nanometres as analogous to the case of excitons [37]. A stronger decrease of the CT energy would be observed in this case from the onset of clustering until the clusters reach a certain size.

Another effect which could cause a red-shift in the CT energy is a stronger delocalisation of the electron in the PCBM clusters. This can be influenced both by the crystallinity, as mentioned by Tvingstedt et al. [53], and by the size of the clusters. In the previous section we showed that the absorption spectra evidenced little intermolecular interaction for low PCBM concentrations and no shift of the absorption peak. The effect on the delocalisation of a single electron (though bound by Coulombic forces to the polymer/fullerene interface) might still be significant. In this case an increasing delocalisation would lower the LUMO level in PCBM and lead thus to a smaller energy gap between the LUMO(acceptor) and the HOMO(donor), i.e. a red-shift of the CT PL. This would be stronger for bigger clusters (or higher crystallinity) which would then qualitatively explain the gradual red-shift for concentrations higher than the solubility limit of PCBM in rra-P3HT.

The delocalisation theory cannot be distinguished from the theory considering mostly the local dielectric environment without some quantitative estimates. But If the global dielectric constant is responsible, then a shift should be observable before clustering occurs. For the shift with the increasing dielectric constant, the amount of PCBM is decisive; for the delocalisation/local dielectric environment, the size of the clusters. Favouring the latter explanation, the fits suggests that the red-shift begins only after 15 %. Unfortunately, as mentioned, below 10 % PCBM the CT emission can be clearly seen, but the position cannot be reliably determined. But in accordance with our fit, Veldman et al. observed the onset of the CT red-shift for PF10DTBT:PCBM between 10 % and 20 % PCBM [56].

On the other hand, the red-shift continues up to 50 % PCBM. At 30 %,

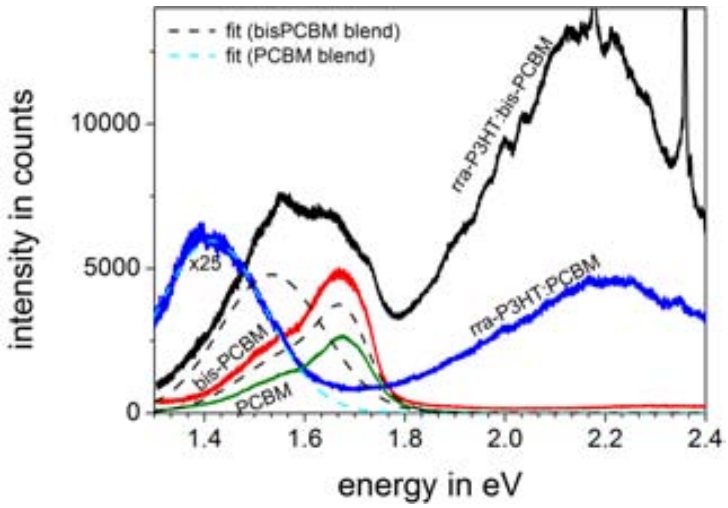

Figure 6.11: PL spectra of rra-P3H:PCBM and rra-P3HT:bisPCBM for fullerene concentrations of 50 %. Also shown are the PL spectra of PCBM and bisPCBM. The fits of the low energy region of the two blends are represented by the dashed lines.

the clusters are already very big (clearly bigger than the dissociation distance of the CT state as shown above) and no cluster size dependent red-shift is expected. Even though a higher crystallinity (DSC measurement) could explain why beyond 30 % the delocalisation increases and red-shifts the emission, the observation favours the explanation of the global dielectric constant.

Further evidence as to which is the reason for the red-shift might be found in the energy for the CT state of rra-P3HT:bisPCBM. As mentioned, the measurements with bisPCBM did not allow for a precise analysis of the CT state at low concentrations. Therefore, we will only compare rra-P3HT:PCBM and rra-P3HT:bisPCBM for a fullerene concentration of 50 %.

Figure 6.11 shows the PL spectra of the two blends in direct comparison. The PCBM and bisPCBM PL spectra and the fits for the CT peaks and bisPCBM emission of the blends are also shown in the same graph. The CT state of the rra-P3HT:bisPCBM blend has an energy of approx. 1.54 eV as compared to 1.41 eV for the rra-P3HT:PCBM blend. This difference is practically identical to the difference in the LUMO levels of the two fullerenes [158]. This shows, as expected, that the LUMO level is a decisive factor for the en-

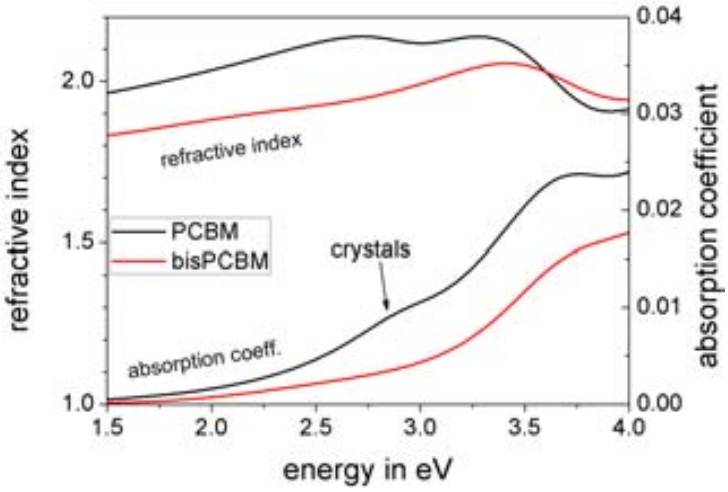

Figure 6.12: Refractive index and absorption coefficient of pure PCBM and bisPCBM

ergy difference of the CT states of the two blends. This translate also directly to a 150 meV higher open circuit voltage [88] in devices with bisPCBM.

Apart from the LUMO level also the morphology of bisPCBM is quite different. Figure 6.12 shows the comparison of the refractive index and absorption coefficient (calculated from the extinction coefficient) of PCBM and bisPCBM on a quartz substrate as obtained from ellipsometry measurements[14]. It shows that bisPCBM films are different with respect to PCBM in two important aspects: they have lower density and they do not crystallise. The former can be seen in the roughly 0.1 lower refractive index and the lower absorption coefficient; the latter in the missing peak at 2.9 eV. Both can be explained by assuming that the additional sidechain has a very disturbing influence on the packing and ordering of bisPCBM. The lack of crystallinity is supported by the fact that bisPCBM does not show any melting peak in DSC measurements [163].

With this we estimate the dielectric constant of bisPCBM to be around 3.6, which should lead in the blend to a dielectric constant of 3.3 compared to 3.42 for PCBM. The higher dielectric constant in the PCBM blend is

[14]Measurement and analysis performed by Anne A. Y. Guilbert and Dr. Mariano Campoy-Quiles.

expected to lead to an additional red-shift of the CT emission of approx. 30 meV compared to the bisPCBM blend. As this change is rather low, this theory is compatible with the observed difference between CT emission energies.

This means that the effect of fullerene crystallinity on the CT emission energy has to be equally low or non-existent in order to be compatible with the measurements. This seems to rule out that increasing crystallinity of PCBM can be the main reason for a red-shift in the CT emission with increasing PCBM concentration.

In summary of the experiments with increasing fullerene concentration, the blends of rra-P3HT:PCBM and rra-P3HT:bisPCBM showed that the fullerenes induce disorder in the polymer and thus cause a blue-shift in their PL emission. The quenching of the CT emission in rra-P3HT:PCBM was explained with an increased charge separation with growing PCBM cluster size. From the concentration dependence of these two effects the formation of clusters was inferred between 15 % and 20 % PCBM. This is lower than the concentration for which first PCBM crystals could be detected, which either means that the DSC measurements and optical measurements were not sensitive enough to detect the small amounts of nanocrystalline PCBM directly, or that up to 30 % PCBM forms clusters with very low crystallinity. The observed red-shift of the CT state is most likely caused predominantly by the increase of the dielectric constant with mixing. A higher electron delocalisation because of growing clusters combined with a higher crystallinity for bigger clusters might be an alternative explanation or, at least, a contributing effect. It was shown that crystallinity alone has only a small effect on the CT energy.

6.3 Influence of temperature

In the measurements at low temperature for the pure polymer samples (chapter 4.1 and chapter 5.2) the emission peaks were getting narrower and the spectra red-shifted. The graphs for a rra-P3HT:PCBM blend with 50 % PCBM at ambient temperature and at 77 K in figure 6.13 show, to the con-

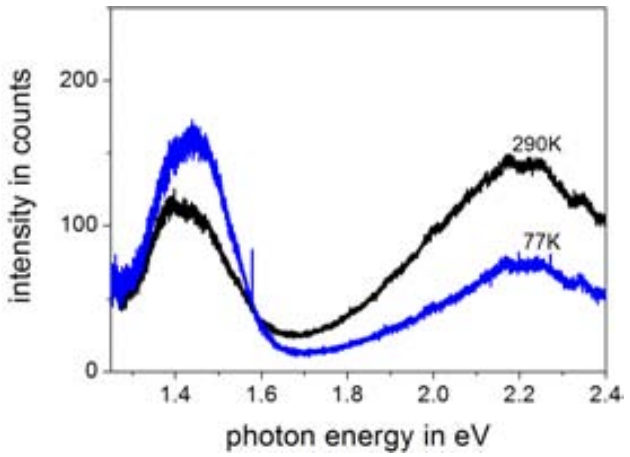

Figure 6.13: PL spectra of rra-P3HT:PCBM with 50 % PCBM at ambient temperature and at 77 K.

trary, that no big changes can be seen for the CT emission peak. It has been suggested that the broad CT peak reflects the distribution of distances between the hole and the electron in each pair [21]. This measurement suggests that this distance is not very sensitive to changes of temperature. However, the intensity increase of the CT PL with cooling is quite significant. As even at room temperature almost all excitons undergo the charge transfer, the most probable explanation for the increased intensity is a more likely radiative geminate recombination rate for a CT state with lowering the temperature. This could be caused by the lower transition rate of non-radiative channels at low temperatures. Alternatively, this observation could also be connected to a less efficient charge separation, which in this case would point to a thermally assisted charge separation. This is a hint that the charge separation occurs in general from the "cold" CT state (see figure 2.4) as in the "hot" exciton picture the energy for the charge separation comes from the surplus energy after the charge transfer, not from thermal energy.

6.4 Blends under high hydrostatic pressure

Most of the discussion in this section will be centred around the CT state. We used PL measurements of rra-P3HT:PCBM under pressure in order to

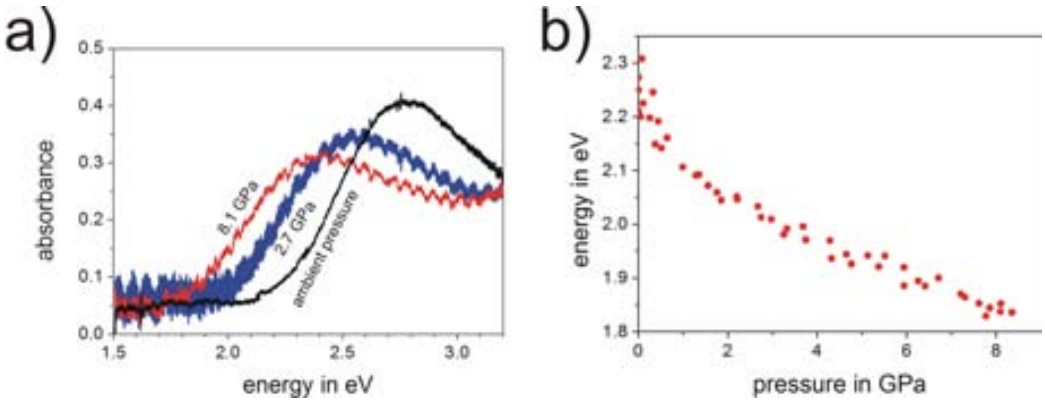

Figure 6.14: (a) Representative absorbance spectra of rra-P3HT:PCBM with 25 % PCBM, (b) energy shift of the absorption with pressure

understand better by which parameters the energy of the CT state and the charge separation can be influenced. Before we can understand the changes of the CT state, we have to find out if the polymer changes its pressure behaviour significantly compared to the pure materials. We have seen small changes in the absorption of the polymer with increasing PCBM concentration, and in the previous chapter, we observed that interchain interaction is an important mechanism for the energy shift under pressure in the pure polymer. With much of the PCBM finely dispersed in the amorphous rra-P3HT, efficient interchain interaction might be inhibited. As the absorption in blends consists mostly of the superposition of the absorption of the different single components, the measurement of absorption under pressure is thus very useful for the investigation of the changes in the polymer energy levels in blends with PCBM.

Figure 6.14 (a) shows some representative absorption spectra of a rra-P3HT:PCBM blend with 25 % PCBM under hydrostatic pressure. The spectra show a red-shift and a broadening with pressure, as for the pure polymer material (compare figure 5.11). Figure 6.14 (b) shows the result of the determination of the absorption onset up to 8 GPa. The shift of this absorption onset is very similar to the one of the pure material (as was shown in figure 5.12). This clearly shows that the mechanisms which cause the shift in the pure material are qualitative and quantitatively comparable to those in the

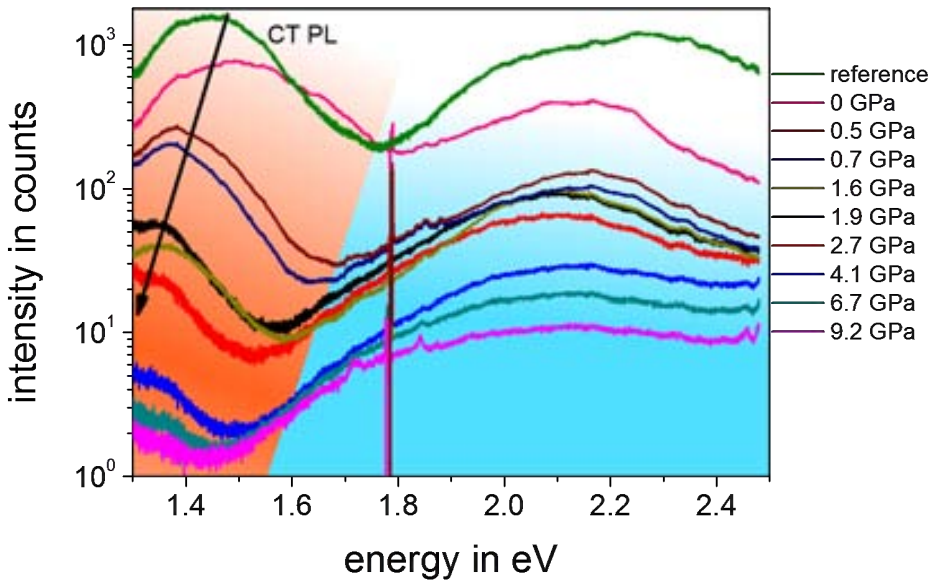

Figure 6.15: Representative examples of the PL of a rra-P3HT:PCBM blend with 50 % PCBM under hydrostatic pressure. On the left the CT peak can be seen to red-shift and get quenched.

blend. Especially, it suggests that the PCBM molecules do not significantly change the interchain interaction between P3HT chains. For RR-P3HT similar results can be expected. The amorphous phase will behave in this sense very similarly to rra-P3HT and the crystalline phase will also behave as the pure material as no intercalation occurs in the crystals.

The PL spectra under high pressure are useful to observe the changes of the CT PL under high hydrostatic pressure. Figure 6.15 shows examples of the PL of a rra-P3HT:PCBM blend with 50 % PCBM. The measurement was performed with cryogenically loaded liquid helium as a pressure transmitting medium, which assures that no chemical reaction with the sample can occur. This sample could be introduced into the pressure cell without any PEDOT:PSS layer (which means that no PL attributed to PEDOT:PSS appears). In most measurements the ruby gave a very strong PL signal at about 1.78 eV. It was partially removed by subtracting a ruby spectrum from the measurements. Apart from the ruby peak, the spectra show the polymer emission on the high energy side. We associate this with high energy sites in the polymer, possibly from trapped excitons. The CT peak on the

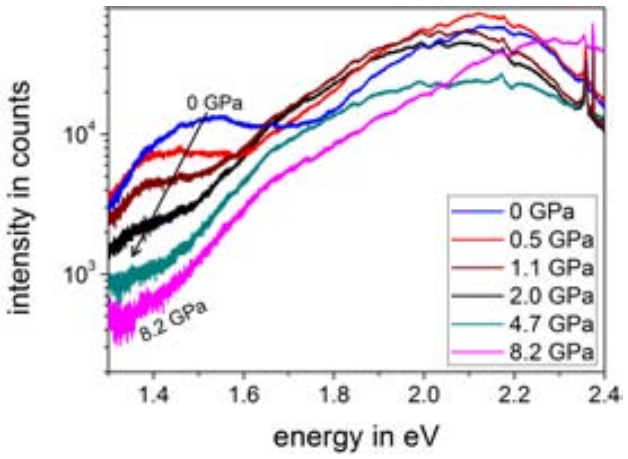

Figure 6.16: Representatives examples of the PL of a rra-P3HT:PCBM blend with 25 % PCBM under hydrostatic pressure.

low energy side decreases in intensity and red-shifts with pressure. It is not clear whether the usual broadening of peaks also occurs. The measurement is unfortunately limited by the range of the Si detector to energies above 1.3 eV, but up to 3 GPa to 4 GPa about half the peak can still be seen which allows for a quantitative analysis up to that point. Beyond this, one can just assume from the graphs that the quenching and red-shifts continues in a similar manner.

In order to observe if there is a concentration dependence of the behaviour of the CT peak under pressure and to see the PL of the polymer simultaneously with the CT peak, a blend with less PCBM was also measured under pressure. Figure 6.16 shows PL spectra for some pressures of a rra-P3HT:PCBM blend with 25 % PCBM. This measurement was performed again in the common manner with a PEDOT:PSS layer and methanol:ethanol as a pressure transmitting medium. For low pressures, the spectra exhibit on the high energy side the pure polymer PL. At higher pressures, the PL gets quenched as we observed before for the pure samples, and at the highest pressure of 8.2 GPa mostly the PEDOT:PSS emission remains. At the low energy side the CT peak can be seen. The CT PL red-shifts and gets quenched like in the sample with 50 % PCBM. At pressure beyond about 2 GPa no CT PL can be observed any longer because of its weak intensity. The CT PL be-

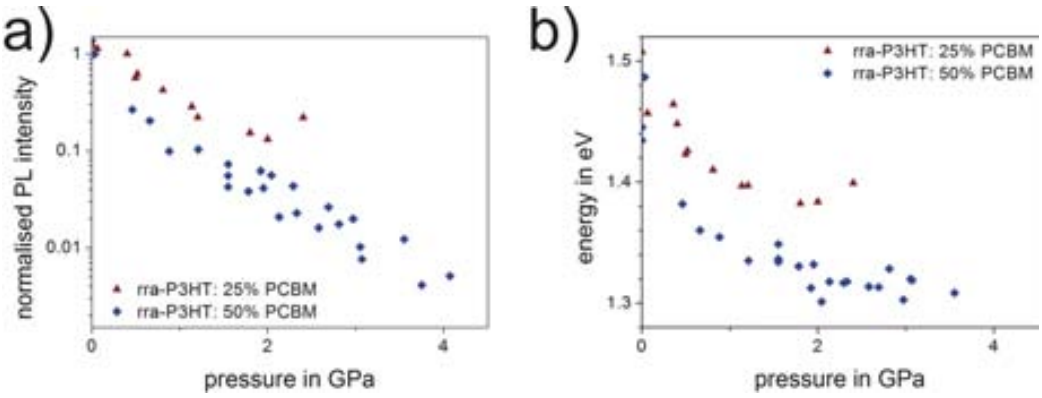

Figure 6.17: Fits of the CT PL for blends of 25 % and 50 % under hydrostatic pressure: (a) normalised intensity; (b) centre energy of the CT peak

haviour at this lower PCBM concentration does not qualitatively differ from the one for 50 %.

For a quantitative analysis, a simple fit of the spectra was performed. The fit of the CT peak was done with one Gaussian peak, the high energy emission was described with another Gaussian peak. In the case of 25 % PCBM, for low pressures also the unquenched (low energy) polymer PL was taken into account assuming it shifts like in the case of pure P3HT (see chapter 5.3). This was necessary in order to fit the CT peak in a reasonable manner because of the overlap of both emissions.

The normalised emission intensities of the CT state for both 25 % and 50 % PCBM are shown in figure 6.17 (a). The CT PL intensities of both blends decrease in a roughly exponential manner with pressure; the CT emission of the blend with 50 % PCBM shows quenching by over 2 orders of magnitude. In figure 6.17 (b) the energy of the CT state (centre of the Gaussian peak) is shown for both the blend of 25 % and 50 % PCBM. As expected from figure 6.7, the CT state of the blend with 25 % PCBM is at slightly higher energies than the one with 50 % and this distance seems to be maintained also under pressure up to at least 2 GPa. The CT state red-shifts these first two gigapascals about 120 meV. Like for the pure materials the shift is significantly stronger in the beginning. The energy shift is roughly between the energy shifts of the pure materials after 2 GPa, rra-P3HT with 200 meV and

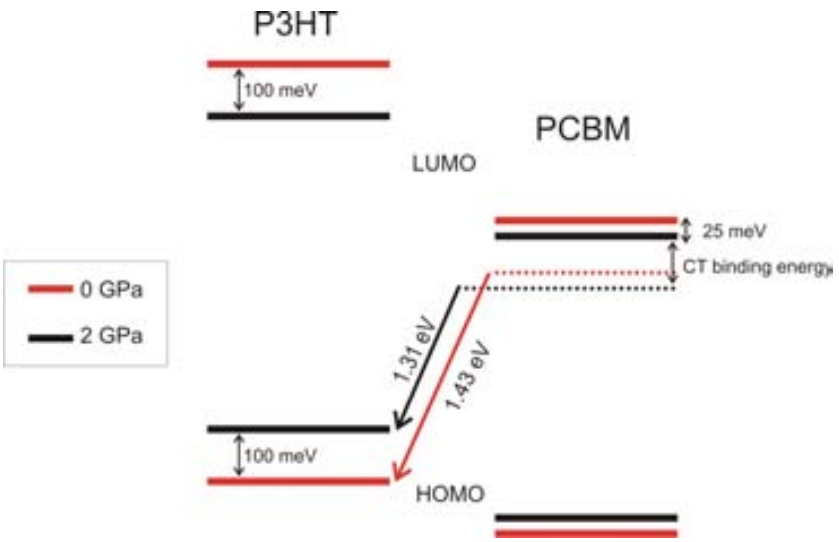

Figure 6.18: Sketch of an energy diagram, showing the shifts of the HOMO and LUMO levels caused by the pressure increase from 0 GPa to 2 GPa. The sketch visualises the possible connexion between the PL red-shift of the pure materials and the one of the CT state.

PCBM 50 meV.

A direct comparison between the shifts in the pure materials and that of the CT state is difficult as the exciton and the CT state are quite different species. The aggregate state which forms in the pure materials for strong intermolecular interaction does not exist for the CT state. However, the transition energies of the excitons under pressure depend largely on the HOMO and LUMO splitting (as well as the mixing of the different excitations) [71]. As the energy of the CT depends on the HOMO (donor) and LUMO (acceptor) levels, probably the splitting of these states due to intermolecular interaction will have comparable effects on the CT state energy. As an estimate it seems therefore plausible to assume that the intermolecular effects which change the exciton transition energies cause similar effects in the CT energy. This seems to be confirmed by the fact that the CT energy shift is roughly the average of the shifts of the excitonic transitions in the pure materials. This would be expected to occur under the assumption that the reduction of the band gap of the pure materials is due to a symmetric shift of the HOMO and LUMO levels under pressure. This idea is depicted

in an energy level sketch in figure 6.18.

It seems reasonable to assume that the CT energy red-shifts for very similar reason as the exciton energy in the pure materials, i.e. mostly intermolecular interaction changing the energy states in the pure materials. But one can also expect the interaction between P3HT chains and the PCBM molecules to change, affecting the order and thus the energy levels at the interface. As mentioned, the distance between electron and hole affects the exciton energy. A closer electron-hole proximity would also lower the CT energy. However, these changes are relatively small. One can expect that CT states are located at the interface where PCBM molecules and P3HT-chains are in direct contact, i.e. as close as the Pauli repulsion allows. Under pressure the changes of the distance (a few percent of a nanometre) will therefore be very low in comparison to the delocalisation of the electron and the hole. It is thus not likely that the CT state is affected by the closer proximity of the hole and the electron.

It was shown that, contrary to the exciton energy, the CT energy is likely to depend on the dielectric constant. Assuming roughly the same change in the dielectric constant with pressure as for PFO (at most 6 % up to 2 GPa, compare chapter 4.3), one can expect the dielectric constant to increase from about 3.4 to at most 3.6 up to 2 GPa for the blend with 50 % PCBM. This would result in an additional red-shift of 30 meV to the ones attributable to changes in exciton energy. This shift is very small and it agrees with the assumption that the shift of the HOMO and LUMO levels in the pure materials are the major cause of the shift.

Regarding the quenching, a very different quenching mechanism has to be responsible than in pure materials. The CT state is trapped at the interface and not very mobile. This makes trapping at defects, as it can happen for the exciton, very unlikely. As trapping by structural defect and by charge transfer depend in the same manner on the migration of the exciton, it is also not likely that pressure inhibits the charge transfer, which would lead to fewer CT states and thus also to less CT PL. It is therefore likely that other decay channels for the CT state open up or increase in strength. The possible decay channels for the CT state are depicted in figure 6.10. As mentioned

before, geminate recombination of the (triplet) CT state to the triplet exciton ($k_{triplet}$) is a possible decay channel. The triplet state in RR-P3HT is around 1.35 eV [172, 173]. In rra-P3HT it can be expected to lie slightly higher than the singlet states because of a similar but much weaker dependence (caused by stronger localisation of the triplet states) on the effective conjugation length [173]. This means, that the energy of the triplet state would be probably in the same range as the CT state energy. In case the triplet state energy decreases more strongly than the CT state energy under pressure, this transition would be activated and become more likely with increasing energy difference between the two states. This way the CT PL (k_{GR}) would be quenched. It would also more importantly lead to a lower charge separation rate ($k_{CS(cold)}$). This mechanism is probably not applicable for RR-P3HT because of the much lower CT energy [174].

Another possibility would be to assume that the quenching occurs because of an increase in the charge separation rate (k_{CS}). This would most likely be connected with a higher delocalisation/mobility of the charges. We suggested that the higher delocalisation of the electron in PCBM with increasing PCBM concentration can be the reason for the strong decrease in the CT PL. Under pressure this could be enhanced. Additionally, the shorter interchain distance in P3HT also increase the mobility of the hole as we showed by the PL quenching under pressure for pure rra-P3HT. Also the dissociation distance is lowered with an increasing dielectric constant as mentioned in the last section. Thus, pressure might assist both the escape of the hole and the electron from the interface and thus increase the rate of the charge separation, which would lead to quenching. RR-P3HT has high mobilities in the crystalline phase [175] and this would explain the good charge separation usually observed in RR-P3HT:PCBM blends as simulated by Deibel et al. by assuming a delocalisation of the hole over several monomers of P3HT [57]. If interchain interaction is enhanced in RR-P3HT crystals, it could strongly affect the charge separation efficiency.

6.5 Chapter conclusions

In this chapter the effects of the blending of P3HT and PCBM have been studied. With increasing concentration of PCBM, the charge transfer (CT) state in rra-P3HT:PCBM blends was shown to red-shift and its emission to get quenched. The increasing dielectric constant is likely to be the major cause of the red-shift. The higher delocalisation of the electron in bigger and more crystalline clusters (lowering of fullerene LUMO level) might additionally contribute to the red-shift. The increased delocalisation of the electron in bigger clusters in the order of the charge transfer dissociation distance was suggested to lead to a higher charge separation rate. We interpreted from this that PCBM molecules are dispersed in the amorphous rra-P3HT matrix up to 15 % of PCBM. We also showed in this context that PCBM seems to have a disturbing influence on the P3HT chain in the amorphous region, blue-shifting PL and absorption of the polymer. Similar results were obtained for the amorphous bisPCBM with the difference that the lower PL quenching suggests some clustering at very low bisPCBM concentrations. Differential Scanning Calorimetry and ellipsometric measurements of rra-P3HT:PCBM blends showed that these initially formed PCBM clusters show no signs of crystallisation or strong intermolecular interaction until 30 % PCBM. This indicates a low crystallinity or nanocrystalline morphology in the PCBM clusters.

We measured PL of two blends of rra-p3HT:PCBM with concentration of 25 % and 50 % PCBM under hydrostatic pressure. The CT state was shown to red-shift about 120 meV up to 2 GPa. It is likely that this shift stems mostly from the shift of the HOMO and LUMO levels in P3HT and PCBM. For the quenching of the charge transfer PL with pressure different explanations were discussed. It was suggested in this context that a higher delocalisation as caused by a higher intermolecular interaction, be it in the PCBM or P3HT, can greatly enhance the charge separation efficiency.

We demonstrated in this chapter the importance of the morphology especially of the PCBM phase when blending P3HT with PCBM. The charge separation and thus the efficiency in real working solar cells are likely to

depend on local mobility/delocalisation of the charges. This also suggests that order and crystallinity are very important for efficient quantum yields in solar cells.

Any one whose disposition leads him to attach more weight to unexplained difficulties than to the explanation of a certain number of facts will certainly reject my theory.

Charles Darwin, **The Origin Of Species**

7

Conclusions and Outlook

The aim of this work is to understand how different mechanisms influence the optical and electronic properties in organic semiconductors. In this chapter, we will summarise the key results of this endeavour and discuss subsequently their implications for the design of molecules and the active layer in optoelectronic devices. And as no work is ever truly finished, we give also suggestions for future work on the subject. A more detailed summary of the experiments and results can be found at the end of the respective chapters.

In this work, PL and absorption properties of the organic semiconductors PFO, rra-P3HT, RR-P3HT and PCBM have been systematically studied in solution, thin films (ambient and low temperature) and high hydrostatic pressure. Additionally, the blends RR-P3HT:PCBM, rra-P3HT:PCBM and rra-P3HT:bisPCBM have been investigated for different fullerene concentrations and rra-P3HT:PCBM under high pressure, mostly with the purpose to understand how this affects the charge transfer (CT) state properties. For the explanation of the energy changes and differences in these experiments, four parameters were used - bond length, planarity, intermolecular interaction and the dielectric environment. In high pressure experiments, these parameters could be changed gradually and in a controlled fashion, making high pressure a powerful tool estimating the contributions of the different parameters to the observed energy shift in the optical spectra.

	PFO, glassy	PFO, gl.+β	RR-P3HT	rra-P3HT	PCBM (4 GPa)
total shift	275 meV	225 meV	450 meV	450 meV	130 meV
bond length	70 meV	70 meV	70 meV	70 meV	$<$ 30 meV
planarisation	50 meV	—	—	0 meV	—
intermol. intera.	155 meV	155 meV	380 meV	380 meV	100 meV to 130 meV
dielectric env.	—	—	—	—	—

Table 7.1: PL red-shift of the measured thin films at about 8 GPa (for PCBM at 4 GPa) and the values assigned to the different parameters.

Intermolecular interaction proved to have a major contribution to the red-shift under pressure. This was shown indirectly for PFO and rra-P3HT and more directly for RR-P3HT crystals by the comparison of the PL red-shift of a semicrystalline RR-P3HT film with the one of the amorphous rra-P3HT film. Additionally, we showed that a higher mobility of the charges caused by intermolecular interaction results in the quenching of Franck-Condon emission in the conjugated materials.

Another contribution to the red-shift under pressure can be the effect of planarisation of the polymer chains. This became most clear in the comparison of the PL red-shifts of the almost planar β-phase with the glassy phase of PFO under hydrostatic pressure. In contrast, Raman measurements indicated that planarisation under pressure plays no significant role in P3HT samples.

The change of the refractive index of a conjugated polymer (PFO) under pressure was determined for the first time. For this purpose, the change in the optical path in a thick glassy PFO film was measured with an interferometric method. The refractive index increased only about 5 percent for a pressure increase of 8 GPa. In addition, the analysis revealed that the oscillator strength and polarisability in these films decrease with pressure.

The estimates for the different contributions for the red-shift under pres-

sure of the pure organic semiconductor films are shown in table 7.1. The red-shift due to the change in bond length was estimated to be very similar in all the polymers (9 meV/GPa). Because PCBM is more rigid, the effect of the bond length change is probably much smaller than for polymers. The dielectric environment was estimated to play no role in the observed red-shifts and the planarisation just for glassy PFO. In each case, the remaining part of the total red-shift was attributed to intermolecular interaction.

The changes in the CT state emission in rra-P3HT:PCBM with increasing PCBM concentration gave indications that the charge separation rate increases with bigger PCBM clusters. These experiments suggest that clusters start to form for PCBM concentrations between 15 % to 20 %. It was shown that under hydrostatic pressure the CT PL is reduced, probably because of higher charge separation as a result of higher delocalisation. The red-shift of the CT state under hydrostatic pressure proved to depend mostly on the energy shifts of the pure materials. Beyond that, the increasing dielectric constant is likely to cause an additional but minor red-shift. The importance of the delocalisation of the charges on the charge separation efficiency underlined the importance of crystallinity at the interface in order to increase the intermolecular interaction and concomitantly the delocalisation.

The results show that we have many ways to influence the optical band gap and emission intensity of polymer films. The control of order seems to be a basic requirement to achieve the desired energy shifts. For an improved photon harvesting of organic solar cells (OSCs) at low energies, above all, the steric effects of the sidechains have to be minimised as they lower the planarity, which increases the optical band gap, and the capability of the polymer to crystallise. But the experiments showed that it would be desirable to decrease the interchain distance even further than what can be found, for example, in P3HT crystals. The intermolecular distance in P3HT in π-stacking direction is about 0.34 nm [133], the covalent bond between two carbon atoms is about 0.14 nm [176]. Even though crosslinking the polymer chains might not be feasible (not to mention potentially detrimental for the conjugated system of the backbone), this shows, at least, that no strong binding forces exist in the crystal and that there is an enormous potential to

reduce the interchain distance from a chemical point of view.

As shown as well, the lower interchain distance has other effects, which have to be taken into account. It improves the mobility of the exciton and quenches the Franck-Condon PL. This quenching is not likely to have negative effects on the device efficiency of OSCs, but for organic light-emitting diodes (OLEDs) it might not be a desired effect.

As this quenching is connected mostly with low-energy traps, probably the same happens for electroluminescence, as it occurs in OLEDs. In this case, the enhancement of the interchain interaction would have to go along with a reduction of the defect sites in the polymer in order to maintain the luminescence quantum yield. However, even for OLEDs the quenching of the Franck-Condon luminescence might not be necessarily detrimental for the device efficiency. In PFO, the Franck-Condon emission is quenched as well, but it leads to a stronger defect/excimer emission. Also, phosphorescent OLEDs require an efficient transport to the phosphorescent sites in the active film [177]. Similar to the transport of the excitons to defect sites in PFO, the emission might even be enhanced this way.

For OSC devices, the absorption is only one part which determines high short circuit currents. Additionally, the charge separation rate of the CT state is important. At the same time, for a high power conversion efficiency, it is desirable to have a high open circuit voltage, i.e. a high CT state energy.

As the low energy absorption increases with pressure but the CT state energy (proportional to open circuit voltage) decreases, it is interesting to estimate how the device efficiency would change with the application of hydrostatic pressure in order to see in which cases it is desirable to achieve pressure-like effects for devices. Scharber et al. [178] made design rules solely based on the polymer band gap and the LUMO position of the donor (while having the PCBM LUMO fixed at $-4.3\,\mathrm{eV}$), or, more to the point, on the difference of the LUMO(donor) and LUMO(acceptor). This graph is shown in figure 7.1. RR-P3HT has a band gap of about $1.9\,\mathrm{eV}$ and a difference in the LUMO levels of RR-P3HT and PCBM of about $1.15\,\mathrm{eV}$ (values between $1.21\,\mathrm{eV}$ [21] and about $1\,\mathrm{eV}$ can be found [101]). According to our results (see sketch in figure 7.1), the red arrow in figure 7.1 would describe

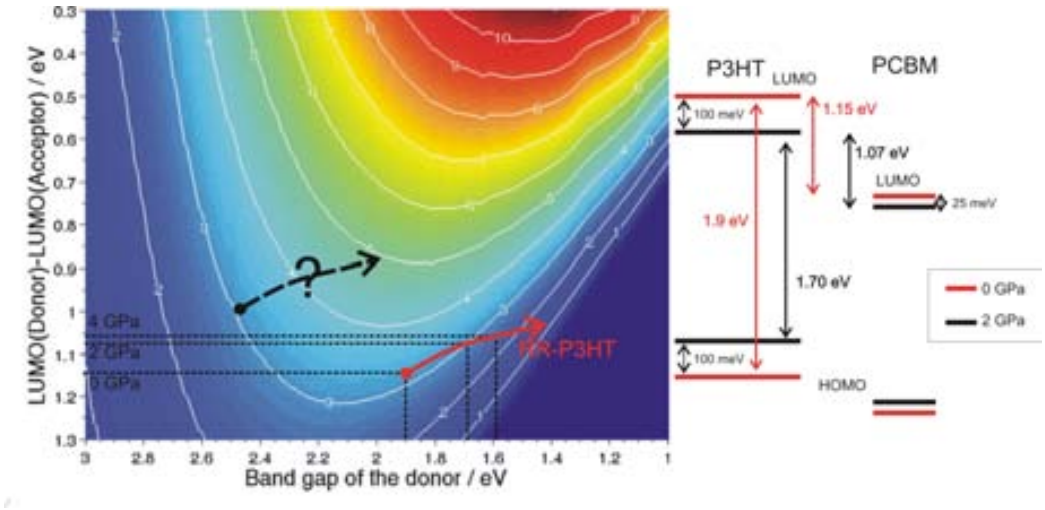

Figure 7.1: Theoretically expected OSC efficiencies; from [8]. The red arrow marks the expected efficiency change of a RR-P3HT:PCBM OSC under high pressure. The black dashed arrow marks a hypothetical example of increasing efficiency under pressure. The sketch on the right hand side shows the changes of the energy levels from 0 GPa to 2 GPa.

the change in efficiency of a hypothetical high pressure OSC.

As can be seen, in such a high pressure OSC based on RR-P3HT:PCBM, the expected efficiency is lowered from just above 3 % to about 2.5 % at 4 GPa. The effect of pressure might not be quite as unfavourable as this path in the graph suggests, for an increase in mobility and a more efficient charge separation are not taken into account in this model. Both are expected to occur at smaller intermolecular distances (high pressure) and would probably increase the expected electrical current of the device considerably.

But with a different polymer there might be very similar but more beneficial changes under pressure. The best polymer to show improved efficiency for high-pressure-like OSCs would have a higher band gap with a maintained or - if possible - lower lying LUMO level. For a hypothetical system this is illustrated by the dashed arrow, which would show a strong increase beyond the efficiency of a RR-P3HT:PCBM system at ambient pressure. This is still not considering the improved mobilities and charge separation. If such pressure-like effects can be applied to high-bandgap polymers the search for a good donor material would in theory be reduced to finding a polymer with

a good LUMO level. Of course, such a material would still have to show that it exhibits good morphologies and mobilities in blends with PCBM. As mentioned both are very important for an efficient charge separation.

This little *gedankenexperiment* is important in order to explore and assess the most direct consequences of the results for OSCs, but the aim of the thesis is more general and the highest benefit for the development of devices is likely to arise from the better understanding of the organic semiconductors obtained with the presented experiments. This better understanding which was gained in course of this work hopefully contributes to design new materials, to get inspiration for new approaches to design active films and eventually to make better organic optoelectronic devices for a future which at the moment might still seem like science fiction.

Concerning future experiments, there are many possible experiments based on the idea to use hydrostatic pressure as a means to explore the properties of organic semiconductors. The thesis dealt with already very good conjugated polymers in their respective field, P3HT for OSCs and PFO for OLEDs. It would be interesting to study systems which - under ambient conditions - do not work well as solar cells and investigate with high pressure if similar changes as for P3HT and PFO can be observed. This can help to understand why a specific material or blend does not work well for OSCs or OLEDs and find solution to improve them.

The changes in the power conversion efficiency under high pressure, which we estimated in this chapter, could also be measured directly. For this, a working OSC has to be introduced into a pressure cell. The experimental set-up requires that both the illumination with a light source and the measurements of electrical currents and voltage are possible. These experiments, especially when combined with PL measurements, could contribute to understand how the performance of OSCs would be affected by pressure. Similar to this experiment, it would be interesting to try to focus more on the electrical properties of the active film by measurements of current-voltage-curves and electroluminescence under pressure. This could give insight into the pressure dependence of the transport properties and bimolecular recombination, which is important both for OLEDs and OSCs.

Bibliography

[1] C. J. Brabec, N. S. Sariciftci, J. C. Hummelen; *Plastic solar cells*; Adv. Funct. Mater.; 11, 1, 15; 2001.

[2] J. W. Park, D. C. Shin, S. H. Park; *Large-area OLED lightings and their applications*; Semicond. Sci. Technol.; 26, 3; 2011.

[3] C. J. Brabec, A. Cravino, D. Meissner, N. S. Sariciftci, T. Fromherz, M. T. Rispens, L. Sanchez, J. C. Hummelen; *Origin of the Open Circuit Voltage of Plastic Solar Cells*; Adv. Funct. Mater.; 11, 5, 374; 2001.

[4] C. Cochrane, L. Meunier, F. M. Kelly, V. Koncar; *Flexible displays for smart clothing: Part I-Overview*; Indian J. Fibre Text. Res.; 36, 4, SI, 422; 2011.

[5] http://www.oled-info.com/sony-oled.

[6] H. Sasabe, J. Kido; *Development of high performance OLEDs for general lighting*; J. Mater. Chem. C; 1, 9, 1699; 2013.

[7] F. So, B. Krummacher, M. K. Mathai, D. Poplavskyy, S. A. Choulis, V.-E. Choong; *Recent progress in solution processable organic light emitting devices*; J. Appl. Phys.; 102, 9, 091101; 2007.

[8] G. Dennler, M. C. Scharber, C. J. Brabec; *Polymer-Fullerene Bulk-Heterojunction Solar Cells*; Adv. Mater.; 21, 13, 1323; 2009.

[9] J. L. Brédas, D. Beljonne, V. Coropceanu, J. Cornil; *Charge-transfer and energy-transfer processes in π-conjugated oligomers and polymers: A molecular picture*; Chem. Rev.; 104, 11, 4971; 2004.

[10] G. Chidichimo, L. Filippelli; *Organic Solar Cells: Problems and Perspectives*; Int. J. Photoenergy; 2010, 1; 2010.

[11] J.-T. Chen, C.-S. Hsu; *Conjugated polymer nanostructures for organic solar cell applications*; Polym. Chem.; 2, 12, 2707; 2011.

[12] A. C. Mayer, S. R. Scully, B. E. Hardin, M. W. Rowell, M. D. McGehee; *Polymer-based solar cells*; Mater. Today; 10, 11, 28; 2007.

[13] H. Hoppe, N. S. Sariciftci; *Organic solar cells: An overview*; J. Mater. Res.; 19, 7, 1924; 2004.

[14] B. Kippelen, J.-L. Brédas; *Organic photovoltaics*; Energy Environ. Sci.; 2, 3, 251; 2009.

[15] P. Nicholson, F. Castro; *Organic photovoltaics: principles and techniques for nanometre scale characterization*; Nanotechnology; 21, 49, 492001; 2010.

[16] B. Ratier, J.-M. Nunzi, M. Aldissi, T. M. Kraft, E. Buncel; *Organic solar cell materials and active layer designs-improvements with carbon nanotubes: a review*; Polym. Int.; 61, 3, 342; 2012.

[17] J. Nunzi; *Organic photovoltaic materials and devices*; C. R. Phys.; 3, 523; 2002.

[18] J. Nelson; *Polymer:fullerene bulk heterojunction solar cells*; Mater. Today; 14, 10, 462; 2011.

[19] http://www.heliatek.com/newscenter/latest_news/neuer-weltrekord-fur-organische-solarzellen-heliatek-behauptet-sich-mit-12-zelleffizienz-als-technologiefuhrer/.

[20] A. Niv, Z. R. Abrams, M. Gharghi, C. Gladden, X. Zhang; *Overcoming the bandgap limitation on solar cell materials*; Appl. Phys. Lett.; 100, 8, 083901; 2012.

[21] D. Veldman, S. C. J. Meskers, R. A. J. Janssen; *The Energy of Charge-Transfer States in Electron Donor-Acceptor Blends: Insight into the Energy Losses in Organic Solar Cells*; Adv. Funct. Mater.; 19, 12, 1939; 2009.

[22] M. Lenes, M. Morana, C. J. Brabec, P. W. M. Blom; *Recombination-Limited Photocurrents in Low Bandgap Polymer/Fullerene Solar Cells*; Adv. Funct. Mater.; 19, 7, 1106; 2009.

[23] V. I. Arkhipov, P. Heremans, H. Bässler; *Why is exciton dissociation so efficient at the interface between a conjugated polymer and an electron acceptor?*; Appl. Phys. Lett.; 82, 25, 4605; 2003.

[24] D. McMahon, D. Cheung, A. Troisi; *Why holes and electrons separate so well in polymer/fullerene photovoltaic cells*; J. Phys. Chem. Lett.; 2, 2737; 2011.

[25] M. T. Dang, L. Hirsch, G. Wantz; *P3HT:PCBM, Best Seller in Polymer Photovoltaic Research*; Adv. Mater.; 23, 31, 3597; 2011.

[26] T. M. Clarke, J. R. Durrant; *Charge Photogeneration in Organic Solar Cells*; Chem. Rev.; 110, 11, 6736; 2010.

[27] M. Knupfer, T. Pichler, M. S. Golden, J. Fink, M. Murgia, R. H. Michel, R. Zamboni, C. Taliani; *Size of Electron-Hole Pairs in Pi-Conjugated Systems*; Phys. Rev. Lett.; 83, 7, 1443; 1999.

[28] I. G. Scheblykin, A. Yartsev, T. Pullerits, V. Gulbinas, V. Sundstrom; *Excited state and charge photogeneration dynamics in conjugated polymers*; J. Phys. Chem. B; 111, 23, 6303; 2007.

[29] K. Hummer, P. Puschnig, C. Ambrosch-Draxl, M. Oehzelt, G. Heimel, R. Resel; *Calculated Optical Absorption of Anthracene under High Pressure*; Synth. Met.; 137, 1-3, 935; 2003.

[30] P. Puschnig, C. Ambrosch-Draxl; *Excitons in organic semiconductors*; C. R. Phys.; 10, 6, 504; 2009.

[31] B. Tian, G. Zerbi, R. Schenk, K. Müllen; *Optical-Spectra And Structure Of Oligomeric Models Of Polyparaphenylenevinylene*; J. Chem. Phys.; 95, 5, 3191; 1991.

[32] E. Havinga, I. Rotte, E. Meijer, W. Hoeve, H. Wynberg; *Spectra and electrical properties of soluble partially alkyl-substituted oligomers of thiophene up to 11 rings*; Synth. Met.; 43, 473; 1991.

[33] C. Brabec, V. Dyakonov, U. Scherf (editors); *Organic photovoltaics: materials, device physics, and manufacturating technologies*; Wiley-VCH, Weinheim; 2008.

[34] Y. Zhao, Z. Y. Xie, Y. Qu, Y. H. Geng, L. X. Wang; *Effects of thermal annealing on polymer photovoltaic cells with buffer layers and in situ formation of interfacial layer for enhancing power conversion efficiency*; Synth. Met.; 158, 21-24, 908; 2008.

[35] P. W. M. Blom, V. D. Mihailetchi, L. J. A. Koster, D. E. Markov; *Device physics of polymer: fullerene bulk heterojunction solar cells*; Adv. Mater.; 19, 12, 1551; 2007.

[36] J. G. Solé, L. Bausá, D. Jaque; *An Introduction to the Optical Spectroscopy of Inorganic Solids*; John Wiley & Sons Ltd, West Sussex; 2005.

[37] M. Pope, C. Swenberg; *Electronic Processes in Organic Crystals and Polymers*; Oxford University Press, New York; 2nd edition; 1999.

[38] A. J. Heeger; *Semiconducting polymers: the Third Generation.*; Chem. Soc. Rev.; 39, 7, 2354; 2010.

[39] S.-H. Lim, T. G. Bjorklund, C. J. Bardeen; *Temperature-dependent exciton dynamics in poly(p-phenylene vinylene) measured by femtosecond transient spectroscopy*; Chem. Phys. Lett.; 342, 5-6, 555; 2001.

[40] K. Paudel, H. Knoll, M. Chandrasekhar, S. Guha; *Tuning Intermolecular Interactions in Dioctyl-Substituted Polyfluorene via Hydrostatic Pressure*; J. Phys. Chem. A; 114, 13, 4680; 2010.

[41] S. Guha, J. D. Rice, Y. T. Yau, C. M. Martin, M. Chandrasekhar, H. R. Chandrasekhar, R. Guentner, P. Scanduicci de Freitas, U. Scherf; *Temperature-dependent photoluminescence of organic semiconductors with varying backbone conformation*; Phys. Rev. B; 67, 12, 125204; 2003.

[42] M. Theander, A. Yartsev, D. Zigmantas, V. Sundström, W. Mammo, M. R. Andersson, O. Inganäs; *Photoluminescence quenching at a polythiophene/C-60 heterojunction*; Phys. Rev. B; 61, 19, 12957; 2000.

[43] R. A. J. Janssen; *Photoexcitations in Conjugated Oligomers*; World Scientific Publishers, Singapore; 1997.

[44] N. S. Sariciftci (editor); *Primary Photoexcitations In Conjugated Polymers: Molecular Exciton Versus Semiconductor Band Model*; World Scientific Publishing, Singapore; 1997; ISBN 978-981-02-2880-4.

[45] V. I. Arkhipov, H. Bässler; *Exciton dissociation and charge photogeneration in pristine and doped conjugated polymers*; phys. stat. sol. (a); 201, 6, 1152; 2004.

[46] M. S. a. Abdou, F. P. Orfino, Y. Son, S. Holdcroft; *Interaction of Oxygen with Conjugated Polymers: Charge Transfer Complex Formation with Poly(3-alkylthiophenes)*; J. Am. Chem. Soc.; 119, 19, 4518; 1997.

[47] M. Muntwiler, Q. Yang, W. Tisdale, X.-Y. Zhu; *Coulomb Barrier for Charge Separation at an Organic Semiconductor Interface*; Phys. Rev. Lett.; 101, 19, 1; 2008.

[48] A. Haugeneder, M. Neges, C. Kallinger, W. Spirkl, U. Lemmer, J. Feldmann; *Exciton diffusion and dissociation in conjugated polymer / fullerene blends and heterostructures*; Phys. Rev. B; 59, 23, 346; 1999.

[49] L. Lüer, H. Egelhaaf, D. Oelkrug, G. Cerullo; *Oxygen-induced quenching of photoexcited states in polythiophene films*; Org. Electron.; 5, 1-3, 83; 2004.

[50] J. E. Kroeze, T. J. Savenije, M. J. W. Vermeulen, J. M. Warman; *Contactless determination of the photoconductivity action spectrum, exciton diffusion length,*

and charge separation efficiency in polythiophene-sensitized tio2 bilayers; J. Phys. Chem. B; 107, 31, 7696; 2003.

[51] X. Y. Zhu, Q. Yang, M. Muntwiler; *Charge-Transfer Excitons at Organic Semiconductor Surfaces and Interfaces*; Acc. Chem. Res.; 42, 11, 1779; 2009.

[52] A. C. Morteani, A. S. Dhoot, J. S. Kim, C. Silva, N. C. Greenham, C. Murphy, E. Moons, S. Cina, J. H. Burroughes, R. H. Friend; *Barrier-free electron-hole capture in polymer blend heterojunction light-emitting diodes*; Adv. Mater.; 15, 20, 1708; 2003.

[53] K. Tvingstedt, K. Vandewal, A. Gadisa, F. Zhang, J. Manca, O. Inganäs; *Electroluminescence from charge transfer states in polymer solar cells*; J. Am. Chem. Soc.; 131, 33, 11819; 2009.

[54] B. C. Thompson, J. M. J. Fréchet; *Polymer-fullerene composite solar cells*; Angew. Chem. Int. Ed. Engl.; 47, 1, 58; 2008.

[55] V. D. Mihailetchi, L. J. A. Koster, J. C. Hummelen, P. W. M. Blom; *Photocurrent generation in polymer-fullerene bulk heterojunctions*; Phys. Rev. Lett.; 93, 21, 216601; 2004.

[56] D. Veldman, O. İpek, S. C. J. Meskers, J. Sweelssen, M. M. Koetse, S. C. Veenstra, J. M. Kroon, S. S. v. Bavel, J. Loos, R. A. J. Janssen; *Compositional and electric field dependence of the dissociation of charge transfer excitons in alternating polyfluorene copolymer/fullerene blends*; J. Am. Chem. Soc.; 130, 24, 7721; 2008.

[57] C. Deibel, T. Strobel, V. Dyakonov; *Origin of the Efficient Polaron-Pair Dissociation in Polymer-Fullerene Blends*; Phys. Rev. Lett.; 103, 3, 36402; 2009.

[58] A. Gadisa, M. Svensson, M. R. Andersson, O. Inganäs; *Correlation between oxidation potential and open-circuit voltage of composite solar cells based on blends of polythiophenes/ fullerene derivative*; Appl. Phys. Lett.; 84, 9, 1609; 2004.

[59] S. Albert-Seifried, J. M. Hodgkiss, F. Laquai, H. A. Bronstein, C. K. Williams, R. H. Friend; *Pressure-Induced Delocalization of Photoexcited States in a Semiconducting Polymer*; Phys. Rev. Lett.; 105, 19, 195501; 2010.

[60] S. Guha, W. Graupner, R. Resel, M. Chandrasekhar, H. R. Chandrasekhar, R. Glaser, G. Leising; *Planarity of para hexaphenyl*; Phys. Rev. Lett.; 82, 18, 3625; 1999.

[61] J. P. Schmidtke, J. S. Kim, J. Gierschner, C. Silva, R. H. Friend; *Optical spectroscopy of a polyfluorene copolymer at high pressure: Intra- and intermolecular interactions*; Phys. Rev. Lett.; 99, 16, 167401; 2007.

[62] A. M. Familia, A. Sarangan, T. R. Nelson; *Gas to crystal effect on the spectral line narrowing of MEH-PPV*; Opt. Express; 15, 13, 8231; 2007.

[63] B. C. Hess, G. S. Kanner, Z. Vardeny; *Photoexcitations In Polythiophene At High-Pressure*; Phys. Rev. B; 47, 3, 1407; 1993.

[64] C. M. Martin, S. Guha, M. Chandrasekhar, H. R. Chandrasekhar, R. Guentner, P. Scanduicci de Freitas, U. Scherf; *Hydrostatic pressure dependence of the luminescence and Raman frequencies in polyfluorene*; Phys. Rev. B; 68, 11, 115203; 2003.

[65] S. Guha, M. Chandrasekhar; *Photophysics of organic emissive semiconductors under hydrostatic pressure*; phys. stat. sol. (b); 241, 14, 3318; 2004.

[66] S. Yang, W. Graupner, S. Guha, P. Puschnig, C. Martin, H. Chandrasekhar, M. Chandrasekhar, G. Leising, C. Ambrosch-Draxl, U. Scherf; *Geometry-dependent electronic properties of highly fluorescent conjugated molecules*; Phys. Rev. Lett.; 85, 11, 2388; 2000.

[67] P. Puschnig, C. Ambrosch-Draxl, G. Heimel, E. Zojer, R. Resel, G. Leising, M. Kriechbaum, W. Graupner; *Pressure studies on the intermolecular interactions in biphenyl*; Synth. Met.; 116, 1-3, 327; 2001.

[68] P. Puschnig, K. Hummer, C. Ambrosch-Draxl, G. Heimel, M. Oehzelt, R. Resel; *Electronic, optical, and structural properties of oligophenylene molecular crystals under high pressure: An ab initio investigation*; Phys. Rev. B; 67, 23, 1; 2003.

[69] M. Oehzelt, R. Resel, A. Nakayama; *High-pressure structural properties of anthracene up to 10 gpa*; Phys. Rev. B; 66, 17, 1; 2002.

[70] K. Hummer, P. Puschnig, C. Ambrosch-Draxl; *Ab initio study of anthracene under high pressure*; Phys. Rev. B; 67, 18, 1; 2003.

[71] J. Cornil, D. D. Santos; *Influence of interchain interactions on the absorption and luminescence of conjugated oligomers and polymers: a quantum-chemical characterization*; J. Am. Chem. Soc.; 7863, 14, 1289; 1998.

[72] S. Yang, W. Graupner, S. Guha; *Influence of the molecular geometry on the photoexcitations of highly emissive organic semiconductors*; SPIE proceedings; 3797, July, 26; 1999.

[73] M. Kasha, H. Rawls, M. El-Bayoumi; *The exciton model in molecular spectroscopy*; Pure Appl. Chem; 11, 371; 1965.

[74] J. Cornil, D. Beljonne, J. P. Calbert, J. L. Bredas; *Interchain interactions in organic π-conjugated materials: Impact on electronic structure, optical response, and charge transport*; Adv. Mater.; 13, 14, 1053; 2001.

[75] R. Farchioni, G. Grosso (editors); *Organic Electronic Materials*; Springer-Verlag, Berlin Heidelberg New York; 2001.

[76] J. Clark, C. Silva, R. Friend, F. Spano; *Role of Intermolecular Coupling in the Photophysics of Disordered Organic Semiconductors: Aggregate Emission in Regioregular Polythiophene*; Phys. Rev. Lett.; 98, 20, 1; 2007.

[77] F. C. Spano; *Modeling disorder in polymer aggregates: The optical spectroscopy of regioregular poly(3-hexylthiophene) thin films*; J. Chem. Phys.; 122, 23, 234701; 2005.

[78] F. C. Spano; *Erratum: Modeling disorder in polymer aggregates: The optical spectroscopy of regioregular poly(3-hexylthiophene) thin films*; J. Chem. Phys.; 126, 15, 159901; 2007.

[79] H. Yamagata, F. C. Spano; *Interplay between intrachain and interchain interactions in semiconducting polymer assemblies: the HJ-aggregate model.*; J. Chem. Phys.; 136, 18, 184901; 2012.

[80] S. Webster, D. N. Batchelder; *Absorption, luminescence and Raman spectroscopy of poly(p-phenylene vinylene) at high pressure*; Polymer; 37, 22, 4961; 1996.

[81] M. A. Loi, A. Mura, G. Bongiovanni, Q. Cai, C. Martin, H. R. Chandrasekhar, M. Chandrasekhar, W. Graupner, F. Garnier; *Ultrafast formation of nonemissive species via intermolecular interaction in single crystals of conjugated molecules*; Phys. Rev. Lett.; 86, 4, 732; 2001.

[82] M. Loi, A. Mura, G. Bongiovanni, Q. Cai, C. Martin; *Pressure-induced quenching of the photoluminescence in sexithiophene single crystals observed by femtosecond spectroscopy*; Synth. Met.; 119, 645; 2001.

[83] L. Rothberg, M. Yan, F. Papadimitrakopoulos, M. Galvin, E. Kwock, T. Miller; *Photophysics of phenylenevinylene polymers*; Synth. Met.; 80, 1, 41; 1996.

[84] V. R. Gangilenka, A. DeSilva, H. P. Wagner, R. E. Tallman, B. A. Weinstein, R. Scholz; *Exciton emission in PTCDA thin films under uniaxial pressure*; Phys. Rev. B; 77, 11, 36; 2008.

[85] R. Buckminster Fuller, E. J. Applewhite; *Synergetics: Explorations in the Geometry of Thinking*; Macmillan, New York; 1975; ISBN 978-0025418707.

[86] P. M. Allemand, A. Koch, F. Wudl, Y. Rubin, F. Diederich, M. M. Alvarez, S. J. Anz, R. L. Whetten; *Two different fullerenes have the same cyclic voltammetry*; J. Am. Chem. Soc.; 113, 3, 1050; 1991.

[87] M. T. Rispens, A. Meetsma, R. Rittberger, C. J. Brabec, N. S. Sariciftci, J. C. Hummelen; *Influence of the solvent on the crystal structure of PCBM and the efficiency of MDMO-PPV : PCBM 'plastic' solar cells*; Chem. Commun.; pages 2116–2118; 2003.

[88] M. Lenes, G.-J. A. H. Wetzelaer, F. B. Kooistra, S. C. Veenstra, J. C. Hummelen, P. W. M. Blom; *Fullerene Bisadducts for Enhanced Open-Circuit Voltages and Efficiencies in Polymer Solar Cells*; Adv. Mater.; 20, 11, 2116; 2008.

[89] http://www.sigmaaldrich.com.

[90] Z. Bao, A. Dodabalapur, A. J. Lovinger; *Soluble and processable regioregular poly(3-hexylthiophene) for thin film field-effect transistor applications with high mobility*; Appl. Phys. Lett.; 69, 26, 4108; 1996.

[91] H. Sirringhaus, P. J. Brown, R. H. Friend, M. M. Nielsen, K. Bechgaard, B. M. W. Langeveld-Voss, A. J. H. Spiering, R. A. J. Janssen, E. W. Meijer, P. Herwig, D. M. de Leeuw; *Two-dimensional charge transport in self-organized, high-mobility conjugated polymers*; Nature; 401, 6754, 685; 1999.

[92] G. Schopf, G. Kossmehl; *Polythiophenes - Electrically Conductive Polymers (Advances in Polymer Science)*; volume 129; Springer-Verlag Berlin; 1997.

[93] R. D. McCullough, R. D. Lowe, M. Jayaraman, D. L. Anderson; *Design, synthesis, and control of conducting polymer architectures: structurally homogeneous poly (3-alkylthiophenes)*; J. Org. Chem.; 58, 904; 1993.

[94] S. Malik, A. K. Nandi; *Crystallization mechanism of regioregular poly(3-alkyl thiophene)s*; J. Polym. Sci. Part B: Polym. Phys.; 40, 18, 2073; 2002.

[95] M. Grell, D. D. C. Bradley, M. Inbasekaran, E. P. Woo; *A glass-forming conjugated main-chain liquid crystal polymer for polarized electroluminescence applications*; Adv. Mater.; 9, 10, 798; 1997.

[96] D. Neher; *Polyfluorene Homopolymers: Conjugated Liquid-Crystalline Polymers for Bright Blue Emission and Polarized Electroluminescence*; Macromol. Rapid Commun.; 22, 17, 1365; 2001.

[97] W. Chunwaschirasiri, B. Tanto, D. L. Huber, M. J. Winokur; *Chain Conformations and Photoluminescence of Poly(di-n-octylfluorene)*; Phys. Rev. Lett.; 94, 10, 3; 2005.

[98] M. J. Winokur, J. Slinker, D. L. Huber; *Structure, photophysics, and the order-disorder transition to the β phase in poly(9,9-(di-n,n-octyl)fluorene)*; Phys. Rev. B; 67, 18, 184106; 2003.

[99] A. L. Khan, M. J. Banach, A. Köhler; *Control of β-phase formation in polyfluorene thin films via Franck-Condon analysis*; Synth. Met.; 139, 3, 905; 2003.

[100] A. Nardes, M. Kemerink, M. de Kok, E. Vinken, K. Maturova, R. Janssen; *Conductivity, work function, and environmental stability of pedot:pss thin films treated with sorbitol*; org. electron.; 9, 5, 727 ; 2008.

[101] C. J. Brabec, J. R. Durrant; *Solution-processed organic solar cells*; MRS Bull.; 33, 7, 670; 2008.

[102] K. Syassen, W. B. Holzapfel; *Physics of solids under high pressure, volume 1*; in K. D. Timmerhaus, M. S. Barber (editors), *High-Pressure Science and Technology*; Plenum, New York; 1979.

[103] A. Jayaraman; *Diamond anvil cell and high-pressure physical investigations*; Rev. Mod. Phys.; 55, 65; 1983.

[104] H. K. Mao, J. Xu, P. M. Bell; *Calibration of the ruby pressure gauge to 800 kbar under quasi-hydrostatic conditions*; Journal of Geophysical Research: Solid Earth; 91, B5, 4673; 1986.

[105] W. Smith, G. Dent; *Modern Raman Spectroscopy - A Practical Approach*; John Wiley & Sons, Ltd; west susse edition; 2005; ISBN 0-471-49668-5.

[106] K. Iwasaki, H. Fujimoto, S. Matsuzaki; *Conformational-Changes Of Poly(3-Alkylthiophene)S With Temperature And Pressure*; Synth. Met.; 63, 2, 101; 1994.

[107] T. Danno, J. Kurti, H. Kuzmany; *Optical Anisotropy And Raman-Scattering From Highly Oriented Poly(Octylthiophene) Films*; Phys. Rev. B; 43, 6, 4809; 1991.

[108] W. C. Tsoi, D. T. James, J. S. Kim, P. G. Nicholson, C. E. Murphy, D. D. C. Bradley, J. Nelson, J.-S. Kim; *The nature of in-plane skeleton Raman modes of P3HT and their correlation to the degree of molecular order in P3HT:PCBM blend thin films.*; J. Am. Chem. Soc.; 133, 25, 9834; 2011.

[109] H. G. Tompkins, E. A. Irene (editors); *Handbook of Ellipsometry*; William Andrew Publishing; Springer, Norwich, Heidelberg; 2005.

[110] H. Cheun, B. Tanto, W. Chunwaschirasiri, B. Larson, M. J. Winokur; *Near-term aging and thermal behavior of polyfluorene in various aggregation states*; Appl. Phys. Lett.; 84, 1, 22; 2004.

[111] A. J. Cadby, P. A. Lane, H. Mellor, S. J. Martin, M. Grell, C. Giebeler, D. D. C. Bradley, M. Wohlgenannt, C. An, Z. Vardeny; *Film morphology and photophysics of polyfluorene*; Phys. Rev. B; 62, 23, 15604; 2000.

[112] M. Grell, D. D. C. Bradley, G. Ungar, J. Hill, K. S. Whitehead; *Interplay of Physical Structure and Photophysics for a Liquid Crystalline Polyfluorene*; Macromolecules; 32, 18, 5810; 1999.

[113] S. Foster, J. Frost, M. Campoy-Quiles, J. Nelson, D. D. C. Bradley; *The limiting role of β-phase in time-of-flight charge transport in poly(9,9-dioctylfluorene), and mobility enhancement through inhibiting its formation*; (in preparation); 2013.

[114] M. Ariu, D. G. Lidzey, D. D. C. Bradley; *Influence of film morphology on the vibrational spectra of dioctyl substituted polyfluorene (PFO)*; Synth. Met.; 111-112, 607; 2000.

[115] S. T. Hoffmann, H. Bässler, A. Köhler; *What determines inhomogeneous broadening of electronic transitions in conjugated polymers?*; J. Phys. Chem. B; 114, 51, 17037; 2010.

[116] W. Barford, D. Trembath; *Exciton localization in polymers with static disorder*; Phys. Rev. B; 80, 16, 165418; 2009.

[117] B. J. Schwartz; *Conjugated polymers as molecular materials : How chain conformation and film morphology influence energy transfer and interchain interactions*; Annu. Rev. Phys. Chem.; 54, 141; 2003.

[118] M. Campoy-Quiles, J. Nelson, D. D. C. Bradley, P. G. Etchegoin; *Dimensionality of electronic excitations in organic semiconductors: A dielectric function approach*; Phys. Rev. B; 76, 235206; 2007.

[119] G. Hartwig; *Polymer Properties at Room and Cryogenic Temperatures*; Plenum, New York; 1994.

[120] A. Cadby, R. Dean, A. M. Fox, R. A. L. Jones, D. G. Lidzey; *Mapping the fluorescence decay lifetime of a conjugated polymer in a phase-separated blend using a scanning near-field optical microscope*; Nano Lett.; 5, 11, 2232; 2005.

[121] E. Zojer, A. Pogantsch, E. Hennebicq, D. Beljonne, J.-L. Brédas, P. Scandiucci de Freitas, U. Scherf, E. J. W. List; *Green emission from poly(fluorene)s: The role of oxidation*; J. Chem. Phys.; 117, 14, 6794; 2002.

[122] S. Guha, W. Graupner, R. Resel, M. Chandrasekhar, H. R. Chandrasekhar, R. Glaser, G. Leising; *Tuning Intermolecular Interactions: A Study of the Structural and Vibrational Properties of p -Hexaphenyl under Pressure*; The Journal of Physical Chemistry A; 105, 25, 6203; 2001.

[123] S. Guha, M. Chandrasekhar, U. Scherf, M. Knaapila; *Tuning structural and optical properties of blue-emitting polymeric semiconductors*; phys. stat. sol. (b); 248, 5, 1083; 2011.

[124] G. Heimel, P. Puschnig, M. Oehzelt; *Chain-length-dependent intermolecular packing in polyphenylenes: a high pressure study*; J. Phys.: Condens. Matter; 3375; 2003.

[125] P. S. Ku; *Equations of State of organic high polymers*; General Electric Company, Philadelphia, Pennsylvania; 1968.

[126] A. Goñi, A. Cantarero, K. Syassen, M. Cardona; *Effect of pressure on the low-temperature exciton absorption in GaAs*; Phys. Rev. B; 41, 10111; 1990.

[127] S. F. Alvarado, P. F. Seidler, D. G. Lidzey, D. D. C. Bradley; *Direct determination of the exciton binding energy of conjugated polymers using a scanning tunneling microscope*; Phys. Rev. Lett.; 81, 1082; 1998.

[128] N. Takeda, S. Asaoka, J. R. Miller; *Nature and energies of electrons and holes in a conjugated polymer, polyfluorene.*; J. Am. Chem. Soc.; 128, 50, 16073; 2006.

[129] M. Tong, C.-X. Sheng, Z. Vardeny; *Nonlinear optical spectroscopy of excited states in polyfluorene*; Phys. Rev. B; 75, 12, 125207; 2007.

[130] J.-W. van der Horst, P. a. Bobbert, M. a. J. Michels, H. Bässler; *Calculation of excitonic properties of conjugated polymers using the Bethe-Salpeter equation*; J. Chem. Phys.; 114, 15, 6950; 2001.

[131] D. Tenery, A. J. Gesquiere; *Effect of PCBM concentration on photoluminescence properties of composite MEH-PPV/PCBM nanoparticles investigated by a Franck-Condon analysis of single-particle emission spectra.*; Chemphyschem.; 10, 14, 2449; 2009.

[132] F. Dias, F. da Costa, A. Maçanita, J. Morgado, H. Burrows, A. Monkman; *Kinetics and thermodynamics of poly (9, 9-dioctylfluorene) beta-phase formation in dilute solution*; Macromolecules; 39, 5854; 2006.

[133] M. Brinkmann; *Structure and morphology control in thin films of regioregular poly(3-hexylthiophene)*; J. Polym. Sci. Part B: Polym. Phys.; 49, 17, 1218; 2011.

[134] M. Theander, M. Svensson, A. Ruseckas, D. Zigmantas, V. Sundström, M. Andersson, O. Inganäs; *High luminescence from a substituted polythiophene in a solvent with low solubility*; Chem. Phys. Lett.; 337, 4Ű6, 277 ; 2001.

[135] X. M. Jiang, R. Österbacka, O. Korovyanko, C. P. An, B. Horovitz, R. A. J. Janssen, Z. V. Vardeny; *Spectroscopic studies of photoexcitations in regioregular and regiorandom polythiophene films*; Adv. Funct. Mater.; 12, 9, 587; 2002.

[136] H. Sirringhaus; *Integrated Optoelectronic Devices Based on Conjugated Polymers*; Science; 280, 5370, 1741; 1998.

[137] P. J. Brown, D. S. Thomas, A. Köhler, J. S. Wilson, J. S. Kim, C. M. Ramsdale, H. Sirringhaus, R. H. Friend; *Effect of interchain interactions on the absorption and emission of poly(3-hexylthiophene)*; Phys. Rev. B; 67, 6, 64203; 2003.

[138] S. Engmann, V. Turkovic, P. Denner, H. Hoppe, G. Gobsch; *Optical order of the polymer phase within polymer/fullerene blend films*; J. Polym. Sci. Part B: Polym. Phys.; 50, 19, 1363; 2012.

[139] T. Kaniowski, W. Luzny, S. Niziol, J. Sanetra, M. Trznadel; *X-ray diffraction and optical studies of fractionalized regioregular poly(3-hexylthiophene)*; Synth. Met.; 92, 1, 7; 1998.

[140] M. Dresselhaus; *Fullerenes*; J. Mater. Res.; 8, 8, 2054; 1993.

[141] S. Kazaoui, R. Ross, N. Minami; *In situ photoconductivity behavior of C60 thin films: Wavelength, temperature, oxygen effect*; Solid State Commun.; 90, 10, 623 ; 1994.

[142] S. Deguchi, R. Alargova, K. Tsujii; *Stable dispersions of fullerenes, C60 and C70, in water. Preparation and characterization*; Langmuir; 17, 6013; 2001.

[143] D. Wasserberg, S. P. Dudek, S. C. Meskers, R. A. J. Janssen; *Comparison of the chain length dependence of the singlet- and triplet-excited states of oligofluorenes*; Chem. Phys. Lett.; 411, 1-3, 273; 2005.

[144] J. Mårdalen, E. J. Samuelsen, O. R. Konestabo, M. Hanfland, M. Lorenzen; *Conducting polymers under pressure: synchrotron x-ray determined structure and structure related properties of two forms of poly(octyl-thiophene)*; J. Phys.: Condens. Matter; 10, 32, 7145; 1998.

[145] A. Zen, M. Saphiannikova, D. Neher, J. Grenzer, S. Grigorian, U. Pietsch, U. Asawapirom, S. Janietz, U. Scherf, I. Lieberwirth, G. Wegner; *Effect of Molecular Weight on the Structure and Crystallinity of Poly(3-hexylthiophene)*; Macromolecules; 39, 6, 2162; 2006.

[146] C. H. Woo, B. C. Thompson, B. J. Kim, M. F. Toney, J. M. J. Fréchet; *The influence of poly(3-hexylthiophene) regioregularity on fullerene-composite solar cell performance.*; J. Am. Chem. Soc.; 130, 48, 16324; 2008.

[147] B. A. Collins, J. R. Tumbleston, H. Ade; *Miscibility, Crystallinity, and Phase Development in P3HT/PCBM Solar Cells: Toward an Enlightened Understanding of Device Morphology and Stability*; J. Phys. Chem. Lett.; 2, 24, 3135; 2011.

[148] B. Sundqvist; *Fullerenes under high pressures*; Advances In Physics; 48, 1, 1; 1999.

[149] G. Louarn, M. Trznadel, J. P. Buisson, J. Laska, A. Pron, M. Lapkowski, S. Lefrant; *Raman Spectroscopic Studies of Regioregular Poly(3-alkylthiophenes)*; J. Phys. Chem.; 100, 30, 12532; 1996.

[150] G. Louarn, J. Y. Mevellec, J. P. Buisson, S. Lefrant; *Comparison Of The Vibrational Properties Of Polythiophene And Polyalkylthiophenes*; Synth. Met.; 55, 1, 587; 1993.

[151] Y. Gao, J. K. Grey; *Resonance chemical imaging of polythiophene/fullerene photovoltaic thin films: mapping morphology-dependent aggregated and unaggregated C=C Species.*; J. Am. Chem. Soc.; 131, 28, 9654; 2009.

[152] S. Garreau, G. Louarn, J. Buisson; *In situ spectroelectrochemical Raman studies of poly (3, 4-ethylenedioxythiophene)(PEDT)*; Macromolecules; 32, 6807; 1999.

[153] Y. Furushima, K. Tazaki, H. Fujimoto; *Raman study on the pressure-induced disordered state of polystyrene*; Solid State Commun.; 140, 5, 240; 2006.

[154] X. Yang, J. K. J. van Duren, M. T. Rispens, J. C. Hummelen, R. A. J. Janssen, M. A. J. Michels, J. Loos; *Crystalline Organization of a Methanofullerene as Used for Plastic Solar-Cell Applications*; Adv. Mater.; 16, 9-10, 802; 2004.

[155] J. K. J. van Duren, X. Yang, J. Loos, C. W. T. Bulle-Lieuwma, A. B. Sieval, J. C. Hummelen, R. A. J. Janssen; *Relating the Morphology of Poly(p-phenylene vinylene)/Methanofullerene Blends to Solar-Cell Performance*; Adv. Funct. Mater.; 14, 5, 425; 2004.

[156] W. Yin, M. Dadmun; *A New Model for the Morphology of P3HT/PCBM Organic Photovoltaics from Small-Angle Neutron Scattering: Rivers and Streams*; ACS Nano; 5, 6, 4756; 2011.

[157] E. Voroshazi, K. Vasseur, T. Aernouts, P. Heremans, A. Baumann, C. Deibel, X. Xue, A. J. Herring, A. J. Athans, T. a. Lada, H. Richter, B. P. Rand; *Novel bis-C60 derivative compared to other fullerene bis-adducts in high efficiency polymer photovoltaic cells*; J. Mater. Chem.; 21, 43, 17345; 2011.

[158] J. M. Frost, M. A. Faist, J. Nelson; *Energetic disorder in higher fullerene adducts: a quantum chemical and voltammetric study.*; Adv. Mater.; 22, 43, 4881; 2010.

[159] A. C. Mayer, M. F. Toney, S. R. Scully, J. Rivnay, C. J. Brabec, M. Scharber, M. Koppe, M. Heeney, I. McCulloch, M. D. McGehee; *Bimolecular Crystals of Fullerenes in Conjugated Polymers and the Implications of Molecular Mixing for Solar Cells*; Adv. Funct. Mater.; 19, 8, 1173; 2009.

[160] D. Chen, A. Nakahara, D. Wei, D. Nordlund, T. P. Russell; *P3HT/PCBM bulk heterojunction organic photovoltaics: correlating efficiency and morphology.*; Nano Lett.; 11, 2, 561; 2011.

[161] K. Tvingstedt, K. Vandewal; *On the Dissociation Efficiency of Charge Transfer Excitons and Frenkel Excitons in Organic Solar Cells: A Luminescence Quenching Study*; J. Phys. Chem. C; 114, 21824; 2010.

[162] J. M. Guo, H. Ohkita, H. Benten, S. Ito; *Charge Generation and Recombination Dynamics in Poly(3-hexylthiophene)/Fullerene Blend Films with Different Regioregularities and Morphologies*; J. Am. Chem. Soc.; 132, 17, 6154; 2010.

[163] A. A. Y. Guilbert, L. X. Reynolds, A. Bruno, A. MacLachlan, S. P. King, M. a. Faist, E. Pires, J. E. Macdonald, N. Stingelin, S. a. Haque, J. Nelson; *Effect of multiple adduct fullerenes on microstructure and phase behavior of P3HT:fullerene blend films for organic solar cells.*; ACS Nano; 6, 5, 3868; 2012.

[164] K. Hasharoni, M. Keshavarz-K., A. Sastre, R. Gonzalez, C. Bellavia-Lund, Y. Greenwald, T. Swager, F. Wudl, A. J. Heeger; *Near IR photoluminescence in mixed films of conjugated polymers and fullerenes*; J. Chem. Phys.; 107, 7, 2308; 1997.

[165] J. Brédas, J. Norton, J. Cornil; *Molecular understanding of organic solar cells: The challenges*; Acc. Chem. Res.; 42, 11, 1691 ; 2009.

[166] L. Onsager; *Initial recombination of ions*; Phys. Rev.; 54, 8, 554; 1938.

[167] M. A. Loi, S. Toffanin, M. Muccini, M. Forster, U. Scherf, M. Scharber; *Charge transfer excitons in bulk heterojunctions of a polyfluorene copolymer and a fullerene derivative*; Adv. Funct. Mater.; 17, 13, 2111; 2007.

[168] H. Oevering, M. N. Paddon-Row, M. Heppener, A. M. Oliver, E. Cotsaris, J. W. Verhoeven, N. S. Hush; *Long-range photoinduced through-bond electron transfer and radiative recombination via rigid nonconjugated bridges: distance and solvent dependence*; J. Am. Chem. Soc.; 109, 11, 3258; 1987.

[169] J. W. Jung, W. H. Jo; *Annealing-Free High Efficiency and Large Area Polymer Solar Cells Fabricated by a Roller Painting Process*; Adv. Funct. Mater.; 20, 14, 2355; 2010.

[170] V. Mihailetchi, J. van Duren, P. Blom, J. Hummelen, R. Janssen, J. Kroon, M. Rispens, W. Verhees, M. Wienk; *Electron Transport in a Methanofullerene*; Adv. Funct. Mater.; 13, 1, 43; 2003.

[171] D. Cheung, D. McMahon, A. Troisi; *Computational study of the structure and charge-transfer parameters in low-molecular-mass P3HT*; J. Phys. Chem. B; 113, 9393; 2009.

[172] K. Sakurai, H. Tachibana, N. Shiga, C. Terakura, M. Matsumoto, Y. Tokura; *Experimental determination of excitonic structure in polythiophene*; Phys. Rev. B; 56, 15, 9552; 1997.

[173] A. P. Monkman, H. D. Burrows, I. Hamblett, S. Navarathnam, M. Svensson, M. R. Andersson; *The effect of conjugation length on triplet energies, electron delocalization and electron–electron correlation in soluble polythiophenes*; J. Chem. Phys.; 115, 19, 9046; 2001.

[174] H. Ohkita, S. Cook, Y. Astuti, W. Duffy, M. Heeney, S. Tierney, I. McCulloch, D. D. C. Bradley, J. R. Durrant; *Radical ion pair mediated triplet formation in polymer-fullerene blend films.*; Chem. Commun.; 100, 37, 3939; 2006.

[175] C. Tanase, E. J. Meijer, P. W. M. Blom, D. M. de Leeuw; *Unification of the Hole Transport in Polymeric Field-Effect Transistors and Light-Emitting Diodes*; Phys. Rev. Lett.; 91, 21, 216601; 2003.

[176] Y. Baskin, L. Meyer; *Lattice Constants of Graphite at Low Temperatures*; Phys. Rev.; 100, 2, 544; 1955.

[177] S. Reineke, M. A. Baldo; *Recent progress in the understanding of exciton dynamics within phosphorescent OLEDs*; phys. stat. sol. (a); 209, 12, 2341; 2012.

[178] M. C. Scharber, D. Mühlbacher, M. Koppe, P. Denk, C. Waldauf, A. J. Heeger, C. J. Brabec; *Design rules for donors in bulk-heterojunction solar cells–towards 10% energy-conversion efficiency*; Adv. Mater.; 18, 6, 789; 2006.

List of publications

Y. Gebremichael, A. Sáchez, X. Borrise, M. Schmidt, A. R. Goñi, M. I. Alonso, R. Rurali, J. Suñé, X. Cartoixa, and F. Pérez-Murano. "Pattern transfer optimization for the fabrication of arrays of silicon nanowires" Microelectronic Engineering 87, no. 5-8 (2010): 1479-1482. doi:10.1016/j.mee.2009.11.086.

M. Campoy Quiles, M. Schmidt, D. Nassyrov, O. Peña, A. R. Goñi, M. I. Alonso, and M. Garriga. "Real-time studies during coating and post-deposition annealing in organic semiconductors" Thin Solid Films 519, no. 9 (2011): 2678-2681. doi:10.1016/j.tsf.2010.12.228.

J. Cabanillas González, Juan, O. Peña-Rodríguez, I. Suarez López, M. Schmidt, M. I. Alonso, A. R. Goñi, and M. Campoy Quiles. "Organic position sensitive photodetectors based on lateral donor-acceptor concentration gradients." Applied Physics Letters 99, no. 10 (2011): 103305. doi:10.1063/1.3631731.

M. Rubio-Roy, O. Vlasin, O. Pascu, J. M. Caicedo, M. Schmidt, A. R. Goñi, N. G. Tognalli, A. Fainstein, A. Roig, G. Herranz "Magneto-optical enhancement by plasmon excitations in nanoparticle/metal structures" Langmuir 28, 9010-9020 (2012). doi: 10.1021/la301239x

J. Cabanillas González, M. Schmidt, O Peña-Rodríguez, M. I. Alonso, A. R. Goñi, M. Campoy-Quiles "Effect of structure and interlayer diffusion in organic position sensitive photodetectors based on complementary wedge donor/acceptor layers" Journal of Nanoscience and Nanotechnology (2012)

M. Schmidt, N. G. Tognalli, M. A. Otte, M. I. Alonso, B. Sepúlveda, A. Fainstein and A. R. Goñi, "Spatial distribution of optical near-fields in plasmonic gold sphere-segment voids" Plasmonics (2013), doi: 10.1007/s11468-013-9491-4

Abstract of "Spatial distribution of optical near-fields in plasmonic gold sphere-segment voids"

We present a comprehensive experimental and computational study on the electromagnetic field distribution in sphere-segment void arrays. Surface plasmon-polaritons can be excited in these void arrays resulting in greatly enhanced electromagnetic fields. With the scanning near-field optical microscope (SNOM) we are able to measure the electromagnetic field distribution at the sample surface. For this purpose an array of relatively large voids with a sphere diameter of 900 nm was fabricated, allowing for an easy access of the scanning glass-fibre tip and yielding very detailed scans. Complementary, finite-difference time-domain (FDTD) calculations on a complete void array have been performed and compared with the SNOM intensity maps and experimental reflectivity data. We show in a direct way both the existence of extended and localised modes in the Au void array for three different void depths. We also show and discuss the changes that the modes undergo for the different void depths and excitation wavelengths. Moreover, since the simulations were performed for two different void geometries, one containing perfectly spherical void surfaces and another more realistic one, which considers the presence of interstitial wall holes and other imperfections, as observed in scanning electron micrographs, we were able to determine by comparison with the experiment under which conditions an array of idealised sphere-segment voids is a meaningful model. This demonstrates that both SNOM and FDTD simulations are powerful tools for understanding the plasmonic response of metallic nanostructures, thus enabling, for instance, a design for applications in ultra-sensitive optical detection.

And thanks to everyone who was not mentioned but made my life in Barna a bit more joyful and chocolaty, my work a bit easier and my thesis a bit better. Because of you I will look back and remember how great this time was.

Los extrañaré...